REPORT DOCUMENTATION PAGE

AFRL-SR-AR-TR-02-

0760

1. AGENCY USE ONLY (Leave Blank)	2. REPORT DATE 7/1/02	3. REPORT TYPE AND DATES COVERED FINAL TECHNICAL REPORT: 5/1/99-9/30/01

4. TITLE AND SUBTITLE	5. FUNDING NUMBERS
Experimental and Analytical Development of Kinetic Rate Data for Radiating Rocket Plume Species	F49620-99-1-0119

6. AUTHOR(S)

E. Ploenjes, P. Palm. I. Adamovich, W. Lempert, V. Subramaniam, J.W. Rich

7. PERFORMING ORGANIZATION NAME(S) AND ADDRESS(ES)	8. PERFORMING ORGANIZATION REPORT NUMBER
Dept. of Mechanical Engineering, The Ohio State University 206 W. 18th Ave., Columbus, OH 43210	

9. SPONSORING / MONITORING AGENCY NAME(S) AND ADDRESS(ES)	10. SPONSORING / MONITORING AGENCY REPORT NUMBER
Space Propulsion and Power Directorate of Aerospace and Materials Sciences Air Force Office of Scientific Research 801 N. Randolph St., Arlington, VA 22203-1977	

11. SUPPLEMENTARY NOTES

The views, opinions and/or findings contained in this report are those of the author(s) and should not be construed as an official Department of the Army position, policy or decision, unless so designated by other documentation.

12 a. DISTRIBUTION / AVAILABILITY STATEMENT	12 b. DISTRIBUTION CODE
Approved for public release; distribution unlimited.	

13. ABSTRACT (Maximum 200 words)

The report presents results of experimental and analytical studies of certain energy transfer mechanisms and rates in high-energy gas flows. The immediate application is to generate kinetic data to aid in the prediction of the radiation emitted by hypervelocity vehicle flowfields, radiation from high altitude rocket plumes, bow shocks, and shock layers around the vehicles. The present report gives data on a newly discovered vibration-to-electronic (V-E) energy transfer process in CO, creating strong UV signal on the CO 4th Positive Bands. This process has been found to be mediated by small amount of free electrons in the flow. Analogous processes populating radiating excited electronic states of NO, CN, and C2 are also presented. In a complementary phase of the work, production of highly vibrationally excited N2 in cold plasmas, and the measurement of vibrational level populations by spontaneous Raman spectroscopy is reported.

14. SUBJECT TERMS		15. NUMBER OF PAGES
ROCKET PLUME RADIATION, ENERGY TRANSFER PROCESSES, HYPERVELOCITY FLOWS, NONEQUILIBRIUM REACTING FLOWS		85
		16. PRICE CODE

17. SECURITY CLASSIFICATION OR REPORT UNCLASSIFIED	18. SECURITY CLASSIFICATION ON THIS PAGE UNCLASSIFIED	19. SECURITY CLASSIFICATION OF ABSTRACT UNCLASSIFIED	20. LIMITATION OF ABSTRACT UL

Enclosure 1

20020903 039

EXECUTIVE SUMMARY

The research reported here, conducted for AFOSR Space Power and Propulsion Program, is an experimental and analytical study of certain energy transfer mechanisms and rates in high-energy gas flows. The immediate USAF application of the current work is to develop the ability to predict the radiation emitted by the exhaust expansion ("plume") of rockets. The goal is to predict the wavelength dependence of the intensity of this radiation as a function of the propellant species and altitude of the rocket. Beyond this, it is also desired to predict the radiation from other regions of flow fields surrounding hypervelocity vehicles such as rockets. These regions include, notably, the bow shock and accompanying shock layers around the vehicle. Large computer modeling codes are being developed for such prediction; they depend critically upon knowledge of the rates of specific chemical reactions and energy transfer processes occurring in the hypervelocity vehicle flow field.

The research by the Ohio State group on this program has concentrated on two major tasks elucidating these rates: 1) Experimental study of the mechanism and rates of energy transfer into excited electronic species that form some of the principal radiators at ultraviolet and visible wavelengths from the flow field. These radiating states include, notably, the CO 4th Positive (UV) Bands (CO $A^1\Pi$ states); NO Beta and Gamma (UV) Bands (NO $B^2\Pi$ and NO $A^2\Sigma^+$ states); C_2 Swan (Visible) Bands (C_2 $A^3\Pi$ states); and CN Violet (Visible) Bands (CN $B^2\Sigma^+$ states); and, 2) Experimental measurements and analytic theory of the rates of vibrational energy transfer among the excited states of common diatomic molecular species (O_2, N_2, CO, NO) in the hypervelocity flow field environment.

The first chapter of the report discusses experiments and analytical research on vibration-to-electronic energy transfer in CO-laser-pumped CO-Ar and CO-N_2 plasmas. The highly vibrationally excited states in CO are populated by resonance absorption of the CO radiation followed by anharmonic (vibration-vibration) V-V pumping. Additionally, N_2 also becomes vibrationally excited due to collisions with vibrationally excited CO. Nonequilibrium ionization in the plasmas is produced by an associative ionization mechanism in collisions of highly vibrationally excited CO molecules. Electron production rate and electron density in these

optically pumped CO-Ar and CO-N₂ plasmas have been measured using a Thomson discharge probe and microwave attenuation. It is shown that adding small amounts of O_2 or NO (50-100 mTorr) to the baseline gas mixtures at P=100 Torr results in an increase of the electron density by up to a factor of 20-40 (from $n_e < 10^{10}$ cm^{-3} to $n_e = (1.5-3.0) \cdot 10^{11}$ cm^{-3}). This occurs while the electron production rate either decreases (as in the presence of O_2) or remains nearly constant within a factor of 2 (as in the presence of NO). It is also shown that the electron-ion recombination rates inferred from these measurements decrease by 2 to 3 orders of magnitude compared to their baseline values (with no additives in the cell), down to $\beta \cong 1.5 \cdot 10^{-8}$ cm^3/sec with 50-100 mTorr of oxygen or nitric oxide added to the baseline CO-Ar mixture, and $\beta \cong (2-3) \cdot 10^{-7}$ cm^3/sec with 75-100 mTorr of O_2 or NO added to the baseline CO-N₂ mixture. The overall electron-ion removal rates in the presence of equal amounts of O_2 or NO additives turn out to be very close, which shows that the effect of electron attachment to oxygen at these conditions is negligible. These results suggest a novel method of electron density control in cold laser-sustained steady-state plasmas and open a possibility of sustaining stable high-pressure nonequilibrium plasmas at high electron densities and low plasma power budget.

Chapter 2 summarizes the experiments showing that vibration-to-electronic mode energy transfer in these plasmas is mediated by free electrons. The experiments depend critically on the novel methods of electron density control reported in Chap.1. It is shown that removal of the electrons from the optically pumped plasmas using a saturated Thomson discharge results in considerable reduction of the UV/visible radiation from the plasma (CO 4th positive bands, NO γ bands, CN violet bands, and C₂ Swan bands). At some conditions, the removal of electrons results in a nearly complete extinguishing of the UV/visible glow of the plasma. This effect occurs even though electron removal results in an increase of the high vibrational level populations of the ground electronic state $CO(X^1\Sigma, v\sim15-35)$. On the other hand, deliberate electron density increase by adding small amounts of O_2 or NO to the optically pumped CO-Ar plasmas produced substantial increase of the UV/visible radiation intensity, which strongly correlates with the electron density. The results of the present experiments indicate that the vibration-to-electronic (V-E) energy transfer process $CO(X^1\Sigma \rightarrow A^1\Pi)$, and, possibly, analogous processes populating radiating excited electronic states of NO, CN, and C₂, in optically pumped plasmas, may be mediated by the presence of electrons which are created in the absence of an

electric field, with low initial energies. Most importantly, this effect occurs at ionization fractions as low as $n_e/N \sim 10^{-9}$-10^{-7}.

Chapter 3 presents a two-dimensional time-dependent model of non-self-sustained DC and RF discharges used for analysis of recent experiments in optically pumped nonequilibrium plasmas. The analysis shows that non-self-sustained DC and RF discharges can be successfully used for measurements of electron production rate, electron recombination rate, and electron density in these plasmas. The inferred rate of electron production per unit volume by the associative ionization mechanism is $S_0 = 1.0 \cdot 10^{15}$ $1/cm^3/s$ and $S_0 = 2.2 \cdot 10^{14}$ $1/cm^3/s$ in CO/Ar=2/100 and in CO/N$_2$=2/100 plasmas, respectively. The inferred electron-ion recombination rate coefficients are $\beta > 6.0 \cdot 10^{-6}$ cm^3/s and $\beta = (7.5 \pm 1.5) \cdot 10^{-6}$ cm^3/s in CO/Ar=2/100 mixtures at P=100 Torr and 20 Torr, respectively. In CO/Ar=2/100 mixtures with a 0.05-0.1 Torr admixture of O$_2$ at P=100 Torr and 20 Torr, the inferred recombination rate coefficients are $\beta = (1.5 \pm 0.3) \cdot 10^{-8}$ cm^3/s and $\beta = (5.1 \pm 2.9) \cdot 10^{-8}$ cm^3/s, respectively. Finally, the inferred electron density in optically pumped CO/Ar/O$_2$ plasmas at the laser beam axis is $n_e = (1.7 \pm 0.2) \cdot 10^{11}$ cm^{-3} at P=100 Torr and $n_e = (6.2 \pm 0.8) \cdot 10^{10}$ cm^{-3} at P=20 Torr.

The concluding Chapter, 4, presents results of spatially resolved Raman measurements of nitrogen vibrational level populations in a nonequilibrium optically pumped plasma sustained by a combination of a continuous wave CO laser and a sub-breakdown radio frequency electric field. The plasma is created in a CO/N$_2$ environment, at a total pressure of 300 Torr. When an RF field is applied to the plasma, collisions between the free electrons heated by the field and the diatomic species create additional vibrational excitation within the plasma region. Note that the reduced electric field, E/N, is sufficiently low to prevent electron impact ionization, which would lead to the glow-to-arc collapse. Vibrational level populations of N$_2$ are measured using spontaneous Raman spectroscopy. The results show that applying the RF field to an optically pumped CO/N$_2$ plasma produces stronger vibrational disequilibrium both in the region occupied by the CO laser beam and outside of this region. The experimental results are compared with kinetic modeling calculations showing a satisfactory agreement.

TABLE OF CONTENTS

CHAPTER 1
ELECTRON DENSITY AND RECOMBINATION RATE MEASUREMENTS
IN CO-SEEDED OPTICALLY PUMPED PLASMAS

1. Introduction

Steady-state nonequilibrium optically pumped environments are produced by resonance absorption of infrared laser radiation by molecules in low vibrational quantum states, with subsequent collisional vibration-to-vibration (V-V) pumping up to high vibrational levels [1,2],

$$AB(v) + AB(w) \rightarrow AB(v-1) + AB(w+1) \tag{1}$$
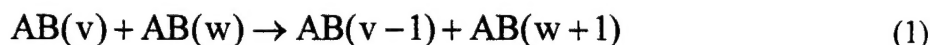
In Eq. (1), AB stands for a diatomic molecule, and v and w are vibrational quantum numbers. This method creates strong vibrational disequilibrium at high densities (up to a few atm in the gas phase), wide temperature range (T=100-1500 K), and a low power budget (~1-10 W/cm^3). In particular, optical pumping by a CO laser has been previously achieved in gas phase CO/Ar/He mixtures [3-8] at pressures of up to 10 atm [3], gas phase nitric oxide [9,10], liquid phase CO [11,12], and solid CO and NO matrices [13,14]. Recently, optical pumping has also been demonstrated in mixtures of CO with infrared inactive gases, such as nitrogen and air, at atmospheric pressure [15,16]. In this case, N_2 and O_2 molecules become vibrationally excited by near-resonance V-V energy transfer from CO,

$$CO(v) + N_2(w) \rightarrow CO(v-1) + N_2(w+1) \tag{2}$$

$$CO(v) + O_2(w) \rightarrow CO(v-1) + O_2(w+1) \tag{3}$$
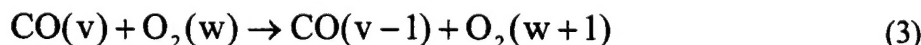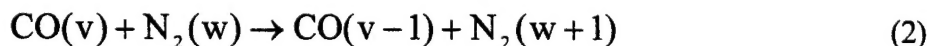
In the experiments of Refs. [2-16], the CO laser power was fairly low, ranging from a few Watts to 200 W c.w.

Ionization in optically pumped gases is produced by an associative ionization mechanism, in collisions of two highly vibrationally excited molecules when the sum of their vibrational energies exceeds the ionization potential [17-20],

$$AB(v) + AB(w) \rightarrow (AB)_2^+ + e^- ,$$
$$E_v + E_w > E_{ion} \tag{4}$$
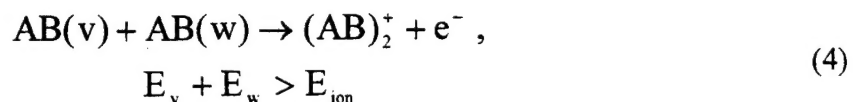
Ionization of carbon monoxide by this mechanism has been previously observed in CO/Ar/He gas mixtures optically pumped by resonance absorption of CO laser radiation [18-20]. The estimated steady-state electron density sustained by a 10 W CO laser in optically pumped CO/Ar/He plasmas with high vibrational level populations of $n_{CO}(v\sim30)\sim10^{15}$ cm^{-3} is $n_e\sim10^{10}$-10^{11} cm^{-3} [19]. Note that unlike electron impact ionization, the ionization mechanism of Eq. (4) is not susceptible to the ionization heating instability, which is responsible for filamentation and the glow-to-arc collapse in high-pressure nonequilibrium plasmas, where ionization is primarily produced by electron impact [21]. Indeed, since the high vibrational level populations of diatomic molecules decrease with temperature due to an exponential rise of the vibration-translation (V-T) relaxation rates [22], there is a negative feedback between the gas heating and the rate of associative ionization. This precludes the ionization instability development and provides a possibility for the use of associative ionization for sustaining unconditionally stable optically pumped nonequilibrium plasmas at high gas pressures (1 atm and above).

The present paper addresses the effect of adding air species, such as O_2 and NO, to optically pumped CO/Ar and CO/N_2 plasmas on the electron production and removal kinetics. Previous results [20] suggest that adding these species produces a significant electron density rise in these plasmas at a nearly constant plasma power budget and electron production rate. Therefore, the main objective of the present study is to investigate the role of these additives on the electron density and on the electron removal rate in the plasma. This would provide insight into the feasibility of sustaining large-volume atmospheric pressure nonequilibrium air plasmas at a minimum power budget.

2. Experimental

The overall schematic of the experimental setup is shown in Fig.1. A carbon monoxide laser is used to excite CO/Ar and CO/N_2 gas mixtures, with additives such as O_2 or NO, slowly flowing through the pyrex glass optical absorption cell shown. The residence time of the gas mixture in the cell is of the order of a few seconds. The liquid nitrogen cooled CO laser [8] is designed in collaboration with the University of Bonn and fabricated at Ohio State. It produces a substantial fraction of its power output on the v = 1→0 fundamental band component in the infrared. In the present experiment, the laser is typically operated at 10-13 W c.w. broadband power on the lowest ten vibrational bands. The output on the lowest bands (1→0 and 2→1) is necessary to start the absorption process in cold CO (initially at 300 K) in the cell. The laser beam can be focused to a focal area of ~1 mm diameter to increase the power loading per CO molecule, producing an excited region 10-20 cm long and 2-3 mm in diameter.

The lower vibrational states of CO, v≤10, are populated by direct resonance absorption of the pump laser radiation in combination with rapid redistribution of population by V-V exchange processes. The V-V processes then continue to populate higher vibrational levels above v=10, which are not directly coupled to the laser radiation (see Eq. (1)). The large heat capacity of the Ar and N_2 diluents, as well as conductive and convective cooling of the gas flow, enables control over the translational/rotational mode temperature in the cell. At steady-state conditions, when the average vibrational mode energy of the CO would correspond to a few thousand degrees Kelvin, the temperature never rises above a few hundred degrees. Thus a strong disequipartition of energy can be maintained in the cell, characterized by very high vibrational mode energy and a low translational/rotational mode temperature. As shown in Fig. 1, the population of the vibrational states of CO in the cell is monitored using a Biorad FTS 175C Fourier transform infrared spectrometer, which records spontaneous emission from the CO fundamental, first and second overtone bands through a CaF_2 window on the side of the cell.

Ionization of highly excited CO molecules in the cell occurs by the associative ionization mechanism of Eq. (4). The electron production rate in this optically pumped plasma is determined from the saturation current of the non-self-sustained DC Thomson discharge [18-20] between two 3 cm diameter brass plate electrodes located in the absorption cell as shown in Fig.

2. Two infrared transparent CaF_2 windows were placed upstream and downstream of the plates (see Fig. 2), so that the laser beam creates a nearly cylindrical excited region between the windows. Thus the plasma generated in the interelectrode space is isolated from the plasma sustained in the remainder of the cell, which significantly reduces the charged species drift and diffusion into the interelectrode space. This allows reaching a well-pronounced current saturation. The electrodes, which are typically 10 to 20 mm apart, are connected to a reversible polarity DC power supply (Thorn EMI GENCOM Inc., Model 3000R), which produces voltage in the range 0-3000 V. The induced current is measured with a Keithley 2001 multimeter, with a 1 MΩ resistor connected in series with the cell to protect the multimeter in case of breakdown. The applied DC voltage is deliberately kept sufficiently low to preclude electron impact ionization. Therefore, in the saturation regime of the Thomson discharge, the applied electric field, which does not produce any ionization by itself, removes as many electrons per second as are produced in the entire discharge volume. The electron production rate per unit volume of the plasma is found from the saturation current as follows [20],

$$S \cong \frac{I_s}{e\pi d^2 D/4},$$

(5)

where d is the diameter of the ionized region created by the focused laser beam, D is the electrode diameter, and $\pi d^2 D/4$ is the volume occupied by the plasma. The plasma diameter, $d=2.5\pm0.5$ mm, is estimated from the diameter of the visible blue glow of the C_2 Swan band radiation, which is strongly coupled with the high vibrational level populations of CO [7].

The electron density in the optically pumped plasma is independently measured by microwave attenuation. The microwave experimental apparatus consists of an oscillator, a transmitting and receiving antenna / waveguide system, and transmitted and reflected microwave power detectors. The phase-locked dielectrically stabilized oscillator generates 20 mW (13 dBm) of microwave radiation at a frequency $\nu=10$ GHz, which is transmitted via SMA-type semi-rigid cable to an antenna within the transmission waveguide. The gap between the waveguides is 1 cm. The receiving waveguide is positioned directly opposite the transmitting waveguide, with the laser-generated plasma located between them (see Fig. 2). The signal transmitted through the

8

plasma is received by an antenna at the back of the receiving waveguide and sent to a tunnel diode detector with a low-noise preamplifier. The detector produces a low-noise DC voltage proportional to the received microwave power, ranging from 0 to 15 V for the transmitted power in the range from –60 dBm to –30 dBm. The voltage noise level is typically 1-2 mV, so that the resultant signal-to-noise ratio is $\sim 10^4$. Power reflected by the plasma is detected by a zero-bias Schottky diode detector through an isolator in the line between the oscillator and the transmitting antenna. This detector produces a DC voltage in the mV range proportional to the reflected microwave power in the range from 0 to 20 mW. In the present experiments, the measured change in reflected power between the laser on and laser off conditions is negligible.

Typical microwave power levels transmitted across the 1 cm gap between the waveguides were in the range of –10 dBm to 0 dBm, decreasing by up to 1 dB when the plasma was generated. To scale the transmitted signal down to the power range over which the detector has the highest sensitivity (that is, down to –60 dBm to –30 dBm range), attenuators were inserted in the line between the receiving antenna and the transmitted power detector. From the relative difference of the transmitted power with and without a plasma the attenuation of the microwave signal across the plasma was determined with an uncertainty of 0.002 dB. This assumes a negligible difference in the power radiated from the gap between the waveguides, with and without the plasma present, which is justified by the negligible change in the measured reflected power at these conditions.

During the microwave attenuation measurements, the laser beam was chopped at a frequency of 57 Hz, providing a square wave laser input into the cell. The laser remained on and off for approximately 8 msec. Our previous time-resolved Fourier transform infrared spectroscopy measurements [8] showed that at CO partial pressures $P_{CO}>0.5$ torr this time is sufficiently long to reach both the quasi-steady state fully V-V pumped distribution and the complete vibrational relaxation of CO in the cell. In addition, the characteristic time scales for associative ionization and for electron-ion recombination, $\tau_{ion} \sim n_e/(k_{ion}n_{CO}^2 f_{v>30}^2) \sim 0.1$ msec and $\tau_{rec} \sim 1/\beta n_e \sim 0.1\text{-}1.0$ msec are both much shorter than the chopper cycle duration. Here $k_{ion}=1.5 \cdot 10^{-13}$ cm^3/sec is the associative ionization rate coefficient [20], $n_{CO}=10^{17}$ cm^{-3} is the CO concentration in the cell (at $P_{CO}=3$ torr), $f_{v>30} \sim 10^{-3}$ is the fraction of the CO molecules

participating in the associative ionization process of Eq. (4) [20], $\beta=10^{-8}-10^{-7}$ cm^3/sec is the electron-ion dissociative recombination rate, and $n_e=10^{11}$ cm^{-3} is the estimated maximum electron density [20]. Therefore the laser on and laser off conditions correspond to the quasi-steady state weakly ionized plasma and nearly fully recombined plasma conditions, respectively. The difference between the incident and transmitted microwave powers between the plasma on and plasma off conditions was determined from the amplitude of the resultant nearly square wave forward power detector signal, $\delta V = V_{inc} - V_{trans}$, modulated by the chopper, and averaged by a Textronix TDS380 oscilloscope over 256 averages. The average electron density in the plasma was inferred from these measurements using the following relation [21],

$$n_e = \frac{m_e c \varepsilon_0}{e^2} \nu_{coll} \frac{\delta V}{V_{inc}} \frac{1}{d} \frac{W}{d},$$ (6)

where ν_{coll} is the electron-neutral collision frequency, $\frac{\delta V}{V_{inc}} = \frac{V_{trans} - V_{inc}}{V_{inc}}$ is the relative attenuation factor in terms of the forward power detector voltage proportional to the incident and the transmitted microwave power, $W=1$ cm is the waveguide width, and $d=2.5\pm0.5$ mm is the diameter of the ionized region. The electron-neutral collision frequency in CO-Ar and CO-N$_2$ mixtures at P=100 torr and T=600 K, $\nu_{coll}=1.1 \cdot 10^{12}$ cm^3/sec and $\nu_{coll}=2.1 \cdot 10^{12}$ cm^3/sec, respectively, was obtained from the Boltzmann equation solution [19] using the experimental cross-sections of elastic and inelastic electron collision processes available in the literature.

O$_2$ or NO were both diluted in nitrogen at the 5000 ppm level to add controlled small amounts (from a few millitorr to a few hundred millitorr) of these species to the cell. The resultant O$_2$/N$_2$ and NO/N$_2$ gas mixtures have been added to the baseline CO/Ar and CO/N$_2$ gas mixtures. The baseline pressure in the cell was P=100 torr, with the CO partial pressure of P$_{CO}$=3 torr. The O$_2$/N$_2$ and NO/N$_2$ mixture partial pressure was varied from 1 torr to 100 torr. Note that adding the same amounts of pure nitrogen (without the additives) to the baseline gas mixtures did not produce significant changes in the measured electron density.

3. Results and Discussion

Figure 3 shows the low-resolution (8 cm^{-1}) CO first overtone infrared emission spectra measured in the optically pumped CO-Ar plasmas with O_2 and NO additives. At these conditions, vibrational levels up to v~35-40 are populated and radiating. From Fig. 3, one can see that adding small amounts (~0.1%) of oxygen to the cell gases results in the depopulation of the high vibrational levels of CO (v>15-20), without producing significant changes in the low vibrational level populations. This is most likely due to the rapid near-resonance V-V energy transfer from highly excited CO to O_2,

$$CO(v) + O_2(0) \rightarrow CO(v-1) + O_2(1), \quad v \sim 25 \tag{7}$$
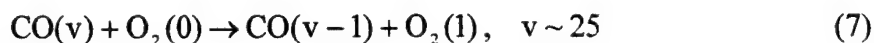
as discussed in our previous publication [15]. On the other hand, adding comparable amounts of nitric oxide to the baseline CO-Ar mixture, in addition to reducing the intensities of the high vibrational bands (v'=20-30) compared to the low bands (v'=2-5), decreases the absolute intensity of the entire spectrum (see Fig. 3). This indicates that the populations of all CO vibrational levels in the range v~2-35 are substantially reduced in the presence of NO. This is consistent with the fact that compared to CO and O_2, NO is a much faster V-T relaxer [23], so that even the low vibrational levels of CO are depopulated by the rapid V-T relaxation processes such as

$$CO(v = 1) + NO \rightarrow CO(v = 0) + NO, \tag{8}$$
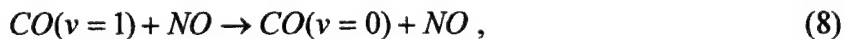
which are competing with the V-V pumping process of Eq. (1). Thus, in both these cases, the concentration of the highly vibrationally excited CO molecules in the cell is reduced. Indeed, Fig. 4 illustrates this effect showing CO vibrational distribution functions inferred from the high-resolution (0.25 cm^{-1}) CO infrared spectra in CO-Ar-O_2 mixtures. Similar behavior has been previously observed from the CO distribution function measurements in CO-Ar-NO mixtures [20]. At these experimental conditions (P=100 torr, P_{CO}=3 torr), the translational/rotational mode temperature inferred from the high-resolution (0.25 cm^{-1}) infrared spectra is in the range of T=500-700 K [8,18,20].

11

Figure 5 displays the microwave signal intensity transmitted through an optically pumped CO-Ar-NO plasma. As discussed in Section 2, the signal is modulated by a chopper providing a square wave laser input into the cell. It can be seen from Fig. 5 that turning on the laser results in the well-pronounced attenuation of the transmitted signal due to the vibrationally stimulated ionization in the cell.

Figures 6 and 7 show the average electron density in the optically pumped CO-Ar plasmas with small admixtures of O_2 and NO, respectively. One can see that in both cases adding 50-75 mtorr of oxygen or nitric oxide to the cell gases increases the electron density by about a factor 20-40, up to $n_e=(1.5-3.0)\cdot10^{11}$ cm^{-3}, compared with the baseline case with only CO and Ar in the cell, $n_e=(3-6)\cdot10^9$ cm^{-3}. This type of behavior is somewhat unexpected since oxygen is known to be an efficient electron attacher by a three-body process,

$$e^- + O_2 + M \rightarrow O_2^- + M \qquad (9)$$

with a rate of $k_{att}N=10^{-11}$ cm^3/s [24], which is likely to reduce the electron density. Further increase of the additive partial pressure up to 400-500 mtorr resulted in the gradual reduction of the electron density back to to $n_e=(1-2)\cdot10^{10}$ cm^{-3} (see Figs. 6,7). The uncertainty in the measured electron density, indicated by the error bars in Figs. 6,7 is mostly due to uncertainty in the diameter of the ionized region, estimated to be in the range between 2.0 and 3.0 mm (see Section 2). The measured maximum electron densities are consistent both with the values predicted by coupled master equation / Boltzmann equation modeling calculations [19] and inferred from RF probe conductivity measurements [20]. Similar behavior of electron density as a function of additive partial pressure was observed in $CO/N_2/O_2$ and $CO/N_2/NO$ mixtures (see Fig. 8), where the electron density also increased by about a factor of 10-20 in the presence of 25-75 mtorr O_2 or NO.

The observed sharp electron density rise with the additive partial pressure between 0 and 100 mtorr (see Figs. 6,7) occurs despite the fact that the CO vibrational level populations have been found to monotonously decrease when oxygen or nitric oxide are added to the cell (see Figs. 3,4 and Ref. [20]). This rise might be interpreted by the participation of O_2 and NO

12

molecules, which both have lower ionization potentials than CO (12.1 eV, 9.6 eV, and 14.0 eV, respectively), in the vibrationally stimulated ionization process of Eq. (4). However, measurements of the net electron production rate at these conditions turn out to be inconsistent with this suggestion. Figure 9 shows current-voltage characteristics of the Thomson discharge sustained between two DC electrodes in the CO-Ar-O_2 plasma (see Fig. 2). One can see that the saturation current of this discharge, proportional to the electron production rate in the plasma, is actually dropping with the O_2 concentration. As discussed in Section 2, in the saturation regime, the applied electric field removes as many electrons per second as are produced in the entire discharge volume. This is illustrated by the measurements of electron density in the Thomson discharge as a function of the applied voltage (see Fig. 10). The fact that the electron density in the plasma drops by about an order of magnitude as the discharge approaches saturation confirms that the saturation current indeed approaches the net electron production rate (within about 10%).

The independent measurements of the electron density and the electron production rate lead us to conclude that the simultaneous electron production rate drop and electron density rise with the additive partial pressure can be only due to the net electron removal rate reduction in the presence of small amounts of O_2 or NO (up to 100 mtorr) in the optically pumped CO-Ar and CO/N_2 plasmas.

To infer the electron removal rate in the optically pumped plasmas, we measured both the electron production rate and the electron density in the same experiment. At these conditions, the electron removal rate is essentially a sum of three processes, (i) ambipolar diffusion of charged species out of the ionized region, (ii) electron-ion recombination, and (iii) electron attachment to oxygen molecules. The time scales for the electron removal by the first two mechanisms differ by about an order of magnitude, $\tau_{diff} \sim d^2/D_a \sim 10$ msec and $\tau_{rec} \sim 1/\beta n_e \sim 0.1-1.0$ msec, where $d \sim 0.2-0.3$ cm is the diameter of the ionized region, $D_a \sim 5$ cm^2/sec is the ambipolar diffusion coefficient at P=100 torr [25], $\beta \sim 10^{-8}-10^{-7}$ cm^3/sec is the dissociative recombination coefficient, and $n_e \sim 10^{11}$ cm^{-3} is the electron density. Therefore in the present work we neglect charge species loss by diffusion. Also, O_2^- ion formation by the three-body electron attachment process of Eq. (9) is neglected. The arguments in favor of this assumption are as follows: (i) adding small amounts of O_2 to the cell gases results in an increase of the electron density in the plasma, which suggests

13

that rapid three-body elecron attachment to oxygen is mitigated to a large extent, (ii) similar results were obtained when comparable amounts of NO, which is not an efficient electron attacher, are added to the cell gases, and (iii) Raman spectroscopy measurements of the O_2 vibrational level populations (v=0-12) in the optically pumped $CO/N_2/O_2$ plasmas [15,16] show that O_2 in these mixtures becomes strongly vibrationally excited, reaching vibrational temperature of $T_v(O_2)$=2200-3600 K. In particular, the latter result suggests that strong vibrational excitation of O_2 might well stimulate detachment of electrons from the weakly bound O_2^- ions (with electron affininity of ~0.43 eV).

With the dominant electron removal process being dissociative recombination, in the steady state its rate can be directly inferred from the electron production rate per unit volume, S, and the electron density, n_e,

$$\beta = \frac{S}{n_e^2} \qquad (10)$$

Figures 11, 12 show the results of simultaneous measurements of the electron production rate inferred from the Thomson discharge saturation current and the electron density in the optically pumped $CO-Ar-O_2$ and in $CO-Ar-NO$ mixtures, respectively. From Fig. 11, one can see that the electron production rate drops with the O_2 partial pressure by about a factor 5, while electron density increases by approximately a factor of 30. Similarly, Fig. 12 shows that the electron production rate weakly changes (approximately within a factor of 2) depending on the NO partial pressure, while the electron density increases with the NO partial pressure almost by a factor of 50. Figure 13 shows the electron-ion recombination rate coefficients inferred from these data using Eq. (10). It can be seen that the recombination rate in $CO-Ar-O_2$ and in $CO-Ar-NO$ mixtures decreases by about three orders of magnitude, from its baseline value of β=2·10^{-5} cm^3/sec (with no additives in the cell) to β~1.5·10^{-8} cm^3/sec with 50-100 mtorr oxygen or nitric oxide added (see Fig. 13). Interestingly, the electron-ion recombination coefficients in both mixtures (with 50-100 mtorr of O_2 or NO added) are very close, which shows that the contribution of electron attachment to oxygen at these conditions is negligible. Similarly, the recombination rate in $CO-N_2-O_2$ and $CO-N_2-NO$ mixtures decreases by about two orders of

14

magnitude, from $\beta = 5 \cdot 10^{-5}$ cm^3/sec with no additives in the cell to $\beta \sim (2-3) \cdot 10^{-7}$ cm^3/sec with 75-100 mtorr O_2 or NO added (see Fig. 14). Here again the difference between the recombination coefficients in O_2 and NO doped CO-N_2 mixtures is small.

Thus, adding small amounts (~0.05-0.1%) of O_2 and NO to the optically pumped CO-Ar and CO-N_2 plasmas allows control and considerable increase of the electron density (from $n_e = (6-8) \cdot 10^9$ cm^{-3} up to $n_e = (1-3) \cdot 10^{11}$ cm^{-3}) by reducing the electron-ion recombination rate (by up to 2-3 orders of magnitude). This result is consistent with the electron density and recombination rate inference from the RF probe plasma conductivity measurements [20].

Quantitative interpretation of the observed effect, i.e. identifying specific kinetic processes responsible for the electron recombination rate reduction, requires knowledge of the ion composition of the optically pumped plasma. However, a qualitative scenario can be suggested based on previous ion composition measurements in a glow discharge in CO-Ar-O_2 mixtures using in situ ion mass spectrometry [26]. The mass spectra taken in CO/Ar mixtures without oxygen show that the dominant ions in the discharge are dimer ions $(CO)_2^+$ and cluster ions of the general form $C_n(CO)_2^+$, n=1-15. However, adding a few tens of millitorr of O_2 to these gas mixtures resulted in nearly complete disappearance of these ions and their replacement by the O_2^+ ions. Note that the electron-ion dissociative recombination rate of the dimer $(CO)_2^+$ ion, $\beta = 2 \cdot 10^{-6}$ cm^3/s [27], greatly exceeds the rate of recombination of the monomer O_2^+ ion, $\beta = (3-5) \cdot 10^{-8}$ cm^3/s at the electron temperature of $T_e \sim 0.3$-0.5 eV [21]. The recombination rate of the large carbon cluster ions can possibly be even higher. A similar process, i.e. destruction of the rapidly recombining carbon-based cluster ions and their replacement by the slowly recombining monomer ions, such as O_2^+ and NO^+, might also occur in optically pumped plasmas. This might occur in rapid exothermic ion-molecule reactions, such as

$$(CO)_2^+ + O_2 \rightarrow CO + CO + O_2^+ \tag{11}$$

$$(CO)_2^+ + NO \rightarrow CO + CO + NO^+ \tag{12}$$
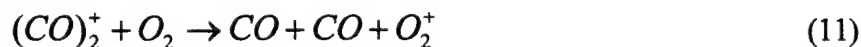
(both O_2 and NO have much lower ionization potential than CO). In addition, rapid resonance charge transfer from the vibrationally excited $O_2(v)$ and $NO(v)$ molecules to O_2^+ and NO^+ ions can produce vibrational excitation of these ions, which may further reduce the dissociative recombination rate [28]. More information on the detailed kinetic mechanism of the observed effect is expected to be obtained from ion mass spectrometry measurements in the optically pumped plasmas.

The observed effects also open a possibility of additional energy coupling to the vibrational modes of diatomic molecules in the optically pumped plasmas (such as CO and N_2). This process, which requires some initial ionization of the gas mixture, relies on free electron heating by an external sub-breakdown RF field with subsequent vibrational excitation by electron impact. Indeed, if the reduced electric field is in the range $E/N=(1-3)\cdot10^{-16}$ $V\cdot cm^2$, which is about an order of magnitude lower than the breakdown threshold, up to 90% of the input electrical power coupled to the plasma goes to excitation of vibrational modes of molecules, such as CO and N_2 [29-31]. The use of this effect would allow sustaining large volumes of strongly nonequilibrium optically pumped gases without using a high-power pump laser.

4. Summary

Electron production rate and electron density in cold optically pumped CO-Ar and CO-N_2 plasmas in the presence of small amounts of O_2 and NO have been measured using a Thomson discharge probe and microwave attenuation. Nonequilibrium ionization in the plasmas is produced by an associative ionization mechanism in collisions of highly vibrationally excited CO molecules. It is shown that adding small amounts of O_2 or NO (50-100 mtorr) to the baseline gas mixtures at P=100 torr results in an increase of the electron density by up to a factor of 20-40 (from $n_e < 10^{10}$ cm^{-3} to $n_e = (1.5-3.0)\cdot10^{11}$ cm^{-3}). This occurs while the electron production rate either decreases (as in the presence of O_2) or remains nearly constant within a factor of 2 (as in the presence of NO). It is also shown that the electron-ion recombination rates inferred from these measurements decrease by 2 to 3 orders of magnitude compared to their baseline values (with no additives in the cell), down to $\beta \cong 1.5\cdot10^{-8}$ cm^3/sec with 50-100 mtorr of oxygen or nitric oxide added to the baseline CO-Ar mixture, or $\beta \cong (2-3)\cdot10^{-7}$ cm^3/sec with 75-100 mtorr of O_2 or NO added to the baseline CO-N_2 mixture. The overall electron-ion removal rates in the presence

of equal amounts of O_2 or NO additives turn out to be very close, which shows that the effect of electron attachment to oxygen at these conditions is negligible. These results suggest a novel method of electron density control in cold laser-sustained steady-state plasmas and open a possibility of sustaining of stable high-pressure nonequilibrium plasmas at high electron densities and low plasma power budget.

5. References

1. J. W. Rich, "Relaxation of Molecules Exchanging Vibrational Energy", in "Applied Atomic Collision Physics", vol. 3, "Gas Lasers", ed. E.W. McDaniel and W.L. Nighan, Academic Press, New York, 1982, pp. 99-1407

2. B.F. Gordiets, V.A. Osipov, and L.A. Shelepin, "Kinetic Processes in Gases and Molecular Lasers", Gordon and Breach, London, 1988

3. J.W. Rich, R.C. Bergman, and M.J. Williams, Measurement of Kinetic Rates for Carbon Monoxide Laser Systems, Final Contract report AFOSR F49620-77-C-0020 (November 1979)

4. J.W. Rich and R.C. Bergman, Chem. Phys., Vol. 44, 1979, p. 53

5. R.L. DeLeon and J.W. Rich, Chem. Phys., vol. 107, 1986, p. 283

6. C. Flament, T. George, K.A. Meister, J.C. Tufts, J.W. Rich, V.V. Subramaniam, J.-P. Martin, B. Piar, and M.-Y. Perrin, Chem. Phys., vol. 163, 1992, p. 241

7. H.L. Wallaart, B. Piar, M.Y. Perrin, and J.P. Martin, Chem. Phys., Vol. 196, 1995, p. 149

8. E. Plönjes, P. Palm, A.P. Chernukho, I.V. Adamovich, and J.W. Rich, Chem. Phys., vol. 256, 2000, p. 315

9. H. Dünnwald, E. Siegel, W. Urban, J.W. Rich, G.F. Homicz, and M.J. Williams, Chem. Phys., Vol. 94, 1985, p. 195

10. S. Saupe, I. Adamovich, M.J. Grassi, and J.W. Rich, Chem. Phys., vol. 174, 1993, p. 219

11. D.S. Anex and G.E. Ewing, J. Phys. Chem., Vol. 90, p. 1604, 1986

12. R.S. Disselkamp and G.E. Ewing, J. Phys. Chem., Vol. 93, p. 6334, 1989

13. J.P. Galaup, J.Y. Harbec, R. Charneau, and H. Dubost, Chem. Phys. Lett., Vol. 120, 1985, p. 188

14. I. Hadj Bachir, R. Charneau, and H. Dubost, Chem. Phys., Vol. 177, 1993, p. 675

15. E. Plönjes, P. Palm, W. Lee, M. D. Chidley, I.V. Adamovich, W.R. Lempert, and J. W. Rich, Chem. Phys., vol. 260, 2000, p. 353

16. W. Lee, I.V. Adamovich, and W.R. Lempert, "Optical Pumping Studies of Vibrational Energy Transfer in High-Pressure Diatomic Gases", Journal of Chemical Physics, vol. 114, 2001, p. 1178

17. L.S. Polak, P.A. Sergeev, and D.I. Slovetskii, Sov. High Temperature Physics, Vol. 15, 1977, p. 15

18. I. Adamovich, S. Saupe, M.J. Grassi, O. Schulz, S. Macheret, and J.W. Rich, Chem. Phys., vol. 173, 1993, p. 491

19. I.V. Adamovich and J.W. Rich, J. Phys. D: Appl. Phys., vol. 30, 1997, p. 1741

20. E. Plönjes, P. Palm, I.V. Adamovich, and J.W. Rich, J. Phys. D: Appl. Phys., vol. 33, 2000, p. 2049

21. Raizer, Y.P., "Gas Discharge Physics", Springer-Verlag, Berlin, 1991

22. Billing, G.D., "Vibration-Vibration and Vibration-Translation Energy Transfer, Including Multiquantum Transitions in Atom-Diatom and Diatom-Diatom Collisions", Nonequilibrium Vibrational Kinetics, Springer-Verlag, Berlin, 1986, Chap. 4, pp. 85-111

23. S. Saupe, I. Adamovich, M.J. Grassi, and J.W. Rich, Chem. Phys., vol. 174, 1993, p. 219

24. H.S.W. Massey, E.H.S. Burhop, and H.B. Gilbody, "Electronic and Ionic Impact Phenomena", Vol. III, "Slow Collisions of Heavy Particles", Oxford, Clarendon Press, 1971

25. E.W. McDaniel, "Collision Phenomena in Ionized Gases", Wiley, New York, 1964

26. Y. Kaufman, P. Avivi, F.Dothan, H. Keren, J. Malinowitz, J. Chem. Phys., Vol. 72, 1980, p. 2606

27. R. Johnsen, "Recombination of Cluster Ions", in B.R. Rowe et al. (eds.), "Dissociative Recombination", Plenum, New York, 1993

28. T. Mostefaoui, S. Laube, G. Gautier, C. rebrion-Rowe, B.R. Rowe, and J.B.A. Mitchell, J. Phys. B: At. Mol. Opt. Phys., Vol. 32, 1999, p. 5247

29. N.L. Aleksandrov, A.M. Konchakov, and E.E. Son, Sov. J. Plasma Physics, Vol. 4, 1978, p. 169

30. N.L. Aleksandrov, A.M. Konchakov, and E.E. Son, Sov. Phys. Tech. Phys., Vol. 49, 1979, p. 661

31. N.L. Aleksandrov, F.I. Vysikailo, R.Sh. Islamov, I.V. Kochetov, A.P. Napartovich, and V.G. Pevgov, Sov. High Temp. Phys., Vol. 19, 1981, p. 22
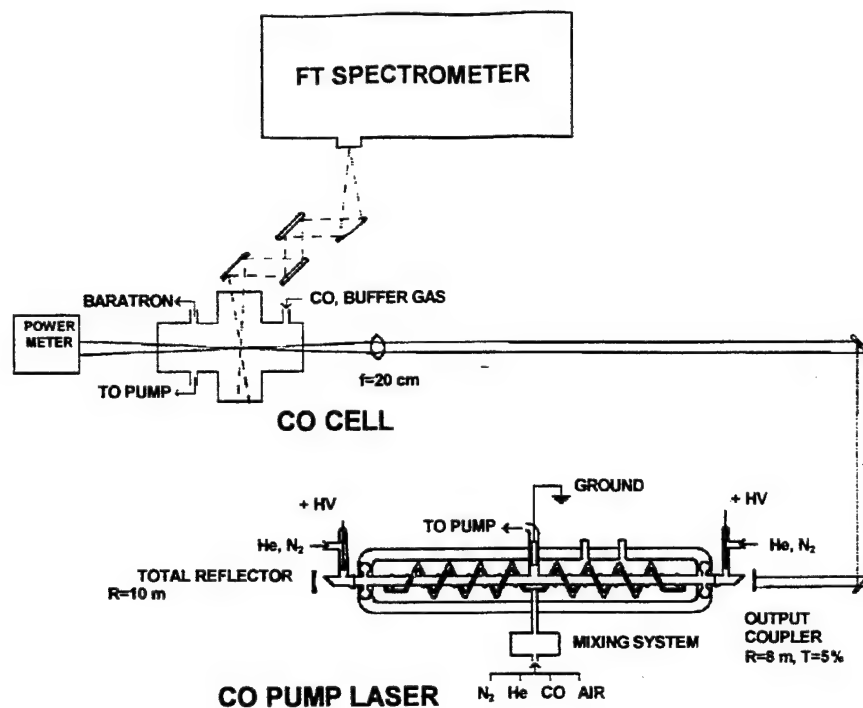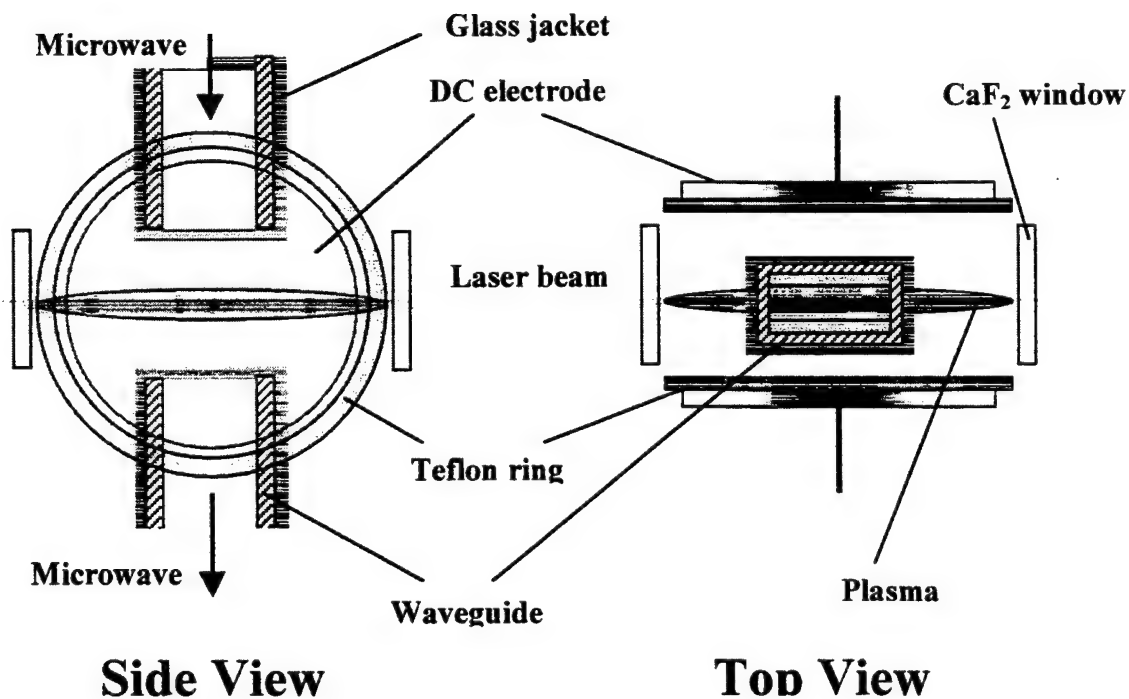
Figure 1. Schematic of the experimental setup

Figure 2. Schematic of the Thomson discharge electrode and microwave waveguide arrangement in the absorption cell
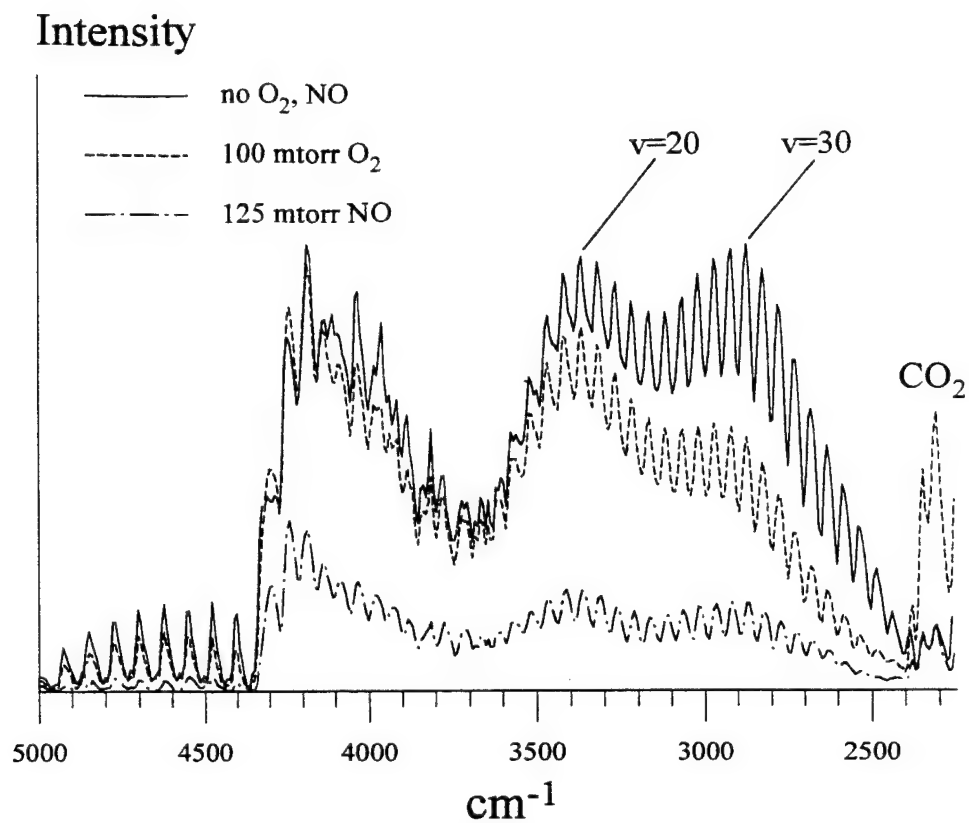
Figure 3. First overtone CO emission spectra in optically pumped CO-Ar mixtures with small amounts of O_2 and NO added. P_{CO}=3 torr, P_{Ar}=100 torr
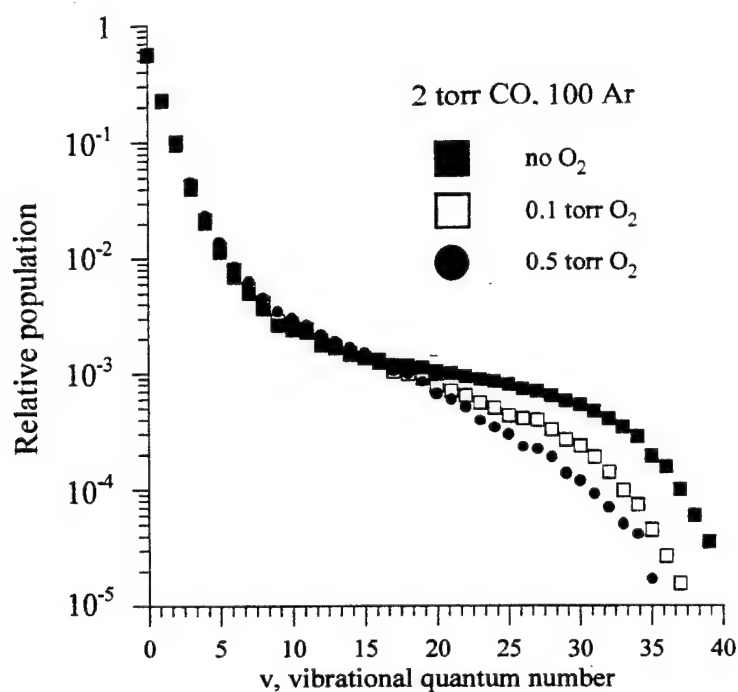
Figure 4. CO vibrational level populations for the conditions similar to those of Fig. 3. P_{CO}=2 torr, P_{Ar}=100 torr
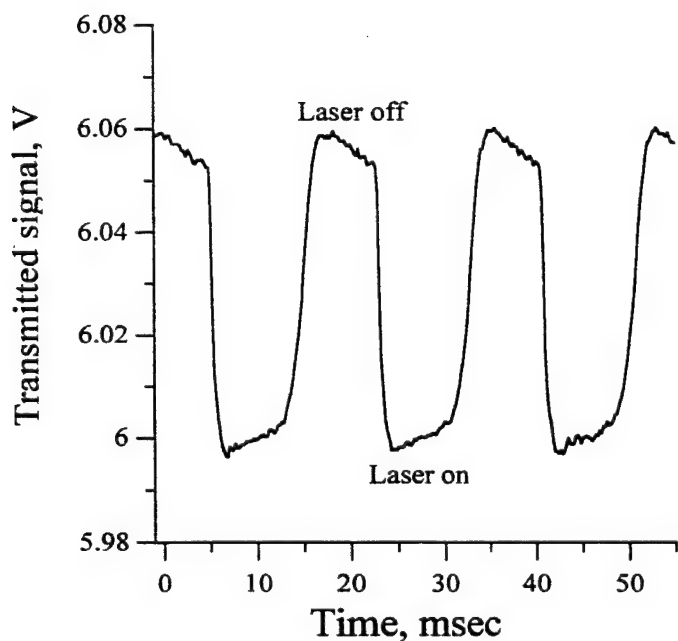
Figure 5. Transmitted microwave signal with the pump CO laser turned on and off. P_{CO}=3 torr, P_{Ar}=100 torr, P_{NO}=50 mtorr
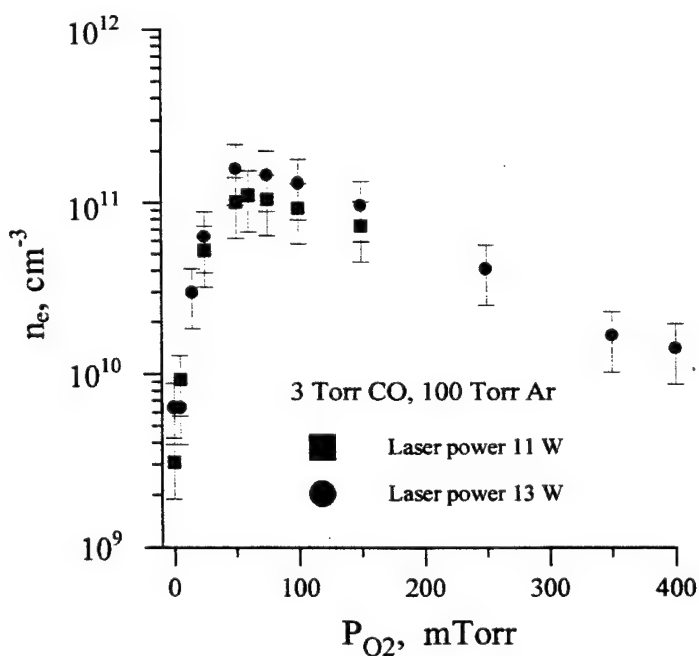
Figure 6. Electron density in CO-Ar-O_2 mixtures as a function of the O_2 partial pressure
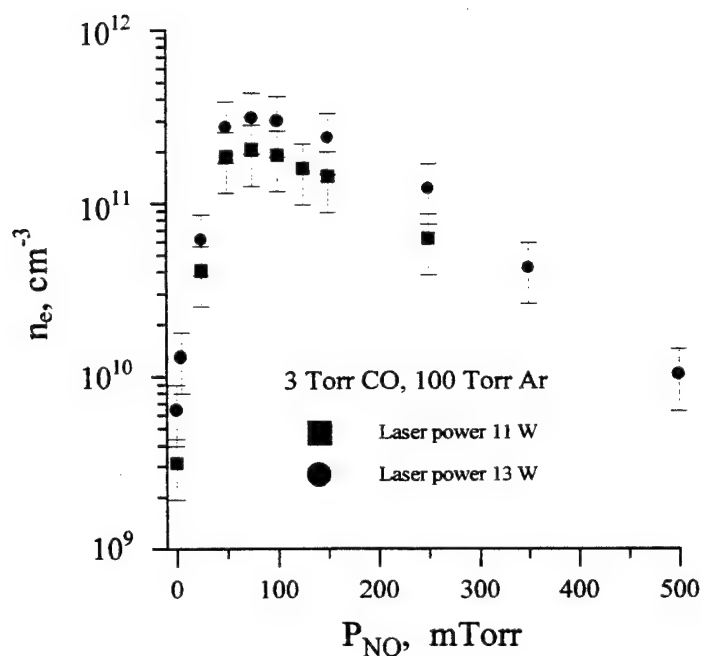
Figure 7. Electron density in CO-Ar-NO mixtures as a function of the NO partial pressure
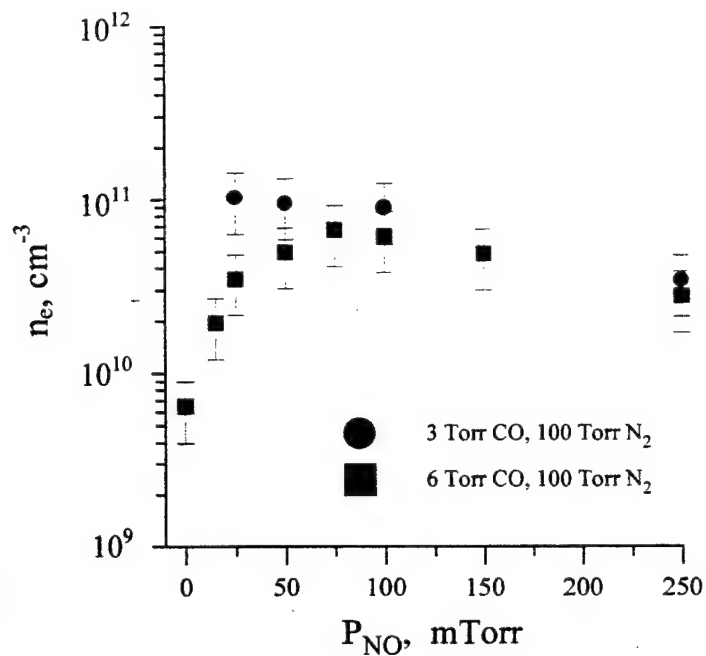
Figure 8. Electron density in CO-N_2 mixtures as a function of the NO partial pressure
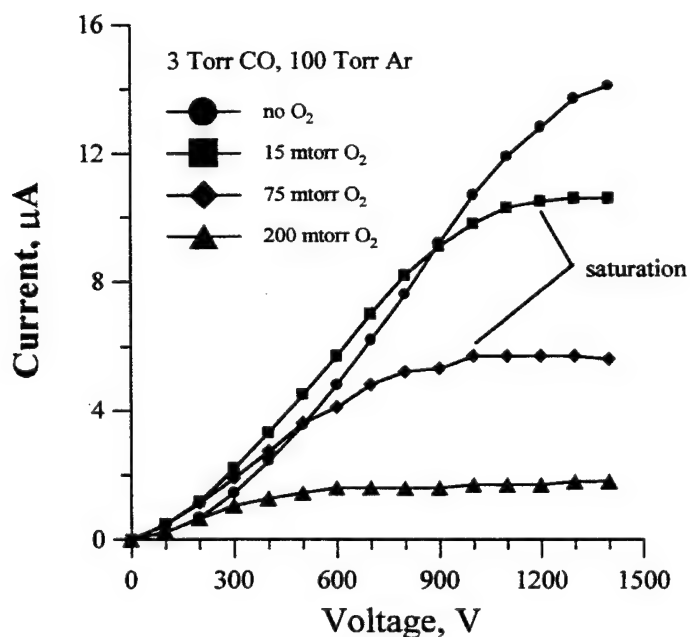

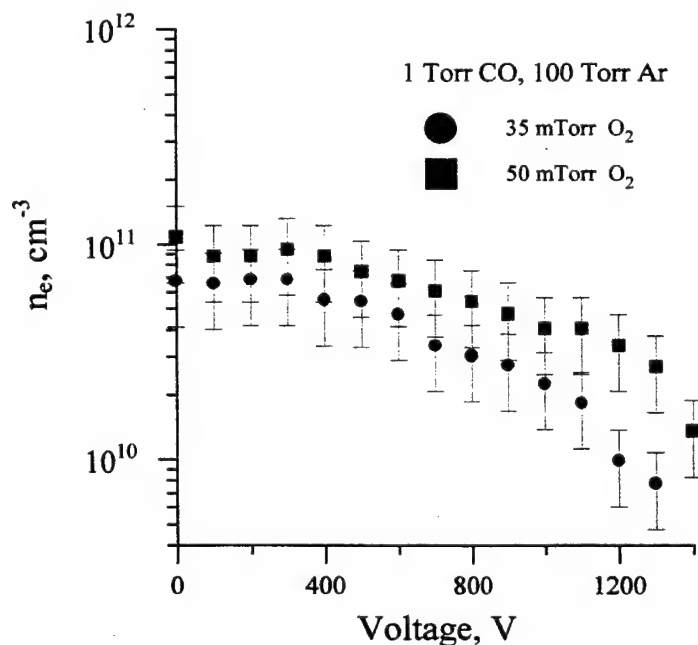Figure 9. Saturation of the Thomson discharge in the optically pumped CO-Ar-O_2 mixtures

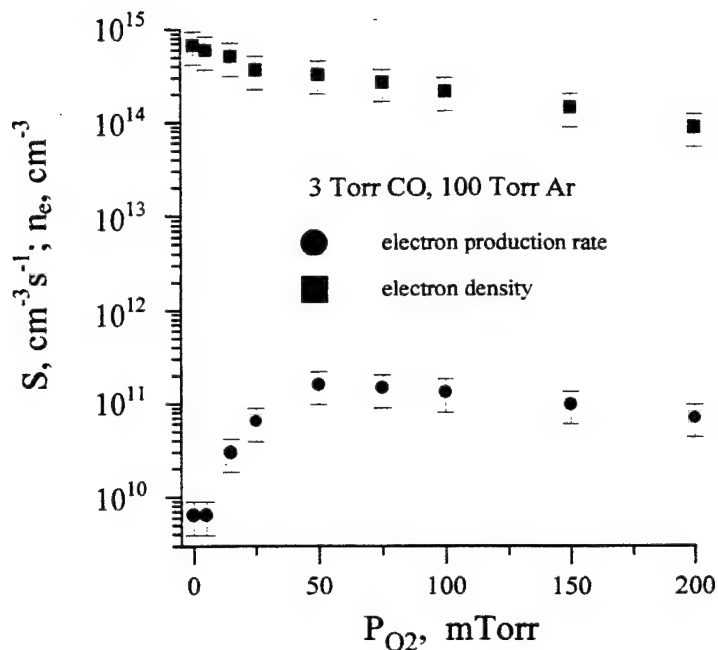Figure 10. Electron removal by the applied field in the Thomson discharge approaching saturation.

Figure 11. Electron production rate and electron density in CO-Ar-O_2 mixtures as a function of O_2 partial pressure.
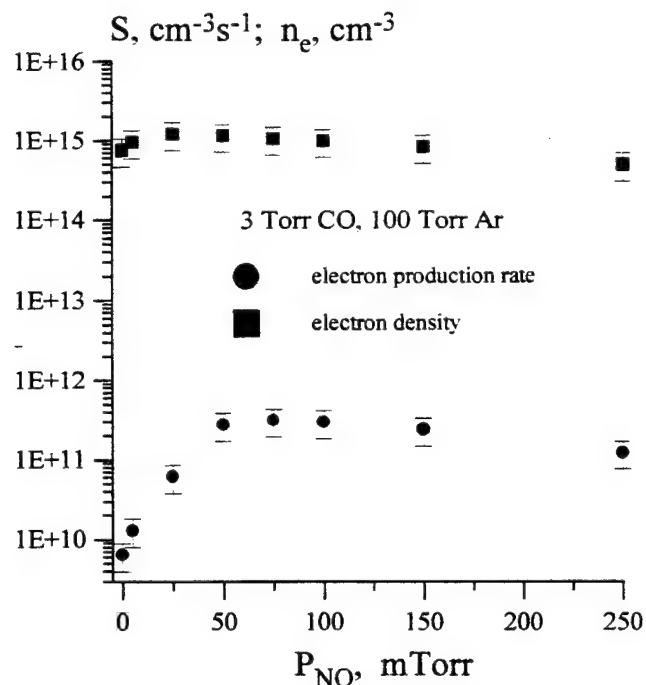

Figure 12 Electron production rate and electron density in CO-Ar-NO mixtures as a function of NO partial pressure
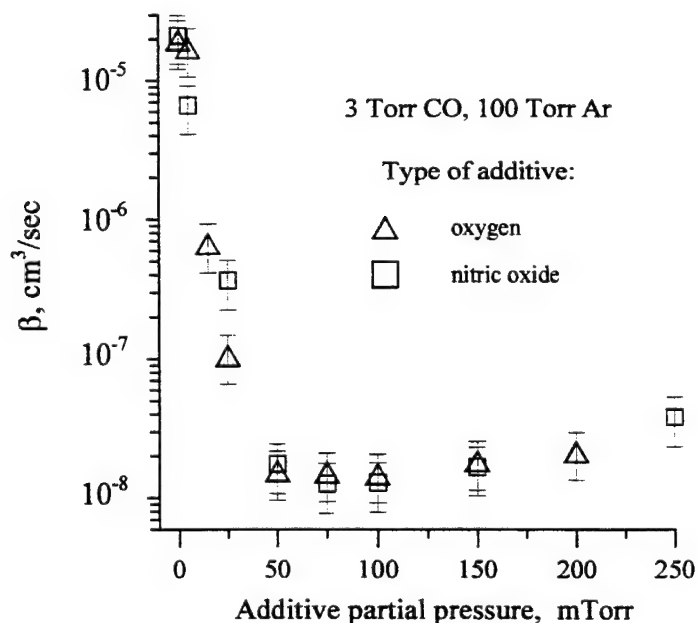

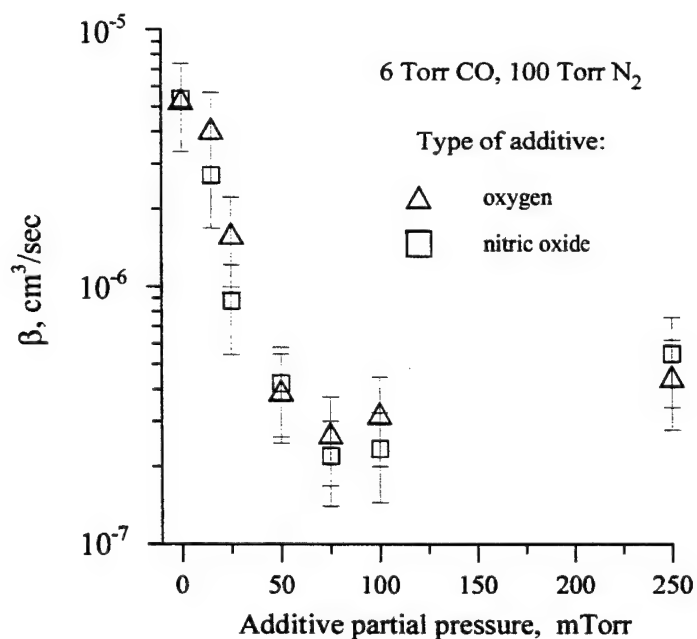Figure 13. Electron recombination rate coefficient in CO-Ar mixtures as a function of additive partial pressure

Figure 14. Electron recombination rate coefficient in CO-N_2 mixtures as a function of additive partial pressure

CHAPTER II

ELECTRON-MEDIATED VIBRATION-ELECTRONIC (V-E) ENERGY TRANSFER IN OPTICALLY PUMPED PLASMAS

1. Introduction

Collisional relaxation of long-lived vibrational and metastable electronic states of molecules is a fundamental problem in plasma physics and chemistry [1]. In particular, energy transfer from the vibrational to the electronic energy mode (V-E energy transfer) has been studied extensively in highly vibrationally excited CO produced by vibration-to-vibration (V-V) pumping [2-10]. Lower vibrational states of CO, $v \leq 10$, can be populated either by electron impact excitation in electric discharges or by direct resonance absorption of CO pump laser radiation. Rapid redistribution of population by V-V exchange processes [11],

$$CO(v) + CO(w) \rightarrow CO(v+1) + CO(w-1), \quad v > w. \tag{1}$$

then continues to populate higher vibrational levels above $v \sim 10$, which are not directly coupled to the initial excitation process. However, population of levels higher than $v=42$ has never been observed. Since vibrational level $v=41$ of the ground electronic state, $X^1\Sigma$, is nearly isoenergetic with the vibrational level $v=1$ of the $A^1\Pi$ excited electronic state [3], it was suggested that $CO(A^1\Pi)$ may be populated by near-resonance vibration-to-electronic (V-E) energy transfer from high vibrational levels of the ground electronic state,

$$CO(X^1\Sigma, v \sim 40) + CO \rightarrow CO(A^1\Pi, v \sim 0) + CO, \tag{2}$$
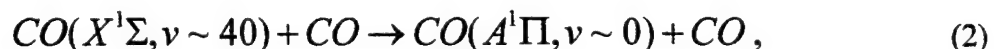
with subsequent rapid decay by emission of UV radiation,

$$CO(A^1\Pi) \rightarrow CO(X^1\Sigma) + h\nu. \tag{3}$$
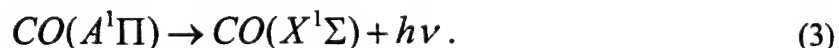
Previous time-resolved measurements of UV radiation in optically pumped CO plasmas [2] support this mechanism since the rise time for the $CO(A^1\Pi, v=1)$ population after the CO pump

laser was turned on was approximately equal to that of the $CO(X^1\Sigma, v=35)$ vibrational level population. In addition, a strong dependence of the $CO(A^1\Pi)$ population on the population of high vibrational levels of the ground electronic state, which can be controlled by fast vibration-to-translation (V-T) relaxers such as helium, has also been observed in steady state experiments [4]. However, a more detailed analysis of these experiments does not support the direct resonant mechanism of Eq. (2), but instead suggests that the energy transfer process involves additional intermediate stages. For example, Wallaart et al. [4] propose a more complex mechanism involving intermediate energy transfer to CO triplet states. A similar direct energy transfer process was also proposed for V-E transfer between vibrational level v~25 and the $CO(a^3\square)$ state in electric discharge plasmas [5]. However, laser magnetic resonance spectroscopy measurements in optically pumped CO-Ar plasmas did not show any detectable population of the $CO(a^3\square)$ state [6].

Previous experiments in the Nonequilibrium Thermodynamics Group at the Ohio State University showed that energy transfer occurs in superelastic collisions between highly vibrationally excited CO molecules and low energy electrons [12, 13]. The present paper presents results indicating that these low-energy electrons also mediate V-E energy transfer in strongly vibrationally excited CO. The kinetics of ionization in CO laser pumped, low-temperature, strongly nonequilibrium CO-Ar and CO-N_2 plasmas have been extensively studied [12-17]. Ionization these plasmas does not require the presence of an electric field and occurs by an associative ionization mechanism, in collisions of two highly vibrationally excited molecules,

$$CO(X^1\Sigma, v) + CO(X^1\Sigma, w) \rightarrow (CO)_2^+ + e^-$$
$$E_v + E_w > E_{ion} \quad , \qquad\qquad (4)$$
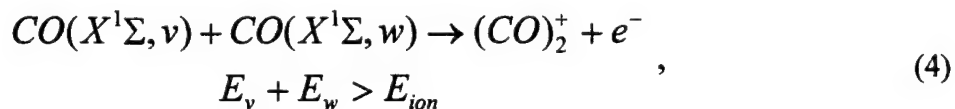
if the total vibrational energy of the reactants, $E_v + E_w$, exceeds the ionization energy of $E_{ion} \cong 14$ eV [12-14]. The mechanism of Eq. (4) creates electrons with rather low initial energies. Both the electron production rate per unit volume, up to $S=2.0 \cdot 10^{15}$ electrons$\cdot$cm^{-3}sec^{-1}, and the associative ionization rate coefficient, $k_{ion}=(1.1-1.8) \cdot 10^{-13}$ cm^{3}sec^{-1}, have been determined from measurements of the saturation current of a non-self-sustained Thomson discharge [12-14]. This

discharge was initiated between two circular probe electrodes placed close to the laser-sustained plasma region. At saturation, the number of electrons removed from the plasma by a weak (sub-breakdown) electric field applied to the electrodes is approximately equal to the rate of electron production, while the electron density in the plasma is much lower than in the absence of the field [12,16]. Basically, this method allows nearly complete removal of electrons from the plasma.

The electron density in the optically pumped CO-Ar and CO-N_2 plasmas, with and without O_2 and NO additives, has been measured by microwave attenuation [16]. These measurements show that the electron density in both CO-Ar and CO-N_2 plasmas without additives is low, $n_e < 10^{10}$ cm^{-3} at a total number density of $N=1.6 \cdot 10^{18}$ cm^{-3} and at an electron production rate of up to $S=0.8 \cdot 10^{15}$ electrons cm^{-3}sec^{-1} [16]. At these conditions, the rate of electron-ion recombination inferred from the electron production rate and the electron density, which are simultaneously measured, is very rapid, $\beta = S/n_e^2 \sim 10^{-5}$ cm^{3}sec^{-1} [15, 16]. However, adding small amounts (up to 0.1%) of either O_2 or NO to the plasma resulted in an electron density increase by a factor of 30-50, up to $n_e=(1-3) \cdot 10^{11}$ cm^{-3} [16]. Remarkably, this occurred while the electron production rate S decreased somewhat, primarily due to the faster V-T relaxation of high vibrational levels of CO by collisions with the additive species [14]. This demonstrates that the electron-ion recombination rate in the presence of small amounts of oxygen or nitric oxide is dramatically reduced, down to $\beta=(1-2) \cdot 10^{-8}$ cm^{3}sec^{-1} in CO-Ar plasmas [15, 16] and $\beta=(2-3) \cdot 10^{-7}$ cm^{3}sec^{-1} in CO-N_2 plasmas [16]. The reduction of the electron-ion recombination rate observed in the presence of small amounts of oxygen or nitric oxide is consistent with the previous results of *in situ* ion composition measurements in glow discharges in CO-Ar-O_2 mixtures [18]. These experiments showed that adding small amounts of O_2 (<1%) to the baseline CO-Ar glow discharge plasma results in replacing of rapidly recombining cluster ions $C_n(CO)_2^+$, n=1-15 by slowly recombining O_2^+ ions (see discussion in [16]). A similar process, i.e. destruction of the rapidly recombining carbon-based cluster ions and their replacement by slowly recombining monomer ions, such as O_2^+ and NO^+, is probably responsible for the observed electron recombination rate reduction and the consequent electron density rise in the optically pumped plasmas.

Finally, our preliminary experiments [12] also demonstrated that removal of electrons from the plasma using a saturated Thomson discharge is accompanied by a noticeable rise of the CO vibrational level populations, v=19-37 (up to about a factor of 2). This behavior is consistent with the depopulation of the high vibrational levels of CO by superelastic collisions with electrons,

$$CO(X^1\Sigma, v) + e^-(\varepsilon) \rightarrow CO(X^1\Sigma, v - \Delta v) + e^-(\varepsilon + \Delta\varepsilon), \qquad (5)$$
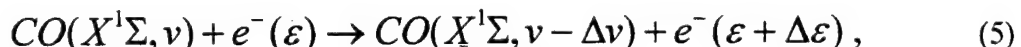
whereas the removal of electrons inhibits this process [13]. The process of Eq. (5), which is known to efficiently transfer up to at least 10 vibrational quanta of CO [19], may substantially increase the energy of electrons formed by associative ionization, Eq. (4). Such electron heating by superelastic collisions can result in populating excited electronic states by electron impact collisions with vibrationally excited ground state CO molecules, such as

$$CO(X^1\Sigma, v) + e^-(\varepsilon + \Delta\varepsilon) \rightarrow CO(A^1\Pi, w) + e^-(\varepsilon). \qquad (6)$$

Similar electron impact excitation can also occur with other vibrationally excited species present in the plasma. The primary objective of the present paper is to study the feasibility of two-stage, electron-mediated vibrational-to-electronic (V-E) energy transfer in CO, given by Eqs. (5) and (6). Optically pumped plasmas present a clean environment for studying such energy transfer processes. Unlike self-sustained electric discharge plasmas, the electron density in optically pumped plasmas can be controlled nearly independently of the CO vibrational level populations, as discussed above.

2. Experimental

The overall schematic of the experimental setup used for our studies of the V-E energy transfer in optically pumped plasmas is shown in Fig. 1. A c.w. carbon monoxide laser is used to excite CO/Ar and CO/N$_2$ gas mixtures, with or without additives such as O$_2$ or NO, slowly flowing through the Pyrex glass optical absorption cell shown. The liquid nitrogen cooled CO laser [10] is designed in collaboration with the University of Bonn [20] and fabricated at Ohio

State. It produces a substantial fraction of its power output on the $v = 1 \rightarrow 0$ fundamental band component in the infrared. In the present experiments, the laser is typically operated at 18-20 W c.w. broadband power on the lowest ten vibrational bands. The output on the lowest bands ($1 \rightarrow 0$ and $2 \rightarrow 1$) is necessary to start the absorption process in cold CO (initially at 300 K) in the cell. The laser beam is focused to a focal area of ~1 mm diameter to increase the power loading per CO molecule, producing an excited region 10-20 cm long and 2-3 mm in diameter.

The lower vibrational states of CO, $v \leq 10$, are populated by direct resonance absorption of the pump laser radiation with subsequent population of high vibrational levels by V-V pumping (see Eq. (1)). The large heat capacity of the Ar and N_2 diluents, as well as conductive and convective cooling of the gas flow, enable control of the translational/rotational mode temperature in the cell. At steady-state conditions, when the average vibrational mode energy of the CO would correspond to a few thousand degrees Kelvin, the temperature never rises above a few hundred degrees. Thus a strong disequipartition of energy can be maintained in the cell, characterized by a very high vibrational mode energy and a low translational/rotational mode temperature. As shown in Fig. 1, the population of vibrational states of CO in the cell is monitored using a Bruker IFS 66 Fourier transform infrared spectrometer, which records spontaneous emission from the CO fundamental, first and second overtone bands through a CaF_2 window on the side of the cell. The infrared spectra are taken at both high (0.25 cm^{-1}) and low (8 cm^{-1}) resolution. Electronically excited radiating molecules are simultaneously detected by an Acton Research VH-504 UV monochromator with a resolution of 0.1 nm through a MgF_2 window on the opposite side of the cell. In the present study, the monochromator was not evacuated.

Ionization of highly excited CO molecules in the cell occurs by the associative ionization mechanism of Eq. (4). The electrons can be removed from the optically pumped plasma by means of a saturated DC Thomson discharge sustained between two 3 cm diameter electrodes placed 10-20 mm apart, as shown in Fig. 2. Two infrared transparent CaF_2 windows placed upstream and downstream of the electrodes (see Fig. 2) isolate the plasma generated in the interelectrode space from the plasma sustained in the remainder of the cell. This significantly reduces the charged species drift and diffusion into the interelectrode space and allows reaching

a well-pronounced current saturation [16]. As discussed in Section 1, at saturation, the number of electrons removed from the plasma by an electric field applied to the electrodes is approximately equal to the rate of electron production, while the electron density in the plasma is much lower than in the absence of the field [12, 16]. The applied voltage was deliberately kept sufficiently low to preclude electron impact ionization. Thus, in the present experiments the Thomson discharge is primarily used for electron removal from the optically pumped plasma. The electron density in the optically pumped plasma is independently measured by attenuation of $\nu=10$ GHz microwave radiation using two waveguides placed 1 cm apart as shown in Fig. 2. Both the Thomson discharge and the microwave apparatus used in the present experiments are discussed in greater detail in Ref. [16].

The experiments were carried out in CO-Ar and CO-N_2 mixtures at pressures of P=100-500 Torr. The CO fraction in the gas mixtures was typically 1%. To add controlled small amounts (on the order of a hundred mTorr) of O_2 and NO to the cell, they were both used diluted in argon at the 5% and 10% level, respectively. The resultant O_2/Ar and NO/Ar gas mixtures have been added to the baseline CO/Ar and CO/N_2 gas mixtures.

3. Kinetic model

The kinetic model used incorporates a coupled master equation for the CO and N_2 vibrational level populations (vibrational distribution function, VDF) and the Boltzmann equation for the symmetric part of the electron energy distribution function (EEDF). The explicit form of the master equation and Boltzmann equation used in the present calculations can be found in [10, 21-23]. The model takes into account CO vibrational excitation by resonance absorption of CO laser radiation, vibration-to-translation (V-T) relaxation and vibration-to-vibration (V-V) exchange in collisions between CO, N_2, and Ar, as well as associative ionization of vibrationally excited CO molecules. For the V-V and V-T processes the same rates are taken as in [10, 21, 22]. The rates of associative ionization and electron-ion recombination used in the calculations have been measured in previous optical pumping experiments at Ohio State [14-16]. The collision integral in the Boltzmann equation incorporates elastic scattering of electrons on

CO and N_2 molecules and Ar atoms, electron impact vibrational excitation / superelastic collisions between molecules and electrons,

$$AB(X^1\Sigma, v) + e^-(\varepsilon) \leftrightarrow AB(X^1\Sigma, w) + e^-(\varepsilon')$$
$$0 \le v, w \le 40, \quad |v - w| \le 10 \qquad (7)$$
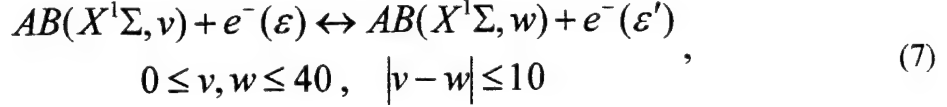
as well as electronic excitation and electron impact ionization of CO, N_2, and Ar. In Eq. (7), AB represents a CO or N_2 molecule, v and w are vibrational quantum numbers, and ε and ε' are the electron energies. Cross sections for the processes of Eq. (7), $\sigma_{v \to w}(\varepsilon)$, have been evaluated using the semi-empirical theory of Ref. [24] and adjusted to fit the few available experimental cross sections, $\sigma_{0 \to w}(\varepsilon)$ (see [25, 26] for more details). The rest of the elastic and inelastic electron scattering cross sections are taken from [27- 29]. The present kinetic model has been validated and extensively used for modeling of various optical pumping experiments [10, 13, 21, 22].

4. Results and Discussion

Figures 3 and 4, taken from Ref. [16], show the current-voltage characteristics of a Thomson discharge between the probe electrodes as well as the electron density in the plasma as a function of the applied voltage. It can be seen that as the Thomson discharge approaches saturation, the electron density is reduced approximately by an order of magnitude, i.e. the electrons are indeed removed by the applied field. Figure 5 shows low-resolution (8 cm^{-1}) CO first overtone emission spectra in an optically pumped CO/Ar=1/100 mixture (with 50 mTorr O_2 additive) at P=100 Torr, with and without a voltage applied to the Thomson discharge electrodes. Oxygen was added to the cell gases to achieve a higher electron density of up to $n_e \sim 10^{11}$ cm^{-3}, as discussed in Section 1. It can be seen that applying a near-saturation voltage to the electrodes (U_s=500 V, I_s=4.6 μA), to remove electrons from the optically pumped gas mixture, results in a substantial increase of the infrared emission intensity from high vibrational levels of CO($X^1\Sigma$). This effect has been first reported in our earlier publication [13]. Figure 6 shows the CO vibrational distribution functions (VDFs) for these conditions, inferred from high-resolution

31

(0.25 cm^{-1}) infrared spectra using a standard technique [30]. One can see that the removal of electrons from the plasma increases the populations of vibrational levels v>15. The populations of levels v=30-38 increase by a factor of 2 to 5. Fig. 7 shows that at the same time the intensity of the UV radiation from the CO 4th positive band system (A$^1\Pi \rightarrow$X$^1\Sigma$) in the absence of electrons is reduced by more than a factor of 2.

These results, i.e. the reduction of the 4th positive system radiation intensity while the high vibrational level populations of the ground electronic state of CO are increased (see Figs. 6, 7) show that the direct V-E energy transfer channel of Eq. (2) is unlikely. This is hardly surprising, since the near-resonance process of Eq. (2), which is essentially Franck-Condon forbidden [3], implies transfer of about 8 eV of energy from the nuclear motion to the electron motion, on a relatively long time scale (of the order of molecular vibrations). Rather, it appears that it is the removal of electrons from the plasma that results in both increase of the high vibrational level populations of CO(X$^1\Sigma$) and reduction of the CO 4th positive system UV radiation intensity. Indeed, without O$_2$ additive present in the cell, when the electron density in the plasma is very low (n$_e$<10^{10} cm^{-3} [16]), applying a saturation voltage to the Thomson discharge electrodes produces only insignificant changes in both CO vibrational level populations and the UV signal intensity. This indicates that the V-E energy transfer CO(X$^1\Sigma \rightarrow$A$^1\Pi$) is indeed mediated by the presence of electrons, as described by Eqs. (5) and (6).
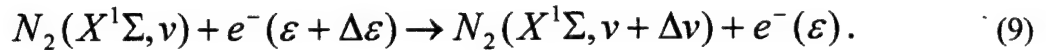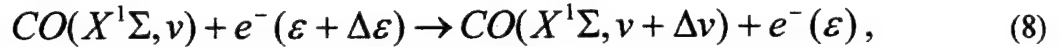
This result is consistent with previous quenching experiments [4], which also did not support a direct V-E transfer mechanism, but instead indicated that an intermediate step, which supplies an additional energy of 1-3 eV, is necessary. Experiments on energy transfer to the CO(a$^3\Box$) state also support the possibility of an electron-mediated V-E process. Indeed, measurements in optically pumped pure CO-Ar mixtures, where the electron density is very low, do not show any detectable population of the a$^3\Box$ state [6]. On the other hand, some evidence of vibration-to-CO(a$^3\Box$) energy transfer is found both in electric discharges [5] and in optically pumped plasmas where the electron density is increased using a small pilot discharge in the absorption cell [7].

A similar effect of electron removal on both the CO vibrational level populations and the UV/visible radiation has been observed in an optically pumped CO/N$_2$=1/100 mixture at P=100 Torr (with 60 mTorr NO additive to achieve a higher electron density). The most substantial difference between CO-Ar and CO-N$_2$ mixtures is that in CO-N$_2$ the UV radiation from the CO 4th positive system is not observed and the most intensive UV/visible bands are NO β and γ bands (in the presence of NO), and CN violet and C$_2$ Swan bands (without NO additive). Again, Fig. 8 shows that the CO vibrational level populations increase in the absence of electrons (U$_s$=800 V, I$_s$=3.5 μA), although the effect is somewhat less pronounced than in CO-Ar plasmas (compare with Fig. 6). The removal of electrons also results in a decrease of UV radiation from NO γ bands by about a factor of 2 (several bands between 200 nm and 280 nm, see Fig. 9), although the NO β band system remains almost unaffected.

The most remarkable effect of electron removal from the optically pumped plasma on the UV/visible radiation intensity has been observed in CO/N$_2$=1/100 mixtures at higher total pressures (P=300-500 Torr). At these conditions, the electron removal results in drastic reduction of the UV/visible radiation from both CN violet and C$_2$ Swan bands (up to a factor of 20, see Fig. 10). This effect is also shown in the photographs in Fig. 11, where the electrode positions are highlighted for clarity. The photographs in Fig. 11 were taken with the CaF$_2$ windows, shown in Fig. 2, removed. The visible CN and C$_2$ glow between the Thomson discharge electrodes nearly disappears when the saturation voltage is applied. Most interestingly, this spectacular effect is produced by reducing the electron density from its low baseline value of n$_e$≅10^{10} cm^{-3} and the total number density of N=1.1·10^{19} cm^{-3}, i.e. from the very low baseline ionization fraction of n$_e$/N~10^{-9}. Although the detailed kinetic mechanisms of population of electronically excited radiating states of NO, CN, and C$_2$ in optically pumped plasmas remain far from understood, these results suggest that the presence of electrons might also mediate the V-E energy transfer from CO(X^{1}Σ, v) to excited electronic states of these molecules.

The rise of high vibrational level populations CO(X^{1}Σ, v>10-15) in the saturated Thomson discharge sustained in an optically pumped plasma, i.e. when the electrons are removed from the plasma (see Figs. 6, 8), is well understood. It was first observed in our previous associative ionization experiments [12] and interpreted with kinetic modeling

33

calculations using a coupled solution of the master equation for the CO VDF and the Boltzmann equation for the EEDF [13]. These modeling calculations show that this effect is caused by the superelastic collisions of Eq. (5) between highly vibrationally excited CO molecules (v≥10-15) and low-energy electrons initially formed by the associative ionization process of Eq. (4). Removal of electrons from the plasma essentially inhibits this mechanism of energy relaxation from high vibrational levels and, consequently, their populations increase. Since the electrons cannot store substantial amounts of energy and since energy transfer in elastic electron-molecule collisions is extremely inefficient [31], the calculations also predict that most of the energy is returned to the vibrational modes of CO and N_2, primarily by exciting the low vibrational levels of CO and N_2 (v≤10) by electron impact [25, 26],

$$CO(X^1\Sigma, v) + e^-(\varepsilon + \Delta\varepsilon) \rightarrow CO(X^1\Sigma, v + \Delta v) + e^-(\varepsilon), \qquad (8)$$

$$N_2(X^1\Sigma, v) + e^-(\varepsilon + \Delta\varepsilon) \rightarrow N_2(X^1\Sigma, v + \Delta v) + e^-(\varepsilon). \qquad (9)$$

Such preferential energy transfer from high to low vibrational levels of CO mediated by electrons (V→e→V-ΔV process [13]) is made possible by the highly non-Boltzmann CO VDF in optically pumped plasmas (see Figs. 6, 8). Qualitatively, the slope of the VDF in the "plateau" region (v>10-15) corresponds to a very high "vibrational temperature", $T_{v,high} \sim \omega_e / \ln(n_v/n_{v+1}) \sim \omega_e v \sim 50,000$ K [13]. On the other hand, the similarly defined "vibrational temperature" for the low vibrational levels, $T_{v,low} \sim \omega_e / \ln(n_1/n_0) \sim 3000$ K, is much lower. Therefore the predominant vibrational energy transfer in collisions of CO molecules with electrons is from high vibrational levels to electrons to low vibrational levels. The average electron energy at these conditions is controlled by competition of the superelastic processes of Eq. (5) and electron impact excitation processes of Eqs. (8,9). Modeling calculations incorporating the V→e→V-ΔV processes of Eqs. (5,8,9) explain both the previously available results on the vibrational level populations in the Thomson discharge [13] and the present experimental data shown in Fig. 6, 8.

It is well established that in electric discharge plasmas in CO, N_2, and air, superelastic collisions of molecules on the low vibrational levels (v≤8-10) with slow electrons significantly

increase their energy, thereby raising the "tail" of the EEDF. This consequently increases the rates of electronic excitation and ionization of *vibrationally non-excited* CO and N_2 molecules by electron impact [25, 26]. The present kinetic model also takes these processes into account. However, the effect of such superelastically heated electrons on electronic excitation of the *vibrationally excited* molecules on the ground electronic state, such as given by Eq. (6), is not well understood and the cross sections for such processes are not available. Qualitatively, strong vibrational excitation of a CO molecule in the process of Eq. (6) would substantially reduce the minimum required electron energy, which may consequently greatly increase its rate. Therefore, some of the energy transferred to the electrons in the superelastic processes of Eq. (5) would not necessarily return to the vibrational modes of CO or N_2 by the electron impact excitation processes of Eqs. (8,9), but instead would go to electronic excitation of already highly vibrationally excited CO molecules, Eq. (6). In optically pumped plasmas, such electron-mediated V-E transfer might produce (i) more significant depopulation of the high vibrational levels of the CO ground electronic state than predicted by the $V \rightarrow e \rightarrow V-\Delta V$ processes of Eqs. (5,8,9) alone, and (ii) stronger UV radiation from $CO(A^1\Pi)$ molecules excited in the presence of electrons. This qualitative scenario certainly appears consistent with the results of the present Thomson discharge experiments shown in Figs. 6-11.

To verify whether the observed reduction of UV signal intensity is indeed due to electron removal by the Thomson discharge, we conducted an additional series of measurements. The electron density in the optically pumped CO-Ar plasmas was deliberately increased by adding varying small amounts (0.05-0.5%) of O_2 and NO to the cell gases. As discussed in Section 1, although, in the presence of these additives, the electron production rate by associative ionization is somewhat reduced, the electron density nevertheless increases by a factor of 20-50 compared to the CO-Ar plasma without additives. If the electron-mediated V-E transfer of Eqs. (5,6) is one of the dominant processes of the $CO(A^1\Pi)$ population in optically pumped plasmas, the electron density increase would have to result in higher CO 4th positive system UV radiation intensity. Indeed, measurements of the CO 4th positive spectra in optically pumped CO/Ar=1/100 mixtures at P=100 Torr with and without additives showed that adding 100 mTorr of either NO or O_2 to the baseline gas mixture increases the UV signal intensity by about a factor of 5 (see Fig. 12). In addition, at these conditions, the UV radiation signal intensity for several CO 4th positive bands

essentially mirrors the electron density as a function of the NO partial pressure (see Figs. 13, 14). Similar results have been obtained using the O_2 as an additive.

Thus, the results of the present experiments indicate that the V-E energy transfer process $CO(X^1\Sigma \rightarrow A^1\Pi)$, and, possibly, analogous processes populating radiating excited electronic states of NO, CN, and C_2, in optically pumped plasmas, are mediated by the presence of electrons which are created in the absence of an electric field, with low initial energies. Most importantly, this effect occurs at ionization fractions as low as $n_e/N \sim 10^{-9} - 10^{-7}$.

Further insight into the detailed kinetic mechanism of the electron-mediated V-E processes would be provided by EEDF measurements in optically pumped CO-Ar and CO-N_2 plasmas. As discussed in Section 1, electrons created by the associative ionization mechanism of Eq. (4) initially have fairly low energies. Therefore, the presence of a substantial fraction of relatively high-energy (up to several eV) electrons in the plasma would provide strong additional evidence in favor of the importance of the highly energetic superelastic collisions of Eq. (5) for electron heating and of mediation of the V-E energy transfer by electrons (see Eq. (6)). Simultaneous EEDF and the CO VDF measurements, together with vacuum UV emission measurements of the entire 4th positive system transitions, $CO(A^1\Pi,v \rightarrow X^1\Sigma,w)$, may provide sufficient experimental data for the development and validation of a quantitative theoretical kinetic model for the electron-mediated V-E energy transfer process of Eqs. (5,6).

5. References

1. M. Capitelli (ed.), "Nonequilibrium Vibrational Kinetics", Springer, Berlin, 1986

2. R.L. DeLeon and J.W. Rich, Chem. Phys., vol. 107, 1986, p. 283

3. C. Flament, T. George, K.A. Meister, J.C. Tufts, J.W. Rich, V.V. Subramaniam, J.-P. Martin, B. Piar, and M.-Y. Perrin, "Nonequilibrium Vibrational Kinetics of Carbon Monoxide at High Translational Mode Temperatures", Chemical Physics, vol. 163, 1992, pp. 241-262

4. H.L. Wallaart, B. Piar, M.-Y. Perrin, J.-P. Martin, "Transfer of Vibrational Energy to Electronic Excited States and Vibration Enhanced Carbon Production in Optically Excited V-V pumped CO", Chem. Phys. vol. 196, 1995, p. 149

5. R. Farrenq, C. Rossetti, G. Guelachvili and W. Urban: Experimental Rovibrational Populations of CO up to v=40 from Doppler-limited Fourier Spectra of the Sequences $\square$v=1, 2 and 3 Emitted by a Laser Type Source", Chem. Phys. vol. 92, 1985, pp. 389-399

6. O. Schulz, J.X. Lin, W. Urban "Vibration to Electronic Energy Transfer in Carbon Monoxide between $X^1\square$ and $a^3\square$", Ber. Bunsenges. Phys. Chem. vol. 99, 1995, p. 348

7. O. Schulz: Umwandlung von Vibrationsenergie in Elektronische Anregung und Lasertätigkeit in Optisch Gepumpten Kohlenmonoxid-Plasmen. Dissertation, Bonn, 1995

8. S. de Benedictis, R. d' Agostino and F. Cramarossa, "Spectroscopic Analysis of the Vibrational Distributions in Dissociative CO-He RF Discharges", Chem. Phys. vol. 71, 1982, pp. 247-256

9. S. de Benedictis, F. Cramarossa, and R. d' Agostino, "Residence time analysis of UV-visible emitting species in CO-He radiofrequency discharges", Chem. Phys. vol. 82, 1983, pp. 395-404

10. E. Plönjes, P. Palm, A.P. Chernukho, I.V. Adamovich, and J.W. Rich, "Time-Resolved Fourier Transform Infrared Spectroscopy of Optically Pumped Carbon Monoxide", Chemical Physics, vol. 256, pp. 315-331, 2000

11. C.E. Treanor, J.W. Rich, R.G. Rehm, "Vibrational Relaxation of Anharmonic Oscillators with Exchange-Dominated Collisions", J. Chem. Phys. vol. 48, 1968, pp. 1798-1807

12. I. Adamovich, S. Saupe, M.J. Grassi, O. Schulz, S. Macheret, and J.W. Rich, "Vibrationally Stimulated Ionization of Carbon Monoxide in Optical Pumping Experiments", Chemical Physics, vol. 173, 1993, pp. 491-504

13. I.V. Adamovich and J.W. Rich, "The Effect of Superelastic Electron-Molecule Collisions on the Vibrational Energy Distribution Function", Journal of Physics D: Applied Physics, vol. 30, No. 12, 1997, pp. 1741-1745

14. E. Plönjes, P. Palm, I.V. Adamovich, and J.W. Rich, "Ionization Measurements in Optically Pumped Discharges", Journal of Physics D: Applied Physics, vol. 33, No. 16, 2000, pp. 2049-2056

15. I.V. Adamovich, "Control of Electron Recombination Rate and Electron Density in Optically Pumped Nonequilibrium Plasmas", Journal of Physics D: Applied Physics, vol. 34, 2001, pp.319-325

16. P. Palm, E. Plönjes, M. Buoni, V.V. Subramaniam, and I.V. Adamovich, "Electron Density and Recombination Rate Measurements in CO-Seeded Optically Pumped Plasmas", Journal of Applied Physics, vol. 89, No. 11, 2001, pp. 5903-5910

17. E. Plönjes, P. Palm, W. Lee, W.R. Lempert, and I.V. Adamovich, "RF Energy Coupling to High-Pressure Optically Pumped Nonequilibrium Plasmas", Journal of Applied Physics, vol. 89, No. 11, 2001, pp. 5911-5918

18. Y. Kaufman, P. Avivi, F.Dothan, H. Keren, J. Malinowitz, J. Chem. Phys., vol. 72, 1980, p. 2606

19. H. Ehrhardt, L. Langhans, F. Linder, and H.S. Taylor, Phys. Rev., vol. 173, p. 222, 1968

20. S. Büscher, O. Schulz, A. Dax, H. Kath, W. Urban, "Improvement of the Performance of CW CO Lasers by Using Externally Ribbed Wall Cooled Discharge Tubes", Applied Physics B (Lasers and Optics), vol. 64, No. 3, 1997, pp. 307-309

21. E. Plönjes, P. Palm, W. Lee, M. D. Chidley, I.V. Adamovich, W.R. Lempert, and J. William Rich, "Vibrational Energy Storage in High-Pressure Mixtures of Diatomic Molecules", Chemical Physics, vol. 260, 2000, pp. 353-366

22. W. Lee, I.V. Adamovich, and W.R. Lempert, "Optical Pumping Studies of Vibrational Energy Transfer in High-Pressure Diatomic Gases", Journal of Chemical Physics, vol. 114, No. 3, 2001, pp. 1178-1186

23. N.A. Dyatko, I.V. Kochetov, and A.P. Napartovich, J. Physics D: Applied Physics, vol. 26, p. 418, 1991

24. J.C.Y. Chen, Journal of Chemical Physics, vol. 40, p. 3513, 1964

25. N.L. Aleksandrov, A.M. Konchakov, and E.E. Son, Sov. Journal of Plasma Physics, vol. 4, p. 663, 1978

26. N.L. Aleksandrov, A.M. Konchakov, and E.E. Son, Sov. Physics - Journal of Technical Physics, vol. 49, p. 1200, 1979

27. Y. Itikawa, M. Hayashi, A. Ichimura et al., J. Phys. Chem. Ref. Data, vol.16, 1986, p.985

28. Y. Itikawa, M. Hayashi, A. Ichimura et al., J. Phys. Chem. Ref. Data, vol.18, 1989, p.23

29. Y. Itikawa, Atomic Data and Nuclear Data Tables, vol. 21, p. 69, 1978

30. K.P. Horn and P.E. Oettinger, J. Chem. Phys., vol. 54, 1971, p. 3040

31. L.G.H. Huxley and R.W. Crompton, "The Diffusion and Drift of Electrons in Gases", Wiley, New York, 1974
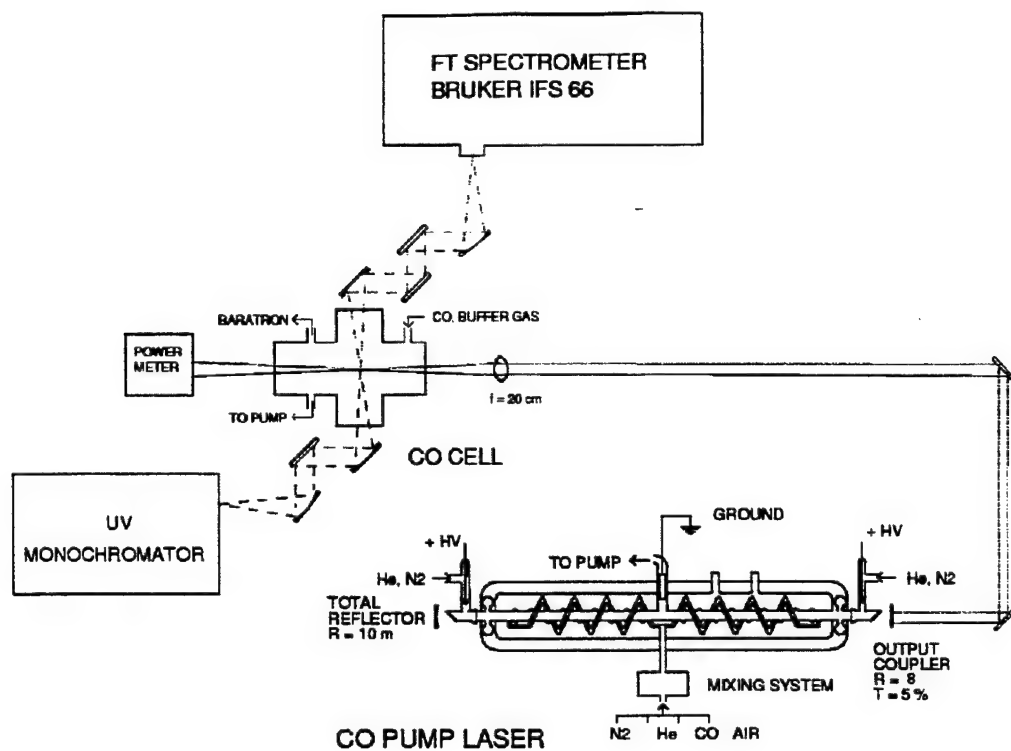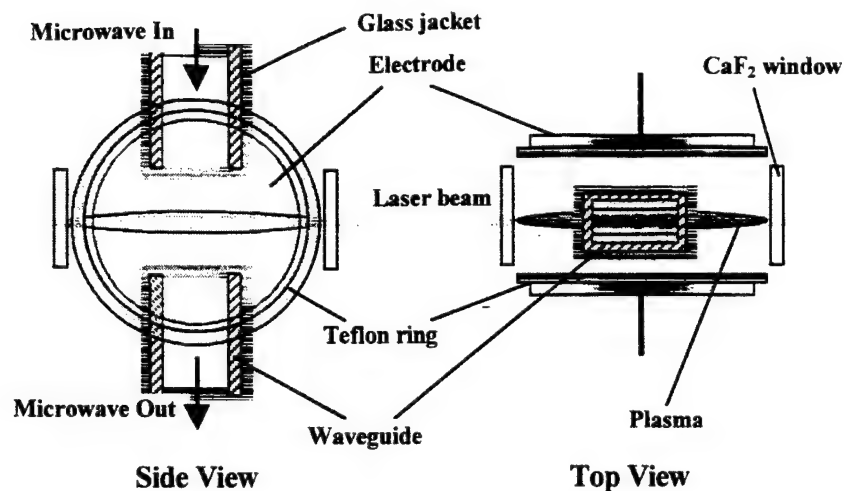
Figure 1. Schematic of the experimental setup

Figure 2. Schematic of the Thomson discharge electrodes and microwave waveguides in the optical absorption cell.
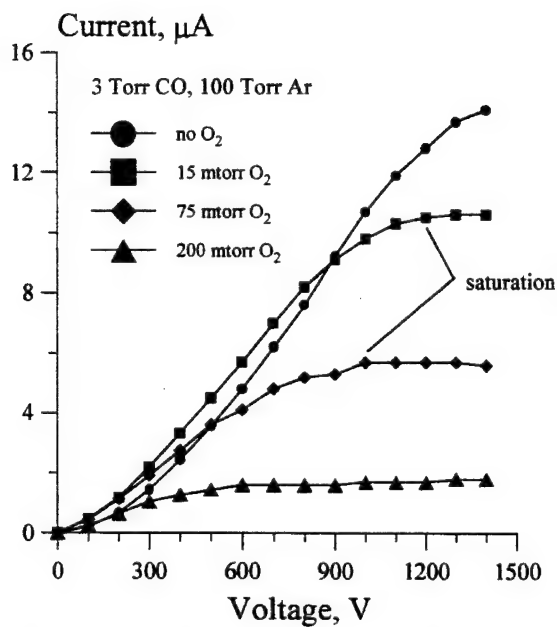

Figure 3. Saturation of the Thomson discharge in optically pumped CO-Ar-O_2 mixtures
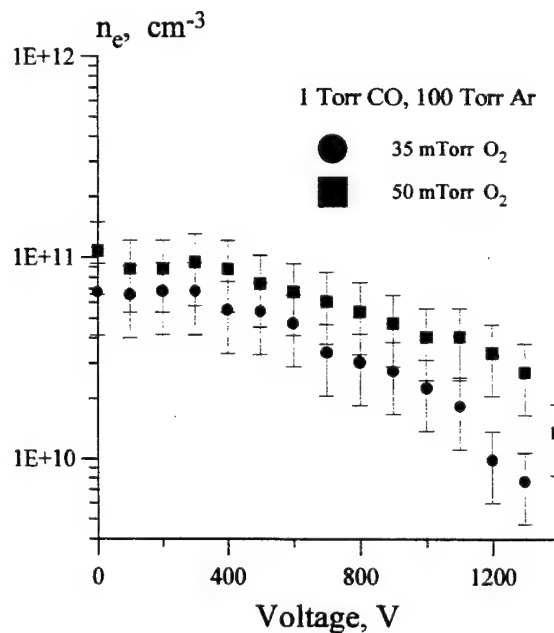

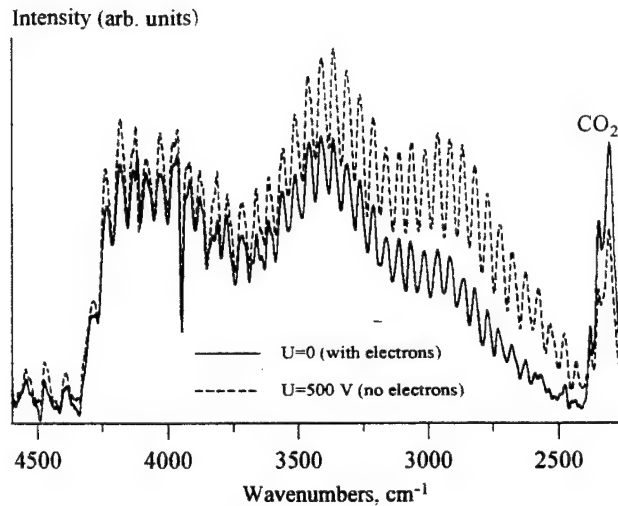Figure 4. Electron removal by the applied field in the Thomson discharge approaching saturation.

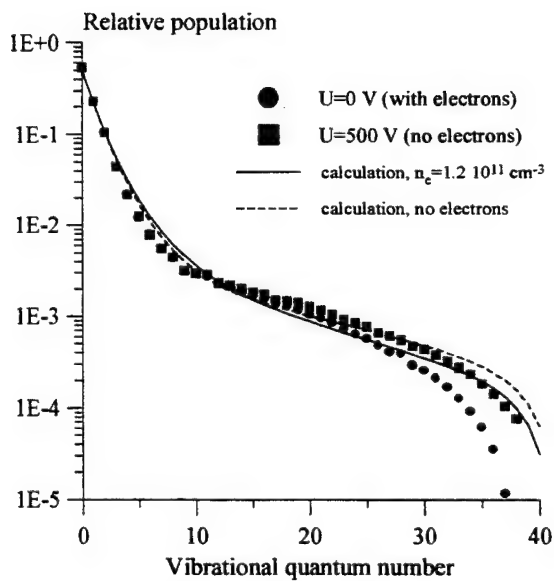Figure 5. Low-resolution CO first overtone emission spectra from an optically pumped CO/Ar=1/100 mixture. P=100 Torr, T=530 K.

Figure 6. Experimental and calculated CO vibrational distribution functions for the conditions of Figure 5.
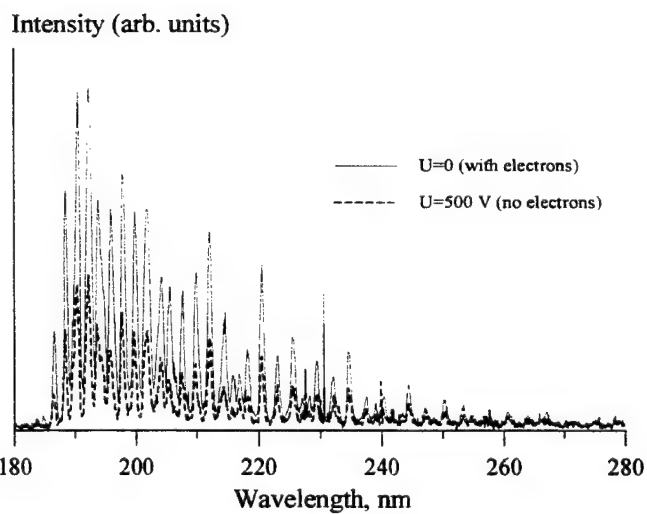
Figure 7. CO UV spectra (4th positive band system) for the conditions of Figure 5.
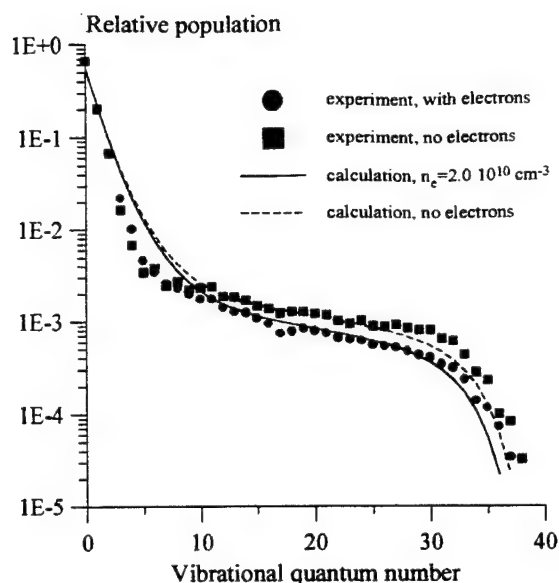
Figure 8. Experimental and calculated CO vibrational distribution functions in an optically pumped $CO/N_2=1/100$ mixture. P=100 Torr, T=420 K.
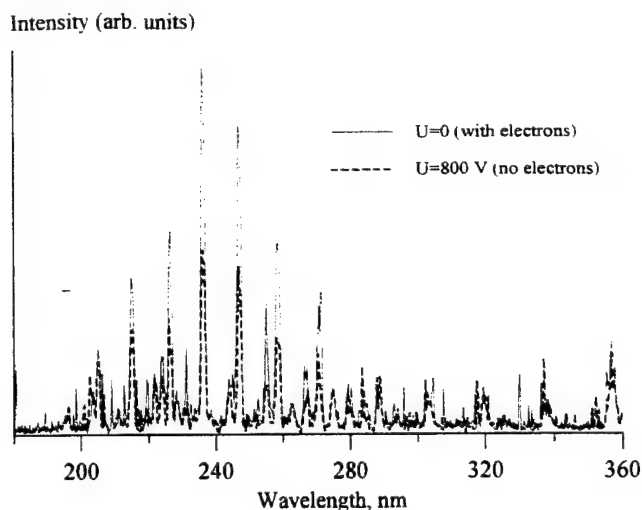

Figure 9. NO UV spectra (β and γ band system) for the conditions of Figure 8.
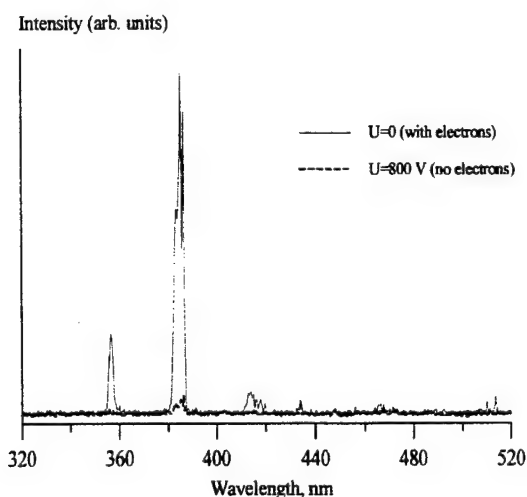
Figure 10. CN violet and C_2 Swan band UV/visible spectra in an optically pumped $CO/N_2=1/100$ mixture. P=420 Torr, T=380 K.
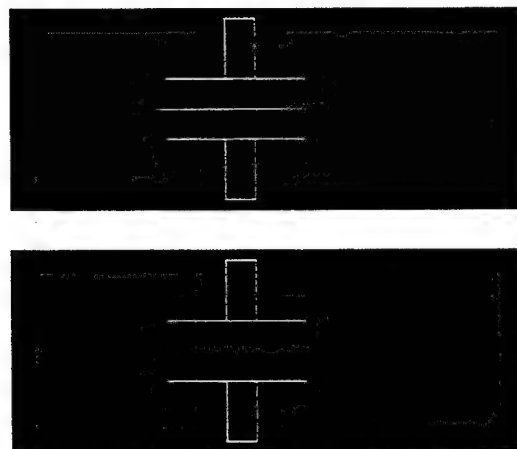

Figure 11. Optically pumped plasmas at the conditions of Fig. 10. Top, no voltage applied; bottom, saturation voltage applied. The location of the Thomson discharge electrodes is highlighted.
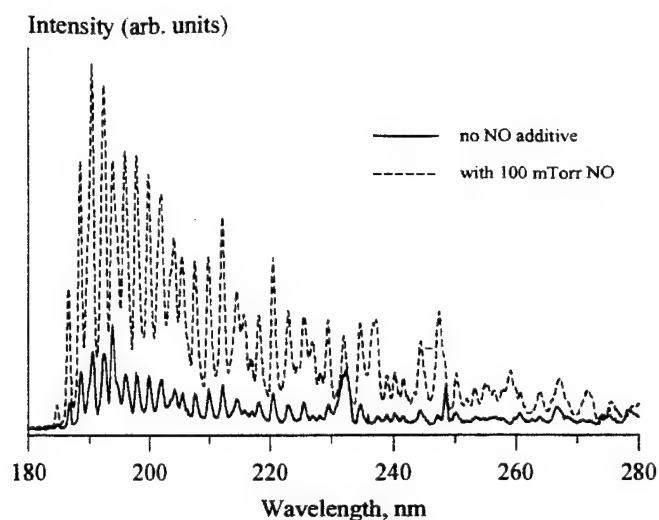
Intensity (arb. units)

no NO additive
with 100 mTorr NO

Wavelength, nm

Figure 12. CO UV spectra (4th positive band system) in an optically pumped CO/Ar=1/100 mixture at P=100 Torr.

n_e, cm^{-3}

3 Torr CO, 100 Torr Ar

Laser power 11 W

Laser power 13 W

P_{NO}, mTorr
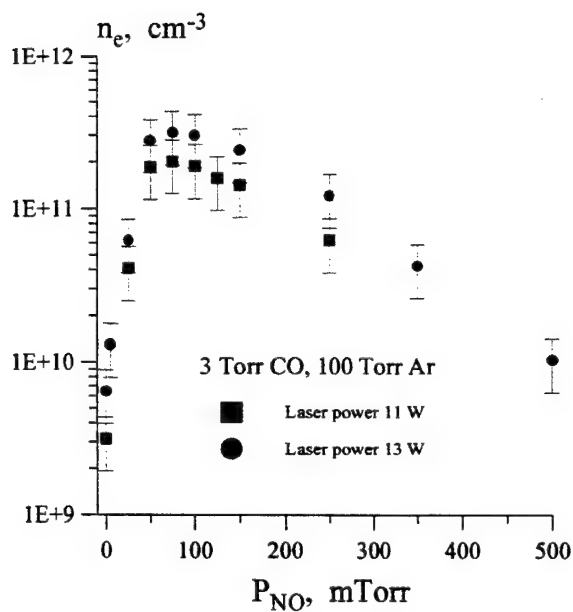
Figure 13. Electron density in CO-Ar-NO mixtures as a function of the NO partial pressure.

Intensty (arb. units)

190.3 nm
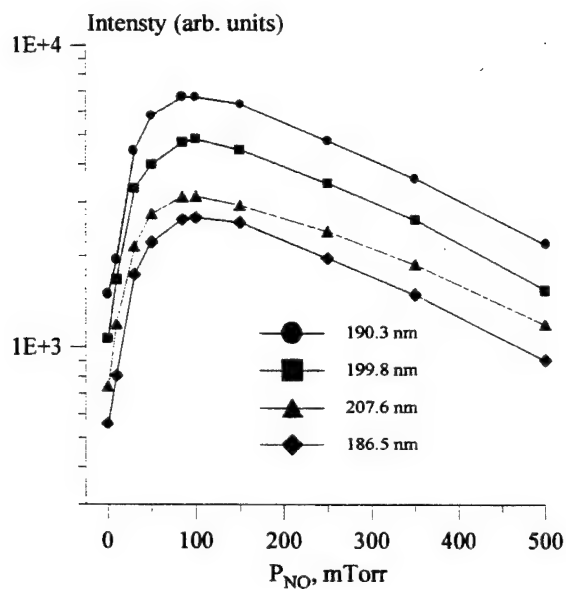199.8 nm
207.6 nm
186.5 nm

P_{NO}, mTorr

Figure 14. UV band radiation intensity (CO 4th positive bands) in CO-Ar-NO mixtures as functions of the NO partial pressure.

43

CHAPTER III
CONTROL OF ELECTRON RECOMBINATION RATE AND ELECTRON DENSITY IN OPTICALLY PUMPED NONEQUILIBRIUM PLASMAS

1. Introduction

The paper addresses analysis of a recent ionization measurement in optically pumped $CO/Ar/O_2$ and $CO/N_2/O_2$ plasmas using non-self-sustained DC and RF discharges [1]. Briefly, the experiments have been conducted in a flowing gas optical absorption cell, where the gas mixture was vibrationally excited by resonance absorption of 20 W continuous wave broadband CO laser radiation. The Gaussian laser beam was focused to increase the power loading per CO molecule, providing an excitation region in the cell of approximately 2 mm in diameter. The absorbed laser power was typically 5-6 W over the absorption length of 12.5 cm, which gives an absorbed power density of 10 W/cm^3. The lower vibrational states of carbon monoxide in the cell, v≤10, are populated by direct resonance absorption of the laser radiation. The higher vibrational levels, v~10-40, which are not directly coupled to the laser radiation, are populated by the rapid redistribution of vibrational energy by the vibration-vibration (V-V) exchange processes,

$$CO(v) + CO(w) \rightarrow CO(v-1) + CO(w+1) \tag{1}$$
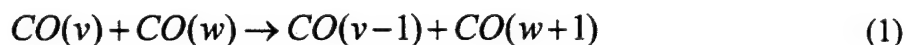
The large heat capacity of the Ar or N_2 diluents, as well as conductive and convective cooling of the gas flow, controls the steady-state translational/rotational mode temperature in the cell, T=400-700 K, while the average vibrational mode energy of CO corresponds to 2000-4000 K degrees K. Thus a strong disequipartition of energy can be maintained in the cell, characterized by very high vibrational mode energy and electron temperature, and a low translational/rotational mode temperature.

Under these conditions, ionization in the optically pumped CO is produced by an associative ionization mechanism, in collisions of two highly vibrationally excited CO molecules when the sum of their vibrational energies exceeds the ionization potential [1-3],

$$CO(v) + CO(w) \rightarrow (CO)_2^+ + e^- ,$$

$$E_v + E_w > E_{ion} \tag{2}$$
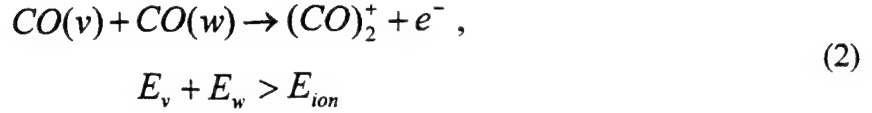
The parameters of the optically pumped plasma created in the cell have been analyzed using two 3 cm diameter brass plate electrodes, placed in the cell as shown in Fig. 1, so that the laser beam created a nearly cylindrical excited region between the electrodes. The electrodes, which were typically 8 to 12 mm apart, were powered either by a DC or by an RF power supply. In both DC and RF experiments, the applied voltage was deliberately kept sufficiently low to completely preclude electron impact ionization [1-3]. Thus, a non-self-sustained DC discharge (sometimes called a Thomson discharge [2,4]) or a non-self-sustained RF discharge can be initiated between the electrodes.

In these experiments, the rate of electron production per unit volume by the associative ionization mechanism of Eq. (2) was estimated from the DC discharge current in the saturation regime, I_S. Saturation occurs when the applied electric field removes as many electrons per second as are produced in the entire discharge volume. This rate is accordingly estimated as

$$S \cong \frac{I_S}{eD\pi a^2 / 4} \cong 10^{14} - 10^{15} \; cm^{-3} \; \sec^{-1} \tag{3}$$

In Eq. (3), obtained in Ref. [3], a is the ionized region diameter and D is the electrode diameter. Note that in the saturation regime the electrons are removed from the discharge much faster than they recombine or attach. Indeed, simple estimates [2] show that the electron residence time in the discharge is much shorter than the time for electron-ion recombination or electron attachment. Therefore measuring the DC saturation current density directly yields the electron production rate per unit volume S, regardless of the ionization mechanism and independently of the electron removal rates. The electron density in the plasma, on the other hand, was estimated from the conduction current of the RF discharge, measured as a difference between the RMS RF discharge currents with the laser turned on and off,

$$n_e \cong \frac{I_C}{e\mu_e Ua} \cong 10^{10} - 10^{11} \ cm^{-3} \tag{4}$$

In Eq. (4), U is the applied RMS RF voltage and μ_e is the electron mobility. Note that Eqs. (3,4) are approximate since they do not account for the electrode edge effects and the spatial nonuniformity of the plasma (in particular, voltage drops across the sheaths in the RF discharge). Therefore they are expected to provide only rather crude estimates of both the electron production rate and the electron density.

The objective of the present paper is to use two-dimensional kinetic modeling of both the DC and the RF discharges for more accurate quantitative inference of the electron production and removal rates, as well as the electron density in the optically pumped plasma.

2. Kinetic Model

The two-dimensional time-dependent model of the non-self-sustained DC and RF discharges used in the optical pumping experiments [1] discussed in Section 1 includes the equations for electron and positive ion concentrations, and the Poisson equation for the electric field [5]:

$$\frac{\partial n_k(x, y, t)}{\partial t} + \nabla \vec{\Gamma}_k = Q_k \ ,$$

$$\vec{\Gamma}_k = D_k \nabla n_k(x, y, t) - \frac{q_k}{|e|} \mu_k \nabla \phi(x, y, t) n_k(x, y, t)$$

$$n_k(x, 0, t) = n_k(x, d, t) = 0 \tag{5}$$

$$\frac{\partial n_k(0, y, t)}{\partial x} = \frac{\partial n_k(\pm W, y, t)}{\partial x} = 0$$

$$n_k(x, y, 0) = 0$$

$$\nabla^2 \phi(x, y, t) = \frac{1}{\varepsilon_0} \sum_k q_k n_k(x, y, t),$$

$$\phi(x, 0, t) = 0, \quad \phi(x, d, t) = U_0 \cos(2\pi\nu t),$$

$$\frac{\partial \phi(0, y, t)}{\partial x} = \frac{\partial \phi(\pm W, y, t)}{\partial x} = 0 \qquad (6)$$

$$\phi(x, y, 0) = U_0 y / d$$

$$Q_e = S(x, y) - \beta n_e n_+$$
$$Q_+ = S(x, y) - \beta n_e n_+ \qquad (7)$$

$$S(x, y) = S_0 \exp\left[-\left(\frac{y - d/2}{a/2}\right)^2 - \left(\frac{x}{a/2}\right)^2 \right] \qquad (8)$$

In Eqs. (5-7), the index k stands for electrons and positive ions, e is the electron charge, n_k and $q_k = \pm e$ are the species concentrations and charges, D_k, μ_k, and $\bar{\Gamma}_k$ are the species diffusion coefficients, mobilities, and fluxes (conduction current density vectors), respectively, ϕ and $\bar{E} = -\nabla\phi$ are the electric potential and electric field, d is the separation between the electrodes, W is the electrode half-width, U_0 and ν are the applied voltage amplitude and frequency, S(x,y) is the rate of electron production by the associative ionization mechanism of Eq. (2), and β is the electron-ion recombination coefficient. In Eq. (8), S_0 and a are the rate of electron production at the laser beam axis and the ionized region diameter. The Gaussian distribution of ionization rate S(x,y) in Eq. (8) is chosen due to the Gaussian power density distribution across the laser beam [6]. At zero frequency, $\nu = 0$, this system of equations describes a non-self-sustained DC discharge.

The electron and ion mobilities and diffusion coefficients in argon and in nitrogen plasmas as functions of the reduced electric field E/N, where N=P/kT is the number density, are taken from [7,8]. The gas pressure and temperature in the optically pumped cell have been previously measured in a wide range of experimental conditions [1-3,6]. Thus, the only unknown

parameters remaining in Eqs. (5-7) are the electron production rate, S, and the electron-ion recombination rate, β.

Eqs. (5-7) are solved numerically until either a steady-state (for a DC discharge) or a periodic (for an RF discharge) solution for $n_k(x,y,t)$ and $\phi(x,y,t)$ is reached. In the latter case this usually takes from a few hundred to a few thousand cycles. The electrode currents in the DC and in the RF discharges are determined as follows,

$$I_{cathode} = L \int_{-W}^{W} dx \sum_{k} \Gamma_{ky}(x,0) \tag{9}$$

$$I_{RMS, cathode} = \left\{ \frac{1}{T} \int_{o}^{T} dt \left[L \int_{-W}^{W} dx \left(\varepsilon_o \frac{\partial E_y(x,0,t)}{\partial t} + \sum_{k} \Gamma_{ky}(x,0,t) \right) \right]^2 \right\}^{1/2} \tag{10}$$

In Eqs. (9,10), Γ_{ky} is the y-component (i.e. perpendicular to the electrode) of the flux of the charged species k, E_y is the y-component of the electric field, L is the length of the electrode along the laser beam, and $T=2\pi/v$ is the RF field oscillation period. The anode current, which is expected to be equal to the cathode current, is calculated in a similar way.

In the calculations discussed in the following section, the 3 cm diameter circular electrodes (see Fig. 1) are modeled as square electrodes of the same surface area. The electrode separation is d=10 mm (for DC discharge) and d=7.5 mm (for RF discharge), the electrode full width and the electrode length are 2W=L=2.66 cm. The ionized region diameter, a=2 mm, is estimated from the apparent diameter of the C_2 Swan band glow, which is strongly coupled to the high vibrational level populations of CO [1]. The applied DC voltage is varied in the range U=0-1000 V. The RF voltage amplitude and frequency are U_0=5 V and v=10 MHz, respectively [1]. Calculations are made at two different pressures, P=100 torr and 20 torr. The gas temperature is taken to be T=500 K, which is in between the temperatures of T=600 K and in T=450 K measured in the optically pumped CO/Ar=2/100 and CO/N_2=2/100 mixtures at P=100 torr [1]. The system of equations (5-7) is solved using standard stiff PDE solver PDECOL [9].

3. Results and Discussion

The first series of modeling calculations have been made for a DC discharge. In these calculations, the electron production rate at the laser beam axis, S_0, was adjusted to match the experimentally measured values of the discharge saturation current, I_S, while the electron recombination rate was assumed to be equal to the rate of dissociative recombination of $(CO)_2^+$ dimer ions, $\beta=2\cdot10^{-6}$ [10]. Figure 2 shows experimental and calculated voltage-current characteristics for two optically pumped gas mixtures, 2 torr CO / 100 torr Ar and 2 torr CO / 100 torr N_2. One can see that the results of calculations reproduce well not only the values of the saturation current, which are controlled exclusively by the electron production rate ($I_s=13.4$ μA in CO/Ar and $I_s=3.1$ μA in CO/N_2) [2,4], but also the entire shape of the voltage-current characteristics. The values of S_0 for the two cases shown in Fig. 2 are $S_0=1.0\cdot10^{15}$ 1/cm^3/s and $S_0=2.2\cdot10^{14}$ 1/cm^3/s, respectively. Varying the other crucial parameter, the recombination rate, in the range $\beta=10^{-7}$-10^{-5} cm^3/sec showed that although it does affect the shape of the current-voltage curves below the saturation limit, the effect is too weak for the accurate inference of the recombination rate coefficient. The best agreement with the experimental data in the entire range of applied voltage (U=0-1000 V) is achieved at $\beta>10^{-6}$ cm^3/sec. Unfortunately, above this value the calculated voltage-current curves become nearly insensitive to the recombination rate variation. Also, variation of the ion mobility μ_+ (within a factor of two) had almost no effect on the calculated voltage-current characteristics.

Figures 3 and 4 show contour plots of electron and ion concentrations, n_e and n_+, as well as electric potential, ϕ, in the optically pumped CO/Ar mixture at U=200 V. In these calculations, $S_0=1.0\cdot10^{15}$ 1/cm^3/s and $\beta=2\cdot10^{-6}$ cm^3/sec. One can see that the applied voltage displaces the highly mobile electrons toward the anode (top electrode in Figs. 3,4), which creates a region of positive space charge with stronger electric field near the center of the cathode (bottom electrode). Figure 5 displays the electron concentration in the DC discharge in the CO/Ar mixture along the axis of symmetry of the discharge (i.e. at x=0) at several values of the applied voltage. It shows that as the applied voltage increases, the electrons are indeed removed from the

49

interelectrode space until the electron concentration is significantly reduced (by more than an order of magnitude) near the saturation point at U=800 V. At these conditions, the rate of electron removal by the field approaches the overall electron production rate, so that

$$I_S \approx eL \int_0^d dy \int_{-W}^{W} dx\, S(x,y) \qquad (11)$$

Figure 5 and Eq. (11) also illustrate the rationale for the inference of the electron production rate per unit volume from the DC discharge saturation current.

In our previous work [1], small amounts of oxygen or air have been added to the baseline CO/Ar gas mixtures to determine the sensitivity of the measured electron production rate S to the level of O_2 impurity in the cell. It was found that addition of O_2 in small concentrations (less than 0.1 torr) only weakly affects the DC discharge saturation current (and therefore the electron production rate). In particular, the electron production rate is reduced by only about 30% if the oxygen partial pressure does not exceed 0.1 torr [1]. As discussed in our previous publication, this effect is most likely due to the reduction of the high CO vibrational level populations in the presence of oxygen, measured by infrared emission spectroscopy [1]. In other words, the rate of electron production by the associative ionization mechanism remains nearly constant (within about 30%) in the presence of trace amounts of O_2.

The results of calculations discussed above show that the non-self-sustained DC discharge measurements indeed allow direct inference of the electron production rate by the associative ionization mechanism. Unfortunately, this method does not allow accurate inference of the electron density in the optically pumped plasma or the recombination rate coefficient since the voltage-current characteristic of the DC discharge is only weakly sensitive to the variation of these parameters. To infer the values of these parameters, we use the results of non-self-sustained RF discharge experiments in optically pumped CO/Ar mixtures containing small amounts of O_2 [1]. In these measurements, the conduction current through the non-self-sustained RF discharge, I_C, has been determined as a difference between the RF currents measured with the CO laser turned on and off. In the latter case, the RF current measured, 190 µA, is the displacement

current. The most important result of these measurements is a sudden increase of the conduction current when small amounts of O_2 (0.05-0.1 torr) are added to the baseline CO/Ar gas mixture (without oxygen), from $I_C<2$ μA to $I_C=90-110$ μA at P=100 torr and from $I_C=15-20$ μA to $I_C=160-220$ μA at P=20 torr [1]. Again, we emphasize that this effect occurs at a nearly constant (within about 30%) electron production rate measured using the DC discharge [1]. A preliminary suggestion made in our previous publication [1] was that adding O_2 to the baseline gas mixture resulted in a significant reduction of the electron removal rate. In the present paper we use the RF discharge modeling to verify this suggestion and to infer the electron removal rate.

A second series of modeling calculations have been made for the RF discharge. Although the kinetic model discussed in Section 2 can be easily modified to incorporate the transport equation for the negative ions, as well as kinetic processes involving formation and decay of negative ions (including the dominant process of O_2^- ions formation by the three-body electron attachment process $O_2+e+M \rightarrow O_2^-+M$), in the present work these processes are neglected. The arguments in favor of this assumption are as follows: (i) adding O_2 to the cell gases results in an apparent increase of the electron density in the discharge, which suggests that rapid three-body elecron attachment to oxygen is mitigated to a large extent, (ii) similar results were obtained when comparable amounts of NO, which is not an efficient electron attacher, were added to the cell gases [1], and (iii) Raman spectroscopy measurements of the O_2 vibrational level populations (v=0-12) in the optically pumped CO/N_2/O_2 plasmas [11] show that O_2 in these mixtures becomes strongly vibrationally excited ($T_v(O_2)$=2200-3600 K). In particular, the latter result suggests that strong vibrational excitation of O_2 might well stimulate detachment of electrons from the weakly bound O_2^- ions (with electron affininity of ~0.43 eV). The electron production rate in these calculations was taken to be equal to the baseline value of $S_0=1.0 \cdot 10^{15}$ 1/cm^3/s inferred from the DC discharge measurements in the CO/Ar mixtures. The electron-ion recombination rate in the calculations was varied in the range $\beta=10^{-9}-10^{-5}$ cm^3/s.

Figures 6,7 show contour plots of the period-averaged electron and ion concentrations, as well as the period-averaged electric potential in the RF discharge. In these calculations, the recombination rate coefficient is taken to be $\beta=2.0 \cdot 10^{-8}$ cm^3/s. One can see that the applied weak RF field displaces the electrons away from the electrodes, thereby creating the positive space

charge areas (sheath) near the electrodes. The electric field in the sheath areas significantly exceeds its value in the quasi-neutral central region, and increases with electron density (i.e. as the recombination rate coefficient is reduced at the constant electron production rate, see Fig. 8). The electric field increase near the electrodes produces the current rise in the external circuit over the level of the displacement current, measured with the laser turned off. The kinetic model used in the present work predicts the RF discharge conduction current as a function of the recombination rate coefficient β (see Fig. 9). Therefore, with the electron production rate $S_0=1.0 \cdot 10^{15}$ 1/cm^3/s known, one can infer the values of the recombination rate in the baseline CO/Ar mixture (without oxygen) and in the mixture with 0.05-1.0 torr of O_2 added by comparing the RF conduction current measurements [1] discussed above and Fig. 9. Using this procedure, for CO/Ar mixtures at 100 torr and 20 torr we obtain $\beta > 6.0 \cdot 10^{-6}$ cm^3/s and $\beta = (7.5 \pm 1.5) \cdot 10^{-6}$ cm^3/s, respectively. For CO/Ar/O_2 mixtures at 100 torr and 20 torr, we infer $\beta = (1.5 \pm 0.3) \cdot 10^{-8}$ cm^3/s and $\beta = (5.1 \pm 2.9) \cdot 10^{-8}$ cm^3/s, respectively. In other words, adding oxygen to the CO/Ar mixture reduces the recombination rate coefficient by more than two orders of magnitude. A similar result is obtained in the CO/N_2 mixtures with small amounts of O_2 added [1]. Figure 10 also shows the RF conduction current as a function of the electron density at the laser beam axis. One can see that the measured values of the RF discharge conduction current correspond to an electron density of $n_e = (1.7 \pm 0.2) \cdot 10^{11}$ cm^{-3} at P=100 torr and $n_e = (6.2 \pm 0.8) \cdot 10^{10}$ cm^{-3} at P=20 torr. The lower electron density at the low pressure (at the same electron production rate) is due both to somewhat faster electron recombination rate and to a more significant contribution of the charged species diffusion out of the ionized region. Variation of the ion mobility within a factor of two had almost no effect on the shape of the curves shown in Figs. 9,10, and therefore on the inferred values of the recombination rate coefficient and electron density.

The inferred electron-ion recombination rates in the absence of oxygen and with O_2 added to the cell are fairly close to the measured rates of recombination of the dimer $(CO)_2^+$ ions, $\beta = 2 \cdot 10^{-6}$ cm^3/s [10] and of the monomer O_2^+ ions, $\beta = (3-5) \cdot 10^{-8}$ cm^3/s at the electron temperature of $T_e \sim 0.3$-0.5 eV [5]. Also, the results of our previous coupled master equation / Boltzmann equation modeling calculations [3] suggest that the electron temperature in the optically pumped plasma, $T_e = 5200$ K, is closely coupled with the CO vibrational temperature, $T_v(CO) = 4100$ K. Therefore, although the detailed kinetic mechanism of the apparent recombination rate reduction

remains uncertain, one might speculate that adding oxygen to the cell gases might result in the replacement of the dominant rapidly recombining dimer $(CO)_2^+$ ions by the more slowly recombining O_2^+ ions, which also have lower ionization potential (12.2 eV vs. 14.0 eV), e.g. in an ion-molecule reaction

$$(CO)_2^+ + O_2 \rightarrow CO + CO + O_2^+ \tag{12}$$
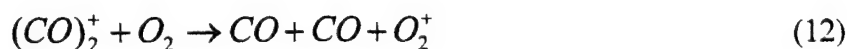
There exist some experimental evidence which is consistent with this qualitative scenario. Kaufman et al. [12] measured the ion composition in glow discharges in $CO/Ar/O_2$ and in $CO/He/O_2$ gas mixtures at P=18 torr using in situ ion mass spectrometry. The resultant mass spectra taken in CO/Ar and in CO/He mixtures without oxygen show that the dominant ions in the discharge are cluster ions of the general form $C_n(CO)_2^+$, n=1-15. However, adding a few tens of millitorr of O_2 to these gas mixtures resulted in nearly complete disappearance of these ions and their replacement by the O_2^+ ions. Additional non-intrusive electron density measurements (such as using microwave attenuation) and ion mass spectrometry measurements in the optically pumped plasmas are desirable to yield more information on the kinetic mechanism of the observed effect.

4. Summary

The analysis of the experiments reported in our previous paper [1] using modeling calculations discussed in the present work show that non-self-sustained DC and RF discharges can be successfully used for measurements of electron production rate, electron recombination rate, and electron density in the optically pumped plasmas. The inferred rate of electron production per unit volume by the associative ionization mechanism is $S_0 = 1.0 \cdot 10^{15}$ $1/cm^3/s$ and $S_0 = 2.2 \cdot 10^{14}$ $1/cm^3/s$ in CO/Ar=2/100 and in CO/N_2=2/100 plasmas, respectively. The inferred electron-ion recombination rate coefficients are $\beta > 6.0 \cdot 10^{-6}$ cm^3/s and $\beta = (7.5 \pm 1.5) \cdot 10^{-6}$ cm^3/s in CO/Ar=2/100 mixtures at P=100 torr and 20 torr, respectively. In CO/Ar=2/100 mixtures with a 0.05-0.1 torr admixture of O_2 at P=100 torr and 20 torr, the inferred recombination rate coefficients are $\beta = (1.5 \pm 0.3) \cdot 10^{-8}$ cm^3/s and $\beta = (5.1 \pm 2.9) \cdot 10^{-8}$ cm^3/s. Finally, the inferred electron density in the optically pumped $CO/Ar/O_2$ plasmas at the laser beam axis is $n_e = (1.7 \pm 0.2) \cdot 10^{11}$

cm^{-3} at P=100 torr and $n_e=(6.2\pm0.8)\cdot10^{10}$ cm^{-3} at P=20 torr. These results demonstrate that electron density in the optically pumped CO/Ar plasmas can be controlled and significantly increased by adding small amounts (up to ~0.1%) of species such as O_2 and NO, which result in reduction of the electron-ion recombination rate.

5. References

1. E. Ploenjes, P. Palm, I.V. Adamovich, and J.W. Rich, "Ionization Measurements in Optically Pumped Discharges", Journal of Physics D: Applied Physics, vol. 33, No. 16, 2000, pp. 2049-2056

2. Adamovich, S. Saupe, M.J. Grassi, O. Schulz, S. Macheret and J.W. Rich, "Vibrationally Stimulated Ionization of Carbon Monoxide in Optical Pumping Experiments", Chemical Physics, vol. 173, 1993, pp. 491-504

3. I.V. Adamovich and J.W. Rich, "The Effect of Superelastic Electron-Molecule Collisions on the Vibrational Energy Distribution Function", Journal of Physics D: Applied Physics, vol. 30, No. 12, 1997, pp. 1741-1745

4. E.P. Velikhov, A.S. Kovalev, and A.T. Rakhimov, "Physical Phenomena in Gas Discharge Plasmas", Moscow, Nauka, 1987

5. Raizer, Y.P., "Gas Discharge Physics", Springer-Verlag, Berlin, 1991

6. E. Ploenjes, P. Palm, A.P. Chernukho, I.V. Adamovich, and J.W. Rich, "Time-Resolved Fourier Transform Infrared Spectroscopy of Optically Pumped Carbon Monoxide", Chemical Physics, vol. 256, pp. 315-331, 2000

7. L.G.H Huxley and R.W. Crompton, "The Diffusion and Drift of Electrons in Gases", Wiley, New York, 1974

8. E.W. McDaniel, "Collision Phenomena in Ionized Gases", Wiley, New York, 1964

9. N.K. Madsen and R.F. Sincovec, ACM Trans. Math. Software, vol. 5, 1979, p. 326

10. R. Johnsen, "Recombination of Cluster Ions", in B.R. Rowe et al. (eds.), "Dissociative Recombination", Plenum, New York, 1993

11. W. Lee, I.V. Adamovich, and W.R. Lempert, "Optical Pumping Studies of Vibrational Energy Transfer in High-Pressure Distomic Gases", submitted to Journal of Chemical Physics, May 2000

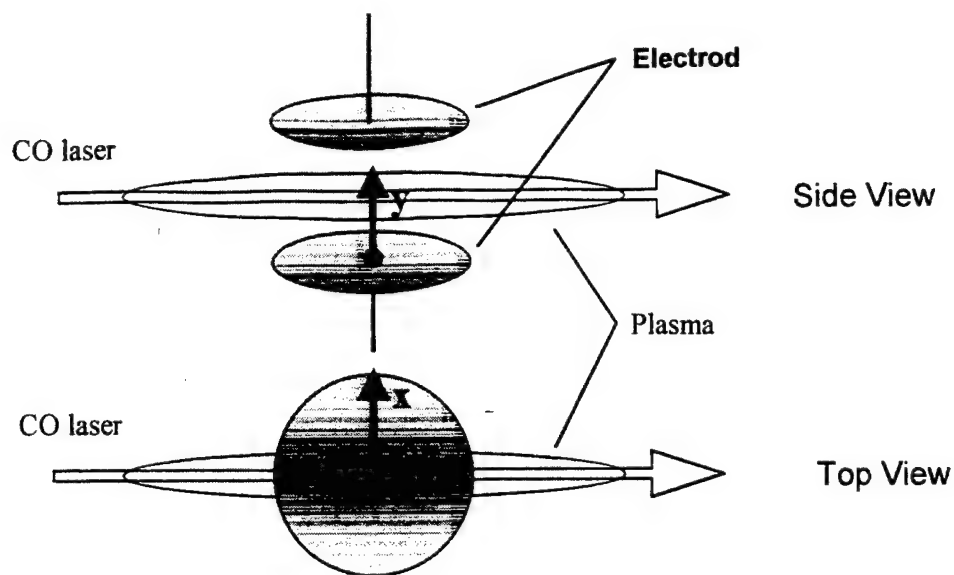12. Y. Kaufman, P. Avivi, F.Dothan, H. Keren, J. Malinowitz, J. Chem. Phys., Vol. 72, 1980, p. 2606

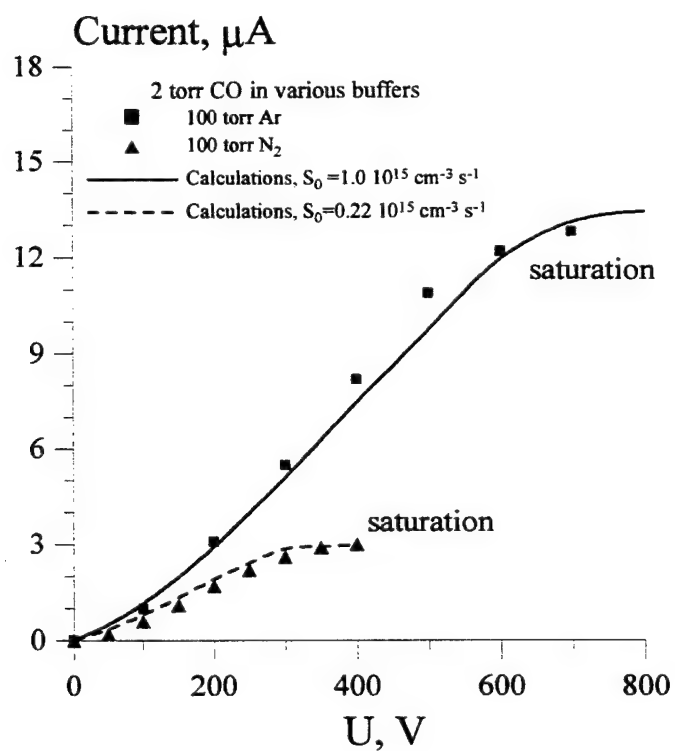Figure 1. Schematic of electrodes in the cell and of the discharge geometry

Figure 2. Experimental and calculated voltage-current characteristics of the DC discharge in the optically pumped plasmas. $\beta = 2 \cdot 10^{-6}$ cm^3/sec

Ion Concentration   Electron Concentration
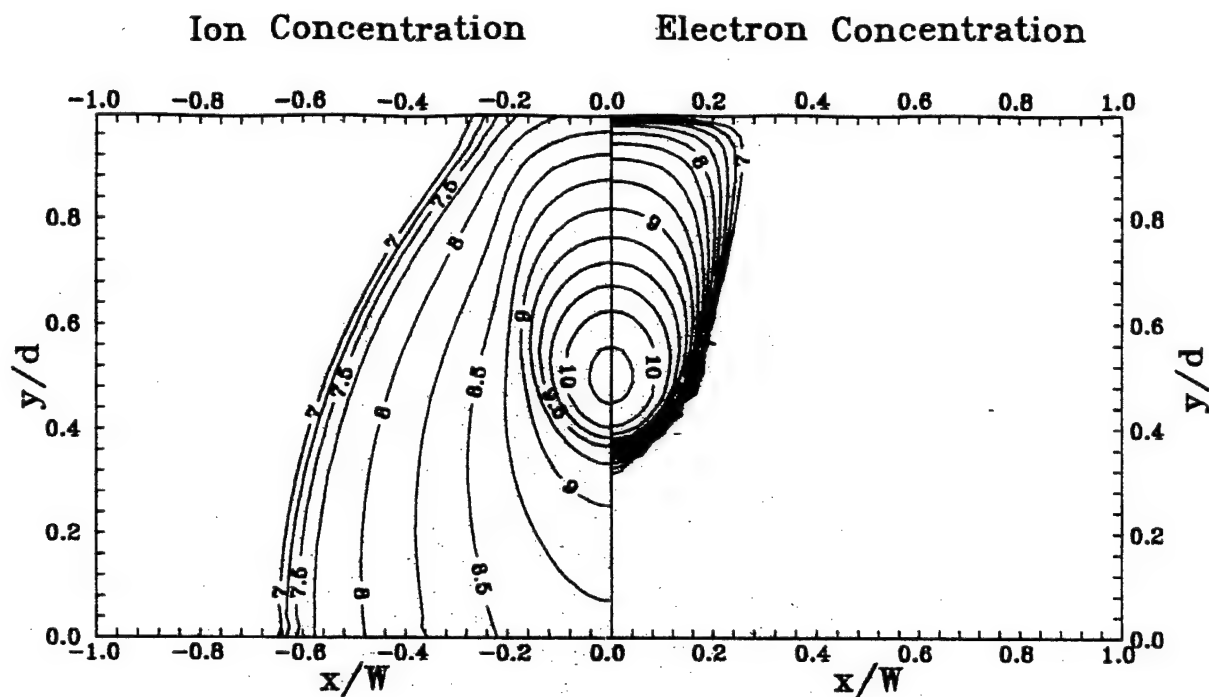
Figure 3. Calculated electron and ion concentration distributions (log scale, in cm^{-3}) in the DC discharge in the optically pumped CO/Ar plasma. $S_0=1.0\cdot10^{15}$ cm^{-3}sec^{-1}, $\beta=2\cdot10^{-6}$ cm^3/sec, U=200 V

Electric Potential
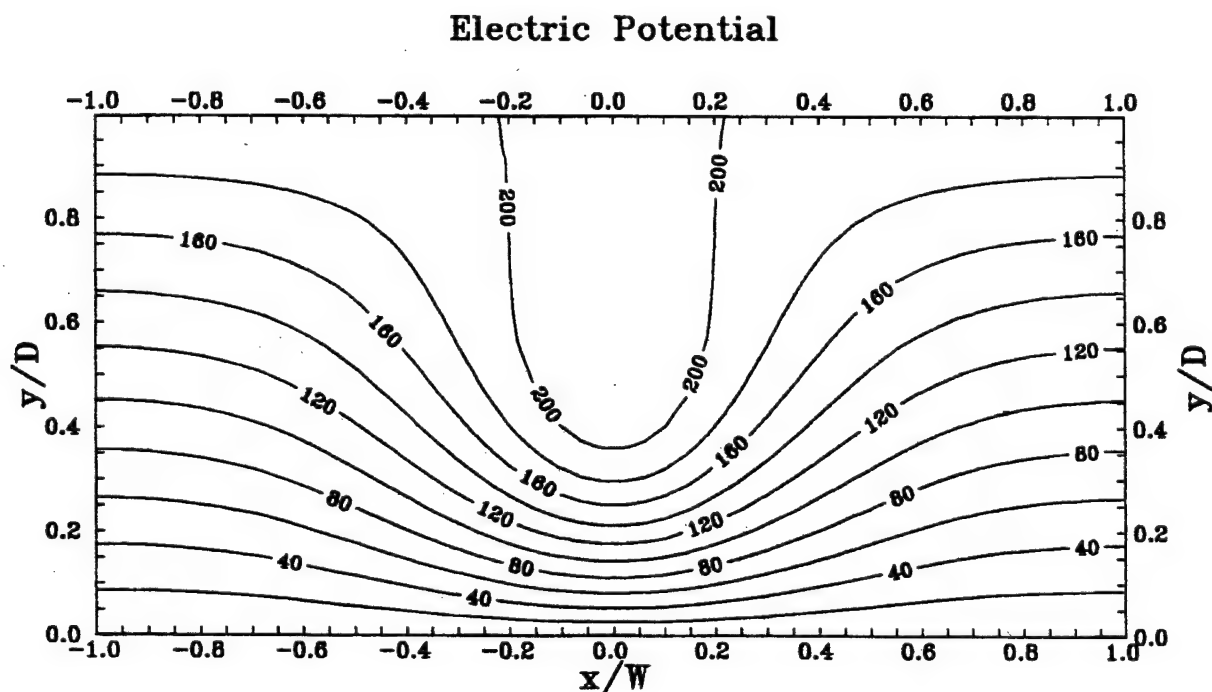
Figure 4. Calculated electric potential distribution (in Volts) in the DC discharge in the optically pumped CO/Ar plasma. $S_0=1.0\cdot10^{15}$ cm^{-3}sec^{-1}, $\beta=2\cdot10^{-6}$ cm^3/sec, U=200 V

Centerline electron concentration, cm^{-3}
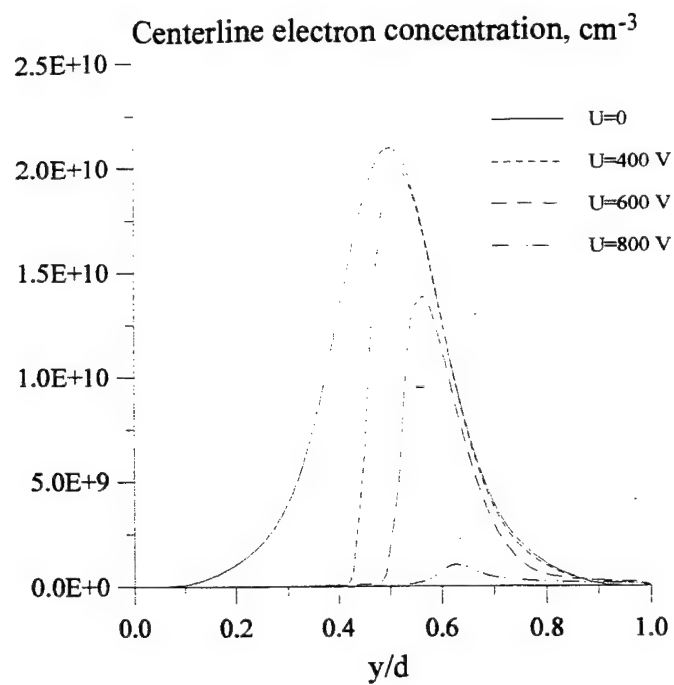
Figure 5. Calculated electron concentration in the CO/Ar plasma at the axis of symmetry of the discharge (x=0) for the conditions of Fig. 2

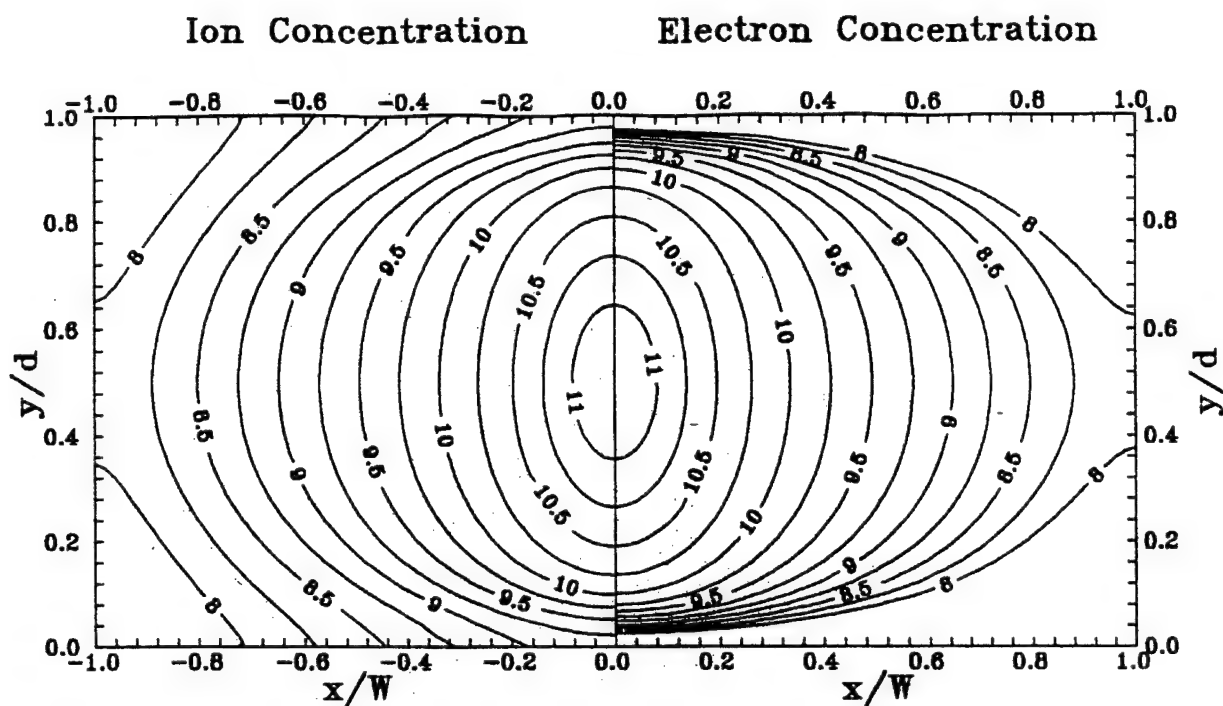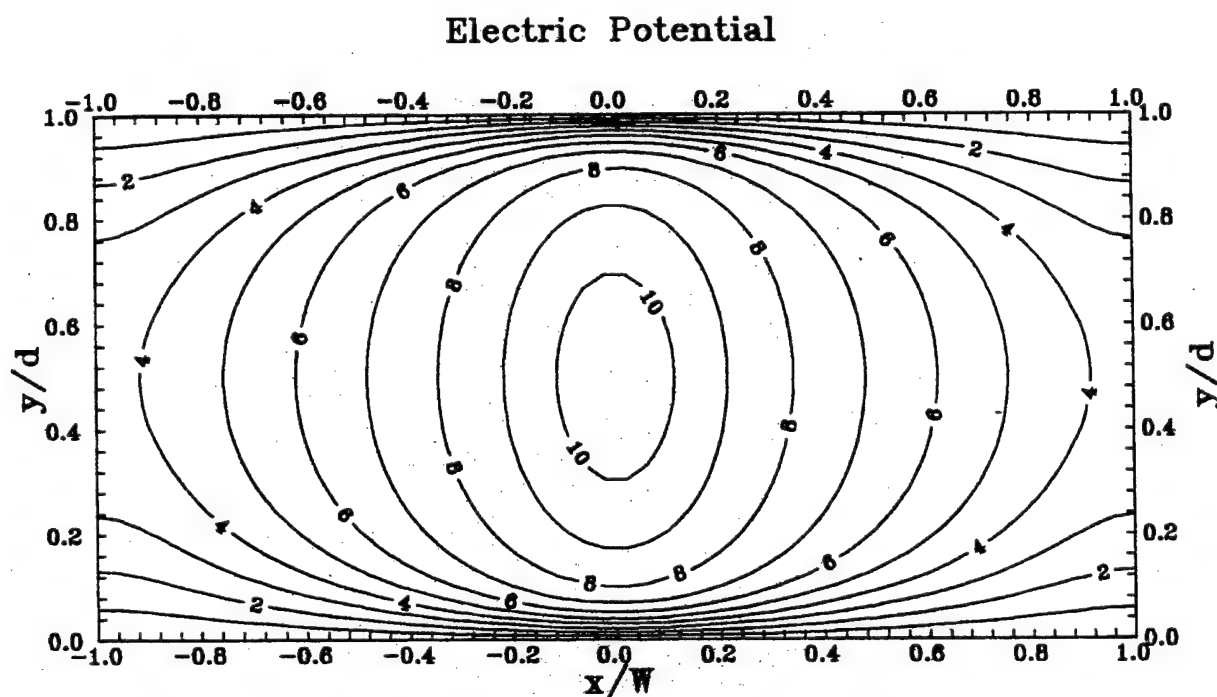Ion Concentration Electron Concentration

Figure 6. Calculated period-averaged electron and ion concentration distributions (log scale, cm^{-3}) in the RF discharge in the optically pumped CO/Ar plasma. $S_0 = 1.0 \cdot 10^{15}$ $cm^{-3}sec^{-1}$, $\beta = 2 \cdot 10^{-8}$ cm^3/sec

Electric Potential

Figure 7. Calculated period-averaged electric potential distribution (in Volts) in the RF discharge in the optically pumped CO/Ar plasma. $S_0 = 1.0 \cdot 10^{15}$ $cm^{-3}sec^{-1}$, $\beta = 2 \cdot 10^{-8}$ cm^3/sec

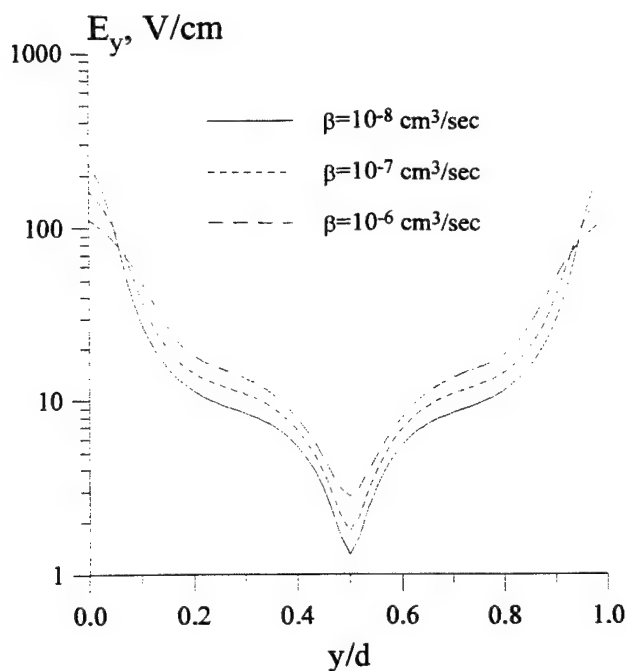Figure 8. Calculated y-component of the RMS electric field in CO/Ar plasma at the axis of symmetry of the RF discharge (x=0).
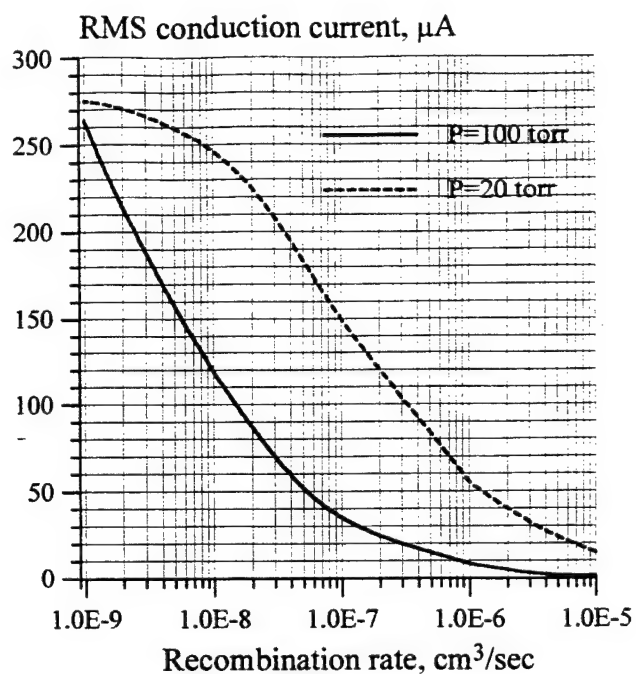

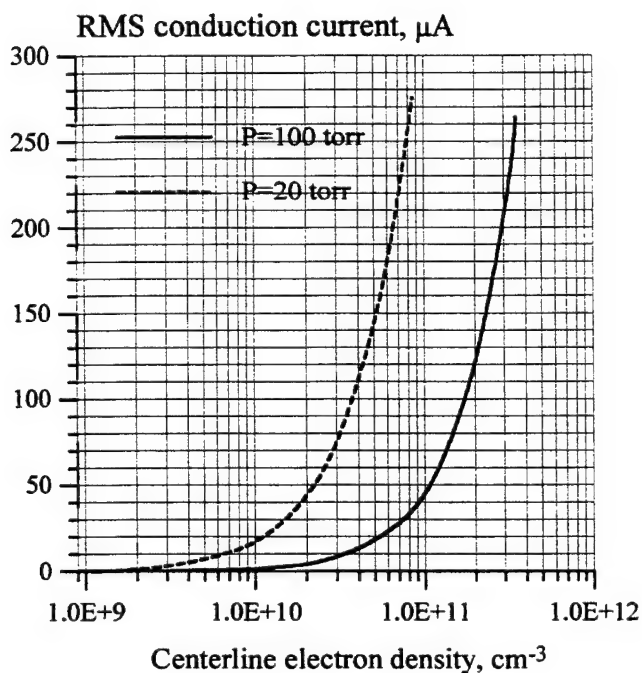Figure 9. Calculated RMS conduction current of the RF discharge as a function of the recombination rate coefficient.

Figure 10. Calculated RMS conduction current of the RF discharge as a function of the electron density at the laser beam axis.

60

CHAPTER IV

SPATIALLY RESOLVED RAMAN MEASUREMENTS OF N_2 VIBRATIONAL LEVEL POPULATIONS IN OPTICALLY PUMPED PLASMAS

1. Introduction

Creating a high-pressure, low-temperature, large-volume plasma has been a challenge to the fields of gas discharge physics and engineering. Large-volume plasmas have traditionally been established at low pressure. At high pressures plasmas become constricted due to rapid instability development. While heating can increase the electron production and diffusion rates, it can quickly lead to runaway ionization due to the ionization heating instability. The runaway ionization causes the glow-to-arc collapse occurring in high-pressure plasmas. By utilizing an ionization method that does not rely on electron impact ionization, it is possible to prevent the thermal instability [1].

The associative ionization mechanism of Eq. (1) produces free electrons in collisions of two vibrationally excited molecules

$$AB(w) + AB(x) \rightarrow (AB)_2^+ + e^-$$
$$E_w + E_x > E_{ion}$$

(1)
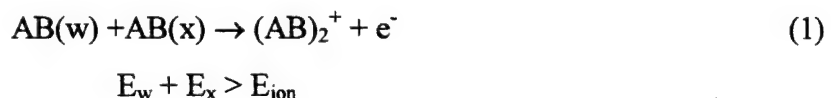
Here E_{ion} is the ionization potential for the molecule of interest. In the case of the CO molecule the ionization potential is on the order of 14 eV.

Associative ionization is produced by collisions of molecules with the total vibrational energy of the collision partners exceeding that of the ionization potential. This type of ionization has been previously observed in CO/Ar and CO/N_2 optically pumped plasmas [2-6]. It has been accomplished by resonance absorption of CO laser radiation followed by vibration-to-vibration (V-V) anharmonic up-pumping [7]. These processes are shown in Eq. (2,3), where v and w are vibrational quantum numbers.

$$CO(v) + h\nu \rightarrow CO(v+1) \tag{2}$$

$$CO(v) + CO(w) \rightarrow CO(v-1) + CO(w+1) \tag{3}$$
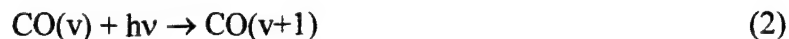
The result is a significant population of high vibrational levels of CO molecules. These molecules can then undergo the associative ionization mechanism illustrated by Eq. (1). It is important to note that while the CO vibrational mode energy at these conditions is a few thousand degrees Kelvin, the translational/rotational temperature never exceeds a few hundred degrees.

While this method can create high-pressure, low-temperature plasmas, it does not produce a large-volume discharge. The optically pumped plasma created by this method is confined to the volume defined by the incident CO laser beam. Outside of the CO laser beam the electrons rapidly recombine and diffusion of the vibrationally excited species is limited due to the high pressure of the system. Additionally, the vibrationally excited species diffusing out of the excitation volume quickly relax to the ground vibrational state.

The main objective of this paper is to demonstrate experimentally the volume increase of the optically pumped plasma outside of the region defined by the incident CO laser beam when an external sub-breakdown RF field is applied. When applied, the RF field couples additional power to the CO and N_2 vibrational energy modes by electron impact excitation. In this case, additional vibrational excitation of both CO and N_2 is produced by free electrons heated by the applied RF field [1]. This in turn produces additional ionization of these species by the associative ionization mechanism of Eq. (1). Note that in the present experiments, the reduced electric field, E/N, is sufficiently low to preclude field-induced electron impact ionization. In the present work, this effect is studied by measuring spatially resolved spontaneous Raman spectra of N_2 with and without an applied RF field.

2. Experimental

A schematic of the experimental set-up is shown in Figs. 1 and 2. A broadband continuous wave CO laser having output at the first 10-12 fundamental bands of CO is used to irradiate a gas mixture. The mixture consists of nitrogen containing approximately 1.5% CO and

trace amounts (approximately 300 ppm) of NO. The total pressure of the gas mixture is approximately 300 torr. The residence time of the gases in the cell is approximately 1 second. The cryogenically cooled CO laser was designed in collaboration with the University of Bonn and constructed at The Ohio State University. It is tuned to emit a substantial percentage of its power on the $v=1 \rightarrow 0$ and $v=2 \rightarrow 1$ fundamental transitions with the majority of the remaining power output in the next 10 vibrational bands. The total output of the laser is approximately 10-15 W.

The output of the CO laser is focused into a six arm cross pyrex absorption cell containing the gas mixture. Focusing the beam increases the power loading per CO molecule along the laser beam. This produces an optically pumped region approximately 2 mm in diameter and 10 cm long. Two circular copper electrodes (3 cm diameter) placed above and below the path of the CO laser beam are used to apply the RF field to the optically pumped plasma. The absorption cell is supported by a vertical translation stage fitted with a micrometer that produced precision movement on the order of ±0.005 mm. This setup permitted the movement of the Raman laser probe beam vertically with respect to the optically pumped plasma.

A nonequilibrium vibrational mode energy distribution of the cell gases is produced by anharmonic V-V up-pumping. In particular, irradiating the gas mixture with a CO laser tuned to the lowest 10-12 vibrational transitions leads to the vibrational excitation of CO molecules to vibrational levels from $v=1$ to $v=10-12$ by direct resonance absorption. Higher vibrational levels $v \sim 10-40$, which are not accessible to the laser, are populated by V-V energy transfer.

In the laser excited CO/N_2 plasma, vibrational energy transfer in collisions between vibrationally excited CO molecules and N_2 molecules also causes vibrational excitation of nitrogen. As shown in Eq. (4)

$$CO(w) + N_2(v) \rightarrow CO(w-1) + N_2(v+1) \tag{4}$$
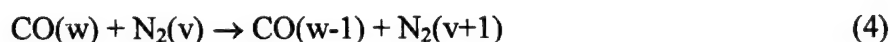
N_2 can be vibrationally excited although it is not directly coupled to the incident CO laser radiation.

Presence of free electrons in the gas mixture may also lead to vibrational excitation of molecular species by electron impact. Basically, free electrons heated by the applied electric field primarily lose their energy by collisional energy transfer to vibrational energy modes of the diatomic species.

$$CO(w) + e^- \rightarrow CO(w+\Delta w) + e^- \qquad (5)$$

$$N_2(w) + e^- \rightarrow N_2(w+\Delta w) + e^- \qquad (6)$$
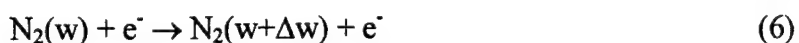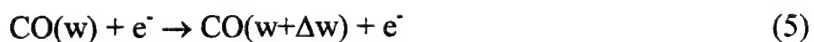
By heating free electrons created by associative ionization of vibrationally excited molecules with an applied RF field, vibrational nonequilibrium can be attained outside of the volume occupied by the CO laser beam. In this experiment, two copper electrodes are placed above and below the optically pumped plasma with a separation of approximately 13 mm. Connected to these electrodes is a 13.56 MHz, 600W ENI ACG-6B RF power supply via a modified MFJ-949E tuner, which is used for plasma impedance matching. Tuning the impedance so that the reflected RF power does not exceed 5-10% of the forward power was typical for these experiments. Setting the output wattage of the RF power supply to 100 W produced a peak-to-peak voltage of 4 kV measured by a high voltage probe. At these conditions, the peak reduced electric field did not exceed $E/N \approx 1 \cdot 10^{-16}$ V·cm^2 [1]. This low value of the reduced electric field precludes electron impact ionization and ionization instability development. Therefore, electrons in the optically pumped plasma enhanced by the RF field are produced only by the associative ionization mechanism.

In these present experiments, the gas mixture in the cell contains approximately 300 ppm of nitric oxide. Addition of trace amounts of NO to the optically pumped plasma is necessary to increase the electron number density. Previous experiments in CO/Ar glow discharge plasmas [8] showed that the dominant ions in the discharge are dimer ions, $(CO)_2^+$, and cluster ions of the general form $C_n(CO)_2^+$, n=1-15. However, adding a few tens of millitorr of O_2 to these gas mixtures resulted in nearly complete disappearance of these ions and their replacement by O_2^+

ions. Note that the electron-ion dissociative recombination rate of the dimer $(CO)_2^+$ ion, $\beta=2\cdot10^{-6}$ cm^3/s [9], greatly exceeds the rate of recombination of the monomer O_2^+ ion, $\beta=(3-5)\cdot10^{-8}$ cm^3/s [10]. The recombination rate of the large carbon cluster ions can possibly be even higher. Our previous measurements [11] showed that electron density in the optically pumped CO/Ar and CO/N_2 plasmas can be considerably increased by adding small amounts of O_2 and NO. This might occur due to a similar process, i.e. destruction of the rapidly recombining carbon-based cluster ions and their replacement by the slowly recombining monomer ions, such as O_2^+ and NO^+.

To acquire spontaneous Raman spectra of the optically pumped plasma, a pulsed Nd:YAG laser tuned to the second harmonic (532 nm) and operated at 10 Hz was used to probe the gas mixture. Each laser pulse has an output energy of 200 mJ and a duration of approximately 10 ns. The Nd:YAG laser probe beam was combined with the CO laser pump beam using a 90° CaF_2 dichroic mirror which was coated to allow transmission of the CO laser beam while reflecting the Nd:YAG beam. Spatial resolution of the Raman spectra was enhanced by focusing of the probe beam using a 0.4 m focal length lens. A notch filter was used to attenuate the 532 nm line resulting from elastic scattering. The Stokes shifted signal was in the range of 600 to 612 nm, which is well outside the attenuation profile of the notch filter. To maximize the signal to noise the image of the plasma was rotated using 2 inch diameter mirrors so that the it was oriented parallel to the vertical input slit of the OMA spectrometer. In addition the signal was focused with $f/4$ lenses to match the 0.25 meter $f/4$ spectrometer. This resulted in a solid angle of approximately 0.049 sr, corresponding to an area defined by the monochromator slits and probe beam of approximately 2mm in length by 100 μm in height. The detector used to acquire the Stokes shifted signal was a microchannel plate intensified charge-coupled device (ICCD) camera. By using a pulser to gate the intensifier the signal to noise increased by eliminating much of the spontaneous emission from the optically pumped cell. The quantum efficiency of the detector was on the order of 6% at the Stokes wavelength and the signal was integrated for a duration of 30s. Within the monochromator, a 1800 line/nm grating was used which resulted in a spectral resolution of approximately 1.5 $\Rightarrow$ and a spectral range of approximately 10 nm. The resolution was adequate to resolve the individual Q-branch vibrational bands, but insufficient to obtain any rotational fine structure.

Uncertainty in the relative band intensities of the Raman spectra of the laser-excited plasma from which the experimental vibrational level populations are derived is estimated to be 10%-20%. For Raman spectra of the optically pumped plasma enhanced by the RF field, the uncertainty is somewhat greater (20-25 %) due to a lower signal-to-noise ratio. Uncertainty in the ratio of vibrational populations of levels v=0 and v=1 is estimated to be 6%.

3. Kinetic model

The two-dimensional time-dependent model of the non-self-sustained RF discharge used in the present optical pumping experiments incorporates the equations for electron and positive ion concentrations, as well as the Poisson equation for the electric field:

$$\frac{\partial n_k(x,y,t)}{\partial t} + \nabla \vec{\Gamma}_k = Q_k ,$$

$$\vec{\Gamma}_k = D_k \nabla n_k(x,y,t) - \frac{q_k}{|e|}\mu_k \nabla \phi(x,y,t) n_k(x,y,t)$$

$$n_k(x,0,t) = n_k(x,d,t) = 0, \quad \frac{\partial n_k(0,y,t)}{\partial x} = \frac{\partial n_k(\pm W,y,t)}{\partial x} = 0$$

$$n_k(x,y,0) = 0$$

(7)

$$\nabla^2 \phi(x,y,t) = \frac{1}{\varepsilon_0}\sum_k q_k n_k(x,y,t) ,$$

$$\phi(x,0,t) = 0, \quad \phi(x,d,t) = U_0 \cos(2\pi \nu t), \quad \frac{\partial \phi(0,y,t)}{\partial x} = \frac{\partial \phi(\pm W,y,t)}{\partial x} = 0$$

(8)

$$\phi(x,y,0) = U_0 y / d$$

$$Q_e = S - \beta n_e n_+$$
$$Q_+ = S - \beta n_e n_+$$

(9)

In Eqs. (7-9), the index k stands for electrons and positive ions, e is the electron charge, n_k and $q_k = \pm e$ are the species concentrations and charges, D_k, μ_k, and $\vec{\Gamma}_k$ are the species diffusion coefficients, mobilities, and fluxes (conduction current density vectors), respectively, ϕ and

$\bar{E} = -\nabla\phi$ are the electric potential and electric field, $\bar{j} = \sum q_k \bar{\Gamma}_k$ is the electric current, d is the separation between the electrodes, W is the electrode half-width, U_0 and ν are the applied voltage amplitude and frequency, S is the rate of electron production by the associative ionization mechanism of Eq. (1), and β is the electron-ion recombination coefficient.

Equations (7-9) are accompanied by equations for vibrational energies of two diatomic species, CO and N_2, as well as the translational-rotational energy equation:

$$\frac{\partial \varepsilon_{vib,j}(x,y,t)}{\partial t} + \nabla\left[D_j \nabla \varepsilon_{vib,j}(x,y,t)\right] = R_j^{las} + R_j^{field} - R_j^{rel},$$

$$\varepsilon_{vib,j}(x,0,t) = \varepsilon_{vib,j}(x,d,t) = \varepsilon_{vib,j}(\pm W,y,t) = \varepsilon_{vib,j}(T_o), \quad \frac{\partial \varepsilon_{vib,j}(0,y,t)}{\partial x} = 0 \qquad (10)$$

$$\varepsilon_{vib,j}(x,y,0) = \varepsilon_{vib,j}(T_o)$$

$$\tfrac{5}{2}kN\frac{\partial T(x,y,t)}{\partial t} + \nabla\left[\lambda\nabla T(x,y,t)\right] = kN(y_{CO}R_{CO}^{rel} + y_{N_2}R_{N_2}^{rel}),$$

$$T(x,0,t) = T(x,d,t) = T(\pm W,y,t) = T_o , \quad \frac{\partial T(0,y,t)}{\partial x} = 0 \qquad (11)$$

$$T(x,y,0) = T_o$$

In Eqs. (10,11), $\varepsilon_{vib,j}$ is the average vibrational energy per molecule, the index j stands for CO or N_2, k is the Boltzmann constant, N is the number density, y_{CO} and y_{N2} are mole fractions of CO and N_2 in the mixture, and R_j^{las}, R_j^{field}, R_j^{rel} are the rates of vibrational excitation by the laser and electron impact and vibrational energy relaxation, respectively.

It is well known that the vibrational distribution functions (VDF) of diatomic species at the conditions of extreme vibrational disequilibrium sustained by the combined laser and electric field excitation can be strongly non-Boltzmann. Determination of the vibrational level populations of CO and N_2 in such nonuniform plasmas, $f_{v,j}$, would require solution of master equation, i.e. approximately 100 coupled 2-D partial differential equations of the general form

$$\frac{\partial f_{v,j}(x,y,t)}{\partial t} + \nabla\left[D_j \nabla f_{v,j}\right] = \left(\begin{array}{c} Laser \\ Excitation \end{array}\right)_{v,j} + \left(\begin{array}{c} Electron \\ Impact \end{array}\right)_{v,j} \tag{12}$$
$$+ (V-T)_{v,j} + (V-V)_{v,j} + (V-E)_{v,j},$$

which would be rather computationally intense. In Eq. (12), $f_{v,j}$ are the relative populations of vibrational levels (vibrational distribution function) and v is the vibrational quantum number. The explicit expressions for the terms in the right-hand-side of Eq. (12) can be found in [12]. The present kinetic model retains only two equations for the vibrational energy modes of CO and N_2 $\varepsilon_{vib,j}$ (Eqs. (10)), obtained from the master equation (12) using the relations

$$\varepsilon_{vib,j} = \sum_v \varepsilon_{v,j} f_{v,j}; \quad \varepsilon_{v,j} = \omega_{e,j} v\left[1 - x_{e,j}(v+1)\right], \tag{13}$$

where $\omega_{e,j}$ and $x_{e,j}$ are the vibrational frequency (in K) and the anharmonicity of the molecules. The vibrational distribution functions (VDFs) of CO and N_2, $f_{v,j}$, have been determined using analytical theory of vibration-vibration (V-V) pumped anharmonic oscillators [13], as a steady-state solution of master equation (12) without space diffusion terms,

$$\frac{f_v}{f_0} = \begin{cases} \exp\left(-\frac{E_1 v}{T_v} + \frac{\Delta E v(v-1)}{T}\right); & v \le v_0 = \frac{1}{2} + \frac{T}{2x_e T_v} \\[3mm] \exp\left(-\frac{v_0^2 \Delta E}{T}\right)\left(\frac{v_a - v}{v_a - v_0}\right)^{1/2} \frac{v_0 + 1}{v+1} \\[3mm] -\frac{T}{12\Delta E} \frac{\delta_{VV}^3}{y_j \widetilde{Q}_{10}} \sum_M \frac{y_M P_{10}^M \exp(\delta_{10}^M v)}{\delta_{10}^M} \frac{1}{v+1}; & v > v_0 \end{cases} \tag{14}$$

In Eq. (14), $E_1 = \omega_e(1-2x_e)$, $\Delta E = \omega_e x_e$, $T_v = E_1/\ln(f_1/f_0)$ is the first level vibrational temperature, P_{10}, $\widetilde{Q}_{10}$, δ_{VT}, and δ_{VV} are the parameters in the expressions for the V-T and V-V rate coefficients,

$$P_{v+1,v}^M = P_{10}^M (v+1) \exp(\delta_{VT}^M v) \,, \tag{15}$$

$$Q_{v+1,v}^{w,w+1} = (v+1)(w+1) \left\{ Q_{10}^S \exp\left(-\delta_{VV}|v-w|\right) \left[\tfrac{3}{2} - \tfrac{1}{2}\exp\left(-\delta_{VV}|v-w|\right)\right] \right.$$
$$\left. + Q_{10}^L \exp\left(-\Delta_{VV}(v-w)^2\right) \right\} \,, \tag{16}$$

$$\widetilde{Q}_{10} = Q_{10}^S + \frac{\delta_{VV}^3}{12\Delta_{VV}} \left(\frac{\pi}{\Delta_{VV}}\right)^{1/2} Q_{10}^L \,, \tag{17}$$

y_M is the V-T relaxation collision partner mole fraction, and $v_a=E_a/E_1$ is the activation level of the vibration-to-electronic (V-E) energy transfer process,

$$CO(X^1\Sigma, v \sim 40) + CO \rightarrow CO(A^1\Pi, v \sim 0) + CO \,, \tag{18}$$
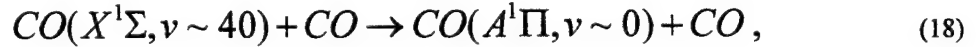
The analytic VDFs of Eq. (14) are in good agreement with steady-state distribution functions obtained by numerical integration of master equation with the V-T and V-V rates given by Eqs. (15,16) [14]. In the present calculations, the two VDFs have been determined iteratively from Eq. (13) using the functional dependence (14) on the first level vibrational temperatures, $T_{v,j}$, as adjustable parameters. This approach greatly reduces the number of equations solved while taking into account the key effect of strongly non-Boltzmann distribution function on the associative ionization rate in the plasma. Note that this approach assumes that both vibrational distributions are quasi-steady-state and that their perturbation by diffusion is weak.

The rate of CO vibrational excitation by resonance absorption of the CO laser radiation, used in Eq. (10), is evaluated as follows [12],

$$R_{CO}^{las} = \sum_{v,J} \frac{A_v B_v}{8\pi ckT} \left(\frac{c}{v}\right)^3 I_v \, \theta \, S_J \exp\left(-\frac{B_v J(J+1)}{T}\right) \varepsilon_v f_v \,, \tag{19}$$

where A_v is the Einstein coefficient for spontaneous radiation, B_v is the rotational constant, v is the laser line frequency, I_v is the laser line power density, θ is the absorption line shape factor, J is the rotational quantum number, and S_J is the Honl-London factor.

The rate of vibrational excitation of CO and N_2 molecules by electron impact in the presence of the RF field is approximated as

$$R_j^{field} = \frac{\bar{j} \cdot \bar{E}}{Nk} \tag{20}$$

The approximation of Eq. (20) is applicable in the range of the reduced electric field $E/N \cong (0.5-5.0) \cdot 10^{-16}$ V·cm^2, where more then 95% of the input electric power, $\bar{j} \cdot \bar{E}$, goes to vibrational excitation of CO and N_2 [10].

The rate of energy relaxation from the vibrational mode of each diatomic species with the vibrational distribution function (VDF) given by Eq. (14) is evaluated as follows [13],

$$\begin{aligned}
R_j^{rel} = E_1 \frac{6\widetilde{Q}_{10}\Delta E}{T\delta_{VV}^3}(v_0+1)^2 \exp\left(-\frac{2v_0^2\Delta E}{T}\right)y_j N \\
+ E_1 Q_{10}^{(01)'} \exp\left(\frac{E_1-E_1'}{T}\right)\left(f_1 f_0' - f_0 f_1'\right)y_j' N ,
\end{aligned} \tag{21}$$

In Eq. (21), the first term in the right-hand-side represents the intra-mode energy relaxation rate due to V-T, V-V, and V-E processes combined, while the second term is the energy relaxation rate due to the V-V′ energy exchange between vibrational modes of CO and N_2,

$$CO(v) + N_2(v') \rightarrow CO(v-1) + N_2(v'+1) \tag{22}$$
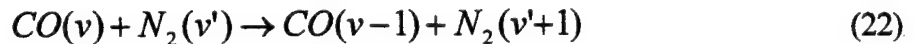
Again, Eq. (21) is in good agreement with the steady-state energy relaxation rate obtained from the numerical solution of the master equation [14].

The electron production rate by the associative ionization mechanism of Eq. (1), used in Eq. (9), is calculated as follows,

$$S = k_{ion} N^2 y_{CO}^2 \sum_{E_v + E_w > E_{ion}} f_{v,CO} f_{w,CO},$$ (23)

The electron and ion mobilities and diffusion coefficients in a nitrogen plasma as functions of the reduced electric field E/N, where N=P/kT is the number density, are taken from [15,16]. The V-V and V-T rates in CO-N_2-He mixtures are taken from [12,17]. The CO pump laser spectum is taken to be the same as in [18].

Direct numerical solution of coupled partial differential equations (7,8,10,11) remains rather problematic due to the fact that the characteristic time scales for reaching the quasi-steady-state distributions of electric field, τ_{RF}~d/w_{dr}, vibrational populations and electron density, τ_{vib}~τ_{ion}~E_1 / R^{rel}, and gas temperature, τ_{HT}~d^2/D, are widely different,

$$\tau_{RF} \sim 10^{-6} \sec \ll \tau_{vib} \sim \tau_{ion} \sim 10^{-4} - 10^{-3} \sec \ll \tau_{HT} \sim 1 \sec$$ (24)

In the above estimates, d~1 cm, w_{dr}=μ_eE~10^6 cm is the electron drift velocity, and D~1 cm^2/s is the diffusion coefficient. The values of τ_{vib} for CO and N_2 are estimated from Eqs. (14,21) for T~300 K, T_v(CO)~3000 K, N~10^{18} cm^{-3}, y_{CO}~0.01, and y_{N2}~1. For this reason, the RMS electric field distribution has been evaluated by integrating Eqs. (7,8) separately, over the time period Δt_1~τ_{RF}, and then assumed to remain unchanged while integrating Eqs. (10,11) over Δt_2~τ_{vib}~τ_{ion}. These two stages were repeated until the steady-state spatial distribution of RMS electric field, RMS charged species concentrations, vibrational level populations, and gas temperature was achieved over Δt_3~τ_{HT}.

In the calculations discussed in the following section, the 3 cm diameter circular electrodes (see Fig. 3) are modeled as square electrodes of the same surface area. The electrode separation and full width are d=1 cm and 2W=2.66 cm. The CO laser beam power distribution is assumed to be Gaussian with the $1/e^2$ radius of 1 mm. Calculations are made for a $CO-N_2$ mixture with 1.4% of CO at P=300 torr. To simulate the effect of additional V-T relaxation produced by addition of small amounts of NO to the plasma, the model gas mixture was also assumed to contain 1% helium. The RF voltage amplitude and frequency are U_0=1500 V and ν=10 MHz, respectively. The system of equations (7,8,10,11) is solved using standard stiff PDE solver PDECOL [19].

4. Results and Discussion

4.1. Experimental Measurements

Previously, it was shown that RF coupling to free electrons produced in an optically pumped CO plasma enhances the vibrational disequilibrium induced in the path of the laser excitation beam [1]. The current results show that this effect is not limited to the volume occupied by the CO laser beam, which is approximately 2 mm in diameter and 10 cm long. Indeed, as can be seen in Figs. 4 and 5, the N_2 Raman spectra band intensities (i.e. the fractional vibrational level populations) increase when the RF field is applied, both at the CO laser beam axis (see Fig. 4), and away from the CO laser beam (see Fig. 5). Note that the Raman spectra with the RF applied have been scaled and baseline corrected to match the intensity of the v=0 peak when the RF is off. This effect is also illustrated in Fig. 6, which shows fractional vibrational level populations. From Fig. 6, one can see that the vibrational level populations for v=1-4 become greater when the RF filed is applied. As discussed in Section 2, the RF power is coupled to the vibrational mode of the diatomic molecules via the free electrons produced in the laser-sustained plasma.

Analysis of the spontaneous Raman spectra of N_2 provides insights into the vibrational population distribution. The vibrational state fractional populations are proportional to the intensity of the corresponding peaks after scaling by 1/(v + 1). When the spectra of the RF and laser sustained plasmas for a coaxial alignment of the pump and probe beams are compared, the increase in fractional population of states with larger v becomes apparent. By comparing the

relative peak heights a greater fractional population is found in states with larger v for the RF sustained plasma. This is illustrated in the Boltzmann plot for that case Fig. 6.

Similar analysis of the case in which the probe and pump beam are not coaxial show a similar result. At a vertical separation of 2.25 mm, when a RF field is not applied, the vibrational nonequilibrium is diminished. However, when a vertically aligned RF field is applied the vibrational loading of the molecule intensifies. This is demonstrated in the Raman spectra and fractional population analysis shown in Figs. 5 and 6. It is important to note that at each probe position the fractional population of states with higher v becomes greater when a RF field is applied. By subjecting the plasma to the RF field a wider distribution of vibrational states is obtained.

The broadening of the vibrational state distribution may be demonstrated quantitatively by defining an equivalent Boltzmann temperature. The equivalent Boltzmann temperature is the slope of the vibrational distribution function at v=0, defined as follows

$$T_v = \frac{\theta_v}{\ln\left(f_0 / f_1\right)} \tag{25}$$

In Eq. (25), θ_v=3353° K is the characteristic vibrational temperature for N_2 and f_0/f_1 is the ratio of the fractional populations for vibrational levels v=0 and v=1. Illustrated in Fig. 12 are the first level equivalent Boltzmann temperatures for varying degrees of separation between the probe and pump beam in the vertical plane. Note that with a vertical displacement between the probe and pump beam the equivalent Boltzmann temperatures never drop below 2000° K when the RF field is applied, even at a displacement of more than 5 mm. Examining the vibrational temperature at the maximum and minimum displacements exhibits this behavior. At coaxial alignment there is a percent gain of approximately 10%. However, at the maximum displacement the percent gain is almost 60%. It is important to note that the increase in vibrational temperature is not due to simple heating of the species present. The

73

translational/rotational temperature does not approach the vibrational temperature in any of the cases presented.

The translational/rotational temperatures were inferred from the Raman spectra by comparing the peak intensities of a vibrationally pumped sample to that of a vibrationally cold sample. These temperatures were calculated as follows,

$$T_H = T_C * \left(\frac{I_C}{I_H} \right) \tag{11}$$

where T_C is the cold gas temperature (300° K), I_C is the intensity of the cold peak and I_H is the integrated scaled intensity $[1/(v+1)]$ of the peaks in the vibrationally hot spectra. Temperatures inferred from the Raman spectra using this method can be found in Fig. 13. Note that this method provides only a rather crude estimate of the temperature since the rotational band structure is ignored. In addition, at large displacement between the pump and probe beam the probe beam path begins to become blocked, causing the probe beam to scatter. This might well introduce an additional error in the temperature inference. Note that the first level vibrational temperature remains much greater than the translational temperature at all data points measured (see in Figs. 12 and 13).

4.2. Modeling Calculations

Figures 7-10 show contour plots of the calculated first level vibrational temperatures of CO and N_2, as well as the translational temperature and the electron density in optically pumped CO/N_2/He plasmas. The left half of each of these plots refers to the parameter distribution in the plasma sustained by a CO laser alone, while the right half shows distribution of the same parameters in the plasma sustained by a combination of the laser and the RF field. For the laser/RF sustained plasma, the parameters shown have been averaged over the RF field oscillation period. From Figs. 7 and 8, it can be seen that applying the RF field to the optically pumped plasma produces a stronger vibrational disequilibrium, with vibrational temperatures of both CO and N_2 considerably increasing (from $T_v(CO)$=3700 K to 4300 K and $T_v(N_2)$=2500 K to 2900 K on the laser beam centerline). Note that with the RF field turned on the size of the

vibrationally nonequilibrium region also substantially increases (roughly by a factor of 2 in the x-direction).

Calculations of the energy balance in the plasma shows that the absorbed laser power in the region between the electrodes is 0.9 W, while the RF power coupled to the plasma is greater by approximately a factor of 2, 1.9 W. In other words, using the sub-breakdown RF field nearly triples the total power added to the plasma. More rapid vibrational energy relaxation in V-V exchange processes in the laser/RF sustained plasma produces additional heat removed from the plasma by conduction. Diffusion of vibrationally excited molecules provides another channel of energy removal from the plasma. In the present calculations, convective cooling of the gas mixture in the slow-flow absorption cell is neglected. From Fig. 9, one can see that the calculated translational temperature on the laser beam axis increases from T=470 K in the laser-sustained plasmas to T=600 K in the laser/RF sustained plasma.

Analysis of Fig. 10 shows that the electron density in the presence of the RF field is greatly reduced, from $n_e=0.8 \cdot 10^{11}$ cm^{-3} to $0.6 \cdot 10^{10}$ cm^{-3}. This result is not surprising since additional heating produced by relaxation processes in the presence of the RF field considerably increases the V-T rates (especially among the high vibrational levels of CO). This results in depletion of the high CO vibrational level populations (at v≥30-35), as shown in Fig. 11, and reduces the rate of ionization by the associative ionization mechanism. This effect, i.e. the negative feedback between the temperature rise and the ionization rate self-stabilizes the plasma and precludes the ionization-heating instability development. On the other hand, the same effect self-limits the amount of RF power coupled to the plasma. However, the electron density and consequently the power coupled to the plasma can both be increased by reducing the translational temperature (e.g. using convective cooling of the plasma in a fast-flow absorption cell). This may considerably increase energy stored in vibrational mode energies of CO-containing molecular gas mixtures at high pressures.

Figure 12 compares the measured and the calculated N_2 vibrational temperatures in the plasma along the line between the electrode centers. One can see that in the absence of the RF field the agreement is quite satisfactory. With the RF field turned on, the calculated vibrational

75

temperature turns out to be somewhat lower than in the experiment. The difference between the experiment and the calculations is within 20% except for one data point taken at y/d=0.94, or less than 1 mm away from the bottom electrode. We believe that at this location scattering of the probe Nd:YAG laser beam off the electrode surface might considerably increase the uncertainty in the measured vibrational level populations. Additional measurements with a smaller separation between the measurement points are necessary to estimate reproducibility of the data and the magnitude of this effect.

Figure 13 shows the measured and the calculated translational temperature of the plasma along the line between the electrode centers. Again, with the RF field turned off and far from the electrodes the agreement is satisfactory. However, temperature measured closer to the bottom electrode (within 2.5 mm) appears to be considerably higher than on the laser beam centerline. The same effect is observed with the RF field turned on (see Fig. 13). Again, probe laser beam scattering off the electrode surface might account for this counterintuitive behavior of the gas temperature in both these cases. With the RF field on, the discrepancy between the calculated and the measured temperature becomes quite substantial, up to 50-100% (see Fig. 13). There are two most likely reasons for such considerable disagreement. First, the translational temperature inferred from the intensities of the rotationally unresolved vibrational bands of the Raman spectra (see Section 2) can be considered only as a fairly crude estimate, since the individual rotational line contribution is not taken into account. Second, there is a considerable uncertainty in the pivotal parameter of the kinetic model controlling the steady-state ionization rate and therefore the RF power coupled to the plasma (as well as the gas temperature), i.e. the temperature dependence of the CO V-T rates among the high vibrational levels ($v \geq 30$-35). Weak V-T rate temperature dependence would produce a fairly strong gas heating before the CO vibrational populations would be depleted thereby slowing down the ionization. On the other hand, steep rise of the V-T rates with temperature would slow down the ionization at more moderate temperatures.

These V-T rates are most likely controlled by collisions of highly vibrationally excited CO molecules with fast relaxer trace species, such as products of the CO disproportionation reaction, including carbon clusters, or NO molecules present in the plasma. Currently, the data

on the rates of these processes are not available. Therefore, in the present calculations, the self-termination of ionization by V-T relaxation is modeled semi-qualitatively, by adding 1% of helium to the baseline CO/N_2 mixture, which might well affect the accuracy of the model predictions. Additional temperature measurements in $CO/N_2/He$ optically pumped plasmas using the rotationally resolved Raman spectra [20] are needed to resolve this issue.

5. References

1. E. Ploenjes, P. Palm, W. Lee, W. R. Lempert, and I.V. Adamovich, "RF Energy Coupling to High-Pressure Optically Pumped Plasmas." Journal of Applied Physics, vol. 89, No. 11, 2001, pp. 5911-5918

2. W. Lee, I.V. Adamovich, and W.R. Lempert, "Optical Pumping Studies of Vibrational Energy Transfer in High-Pressure Diatomic Gases", Journal of Chemical Physics, vol. 114, 2001, p. 1178-1186

3. I. Adamovich, S. Saupe, M.J. Grassi, O. Schulz, S. Macheret, and J.W. Rich, Chem. Phys., vol. 173, 1993, p. 491

4. I.V. Adamovich and J.W. Rich, J. Physics D: Applied Physics, vol. 30, 1997, p. 1741

5. E. Plönjes, P. Palm, I.V. Adamovich, and J. W. Rich, "Ionization Measurements in Optically Pumped Discharges", Journal of Physics D: Applied Physics, vol. 33, No. 16, 2000, p. 2049

6. I.V. Adamovich, "Control of Electron Recombination Rate and Electron Density in Optically Pumped Nonequilibrium Plasmas", Journal of Physics D: Applied Physics, vol. 34, 2001, p.319

7. J. W. Rich, "Relaxation of Molecules Exchanging Vibrational Energy", in "Applied Atomic Collision Physics", vol. 3, "Gas Lasers", ed. E.W. McDaniel and W.L. Nighan, Academic Press, New York, 1982, pp. 99-140

8. Y. Kaufman, P. Avivi, F.Dothan, H. Keren, J. Malinowitz, J. Chem. Phys., Vol. 72, 1980, p. 2606

9. R. Johnsen, "Recombination of Cluster Ions", in B.R. Rowe et al. (eds.), "Dissociative Recombination", Plenum, New York, 1993

10. Raizer, Y.P., "Gas Discharge Physics", Springer-Verlag, Berlin, 1991

11. P. Palm, E. Plönjes, M. Buoni, V.V. Subramaniam, and I.V. Adamovich, "Electron Density and Recombination Rate Measurements in CO-Seeded Optically Pumped Plasmas", Journal of Applied Physics, vol. 89, No. 11, 2001, pp. 5903-5910

12. C. Flament, T. George, K.A. Meister, J.C. Tufts, J.W. Rich, V.V. Subramaniam, J.-P. Martin, B. Piar, and M.-Y. Perrin, "Nonequilibrium Vibrational Kinetics of Carbon Monoxide at High Translational Mode Temperatures", Chemical Physics, Vol. 163, 1992, p. 241

13. B.G. Gordiets and S.A. Zhdanok, "Analytic Theory of Ahnarmoinic Oscillators", in Nonequilibrium Vibrational Kinetics, "ed. by M. Capitelli, Springer, Berlin, 1986

14. I.V. Adamovich, S.O. Macheret, and J.W. Rich, "Spatial Nonhomogeneity Effects in Nonequilibrium Vibrational Kinetics", Chemical Physics, vol. 182, 1994, pp. 167-183

15. L.G.H Huxley and R.W. Crompton, "The Diffusion and Drift of Electrons in Gases", Wiley, New York, 1974

16. E.W. McDaniel, "Collision Phenomena in Ionized Gases", Wiley, New York, 1964

17. E. Ploenjes, P. Palm, W. Lee, M. D. Chidley, I.V. Adamovich, W.R. Lempert, and J. William Rich, "Vibrational Energy Storage in High-Pressure Mixtures of Diatomic Molecules", Chemical Physics, vol. 260, 2000, pp. 353-366

18. E. Ploenjes, P. Palm, A.P. Chernukho, I.V. Adamovich, and J.W. Rich, "Time-Resolved Fourier Transform Infrared Spectroscopy of Optically Pumped Carbon Monoxide", Chemical Physics, vol. 256, pp. 315-331, 2000

19. N.K. Madsen and R.F. Sincovec, ACM Trans. Math. Software, vol. 5, 1979, p. 326

20. W. Lee and W.R. Lempert, AIAA Paper 2002-0394
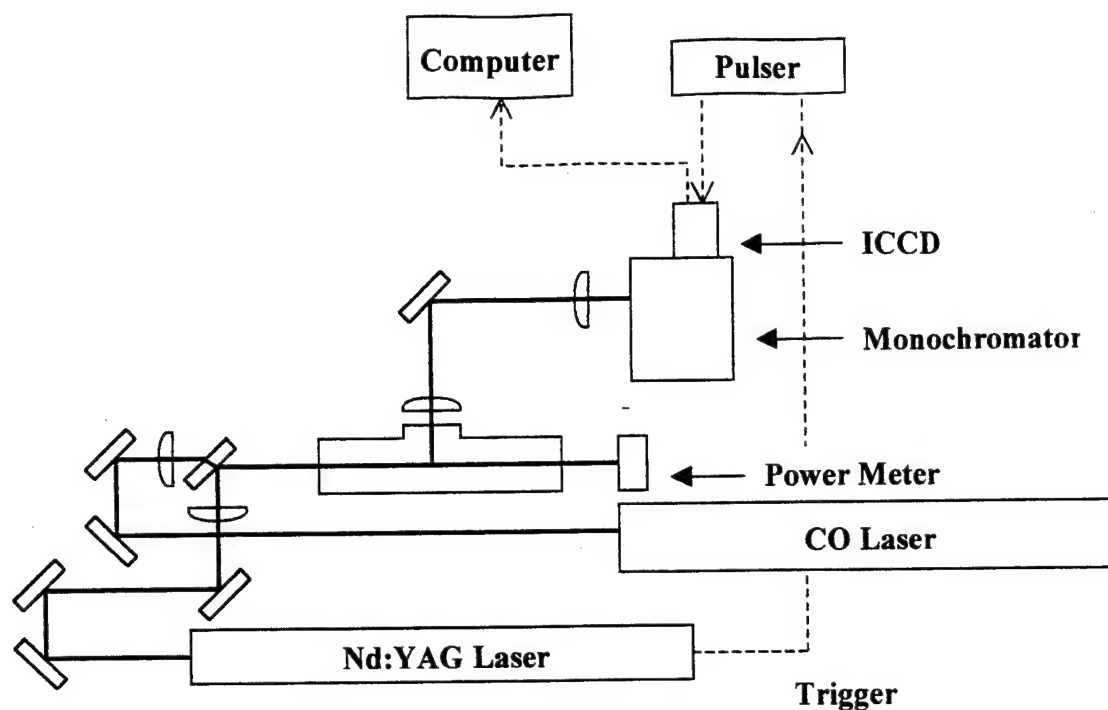
Figure 1. Experimental apparatus for spatially resolved Raman measurements.
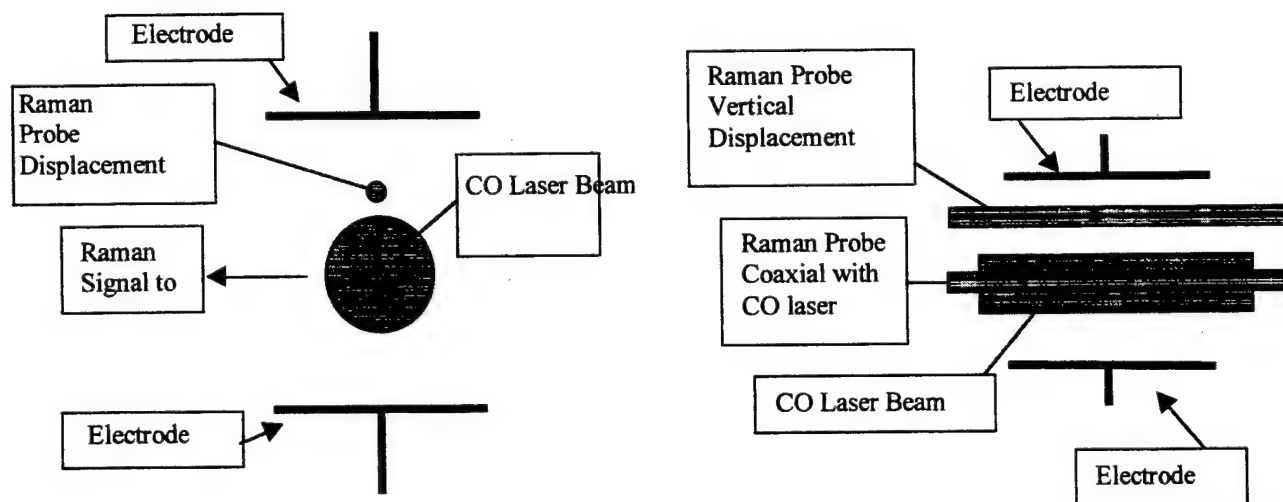

Figure 2. Schematic of electrode arrangement and CO laser and Nd:YAG laser beams at various measurement point locations.
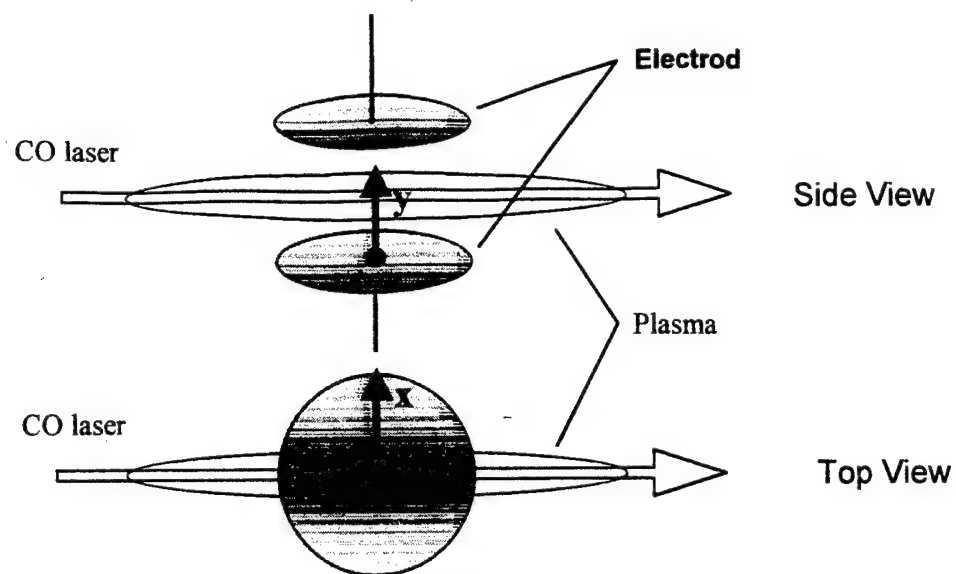
Figure 3. Schematic of electrodes in the cell and of the discharge geometry
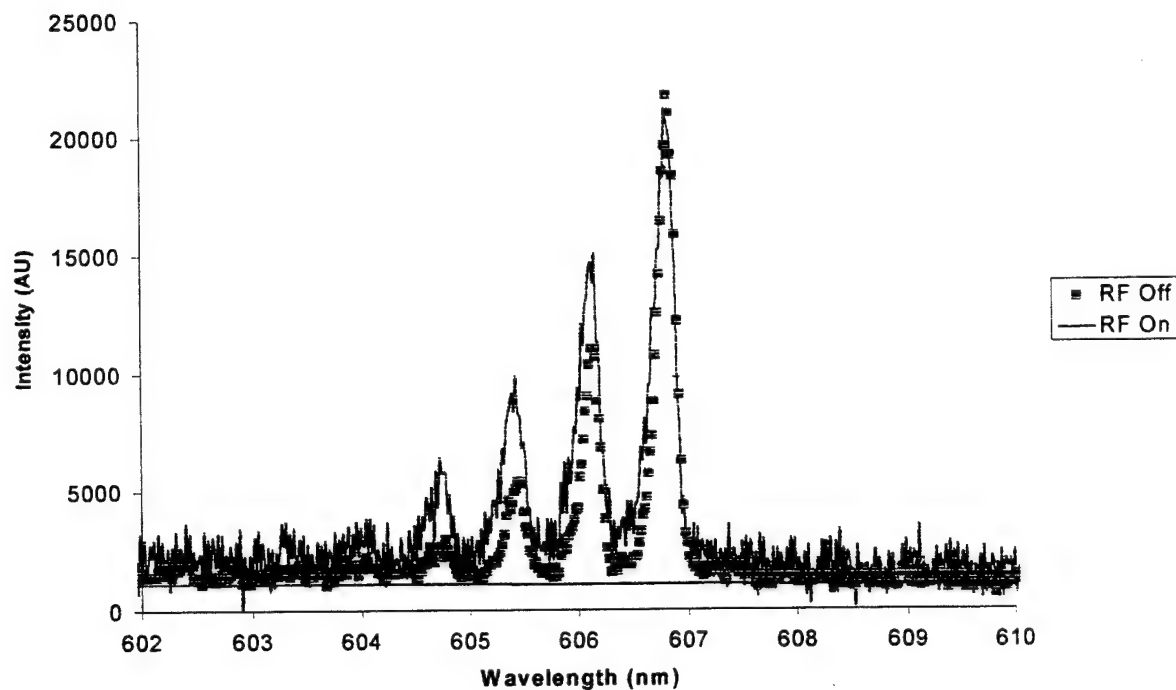
Figure 4. Raman spectra of vibrationally excited N_2 for the coaxial orientation of the pump and the probe laser beams, with the RF field on and off.
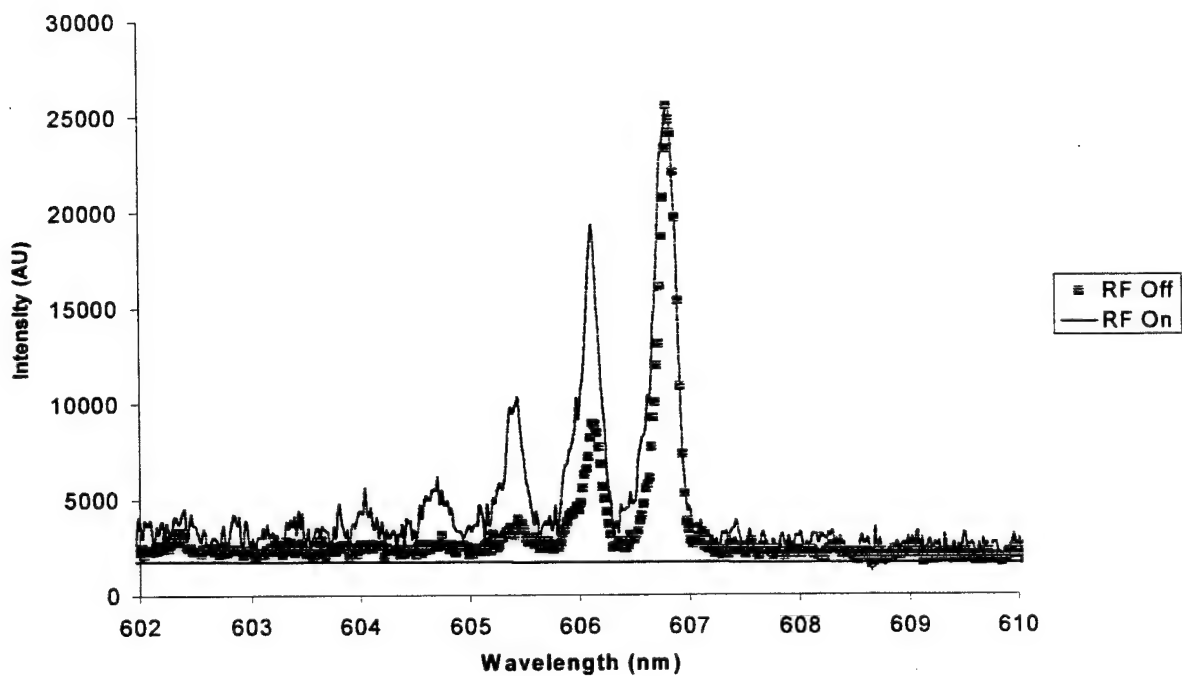

Figure 5. Raman spectra of vibrationally excited N_2 with a 2.25 mm vertical separation between the pump and the probe laser beams, with the RF field on and off.
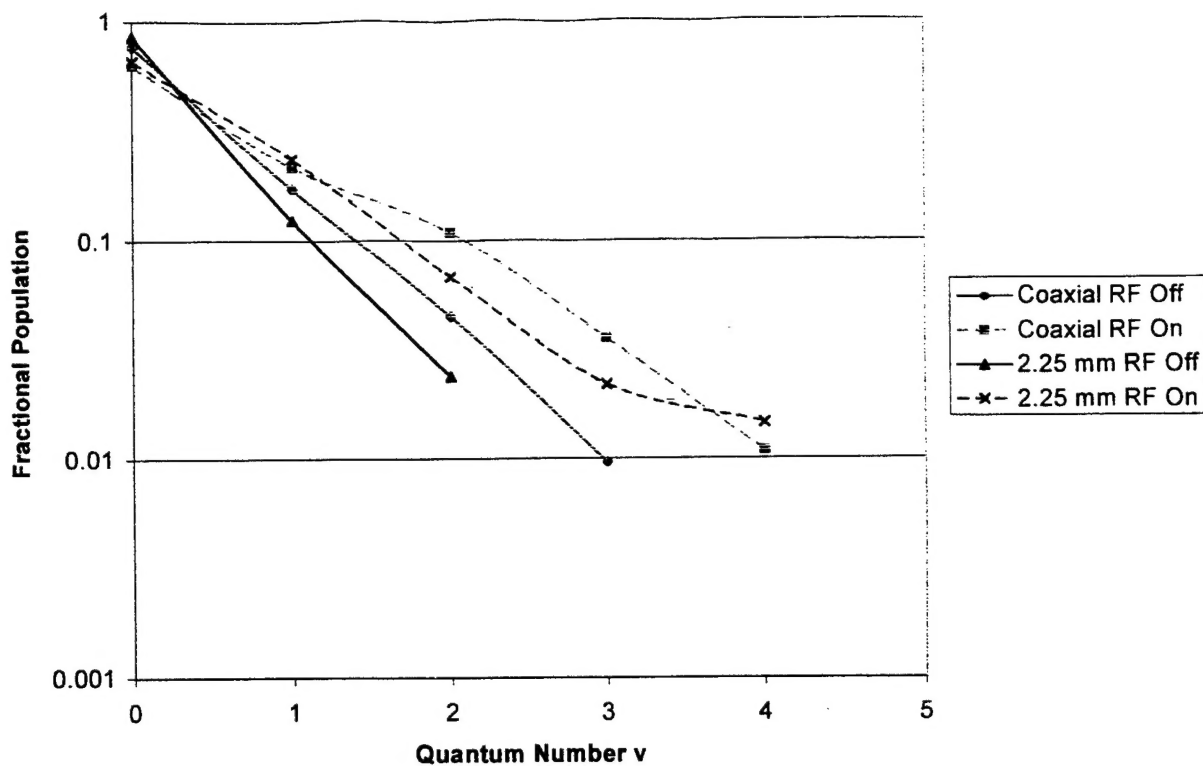
Figure 6. N_2 vibrational level populations for two different locations of the probe laser beam.
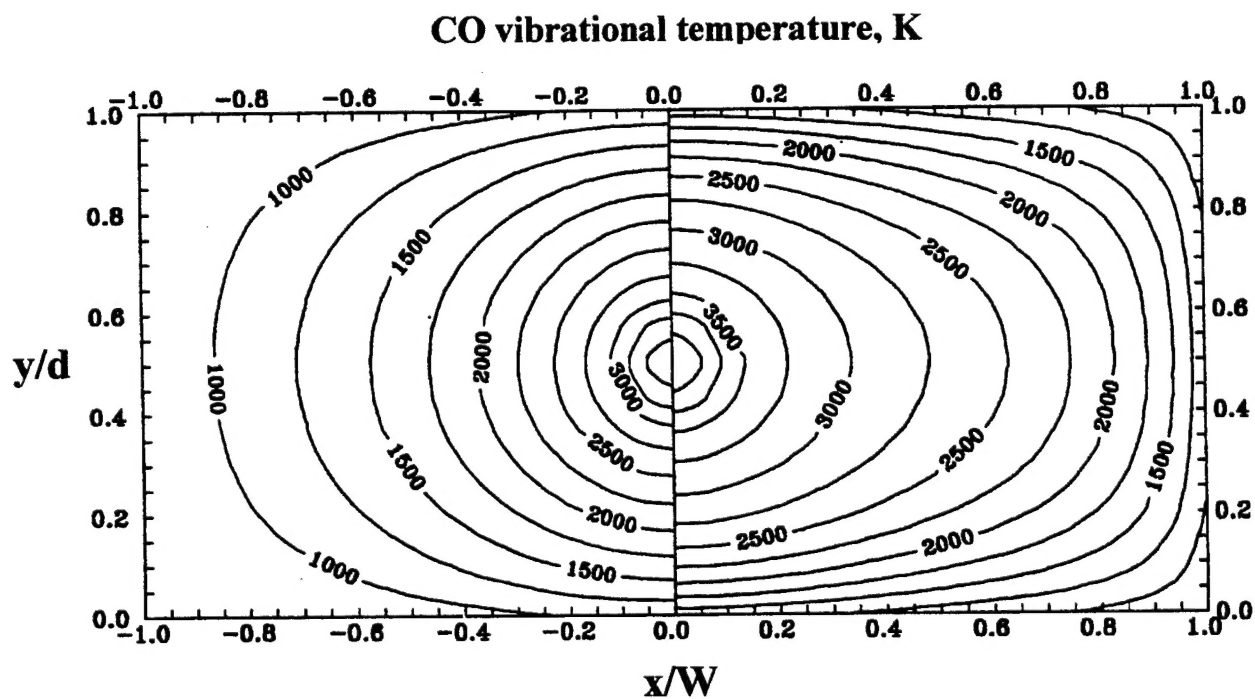
Figure 7. First level vibrational temperature of CO in the optically pumped CO/N_2 plasma without (**left**) and with (**right**) RF field applied.
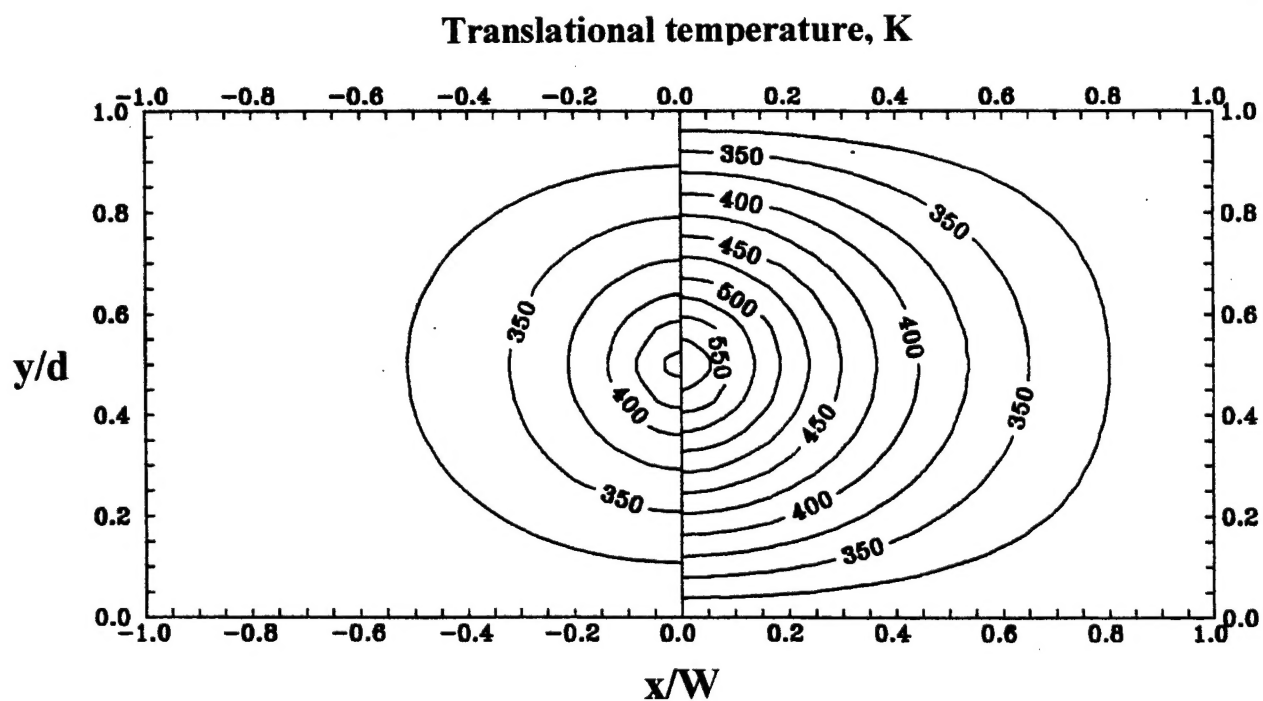
N₂ vibrational temperature, K
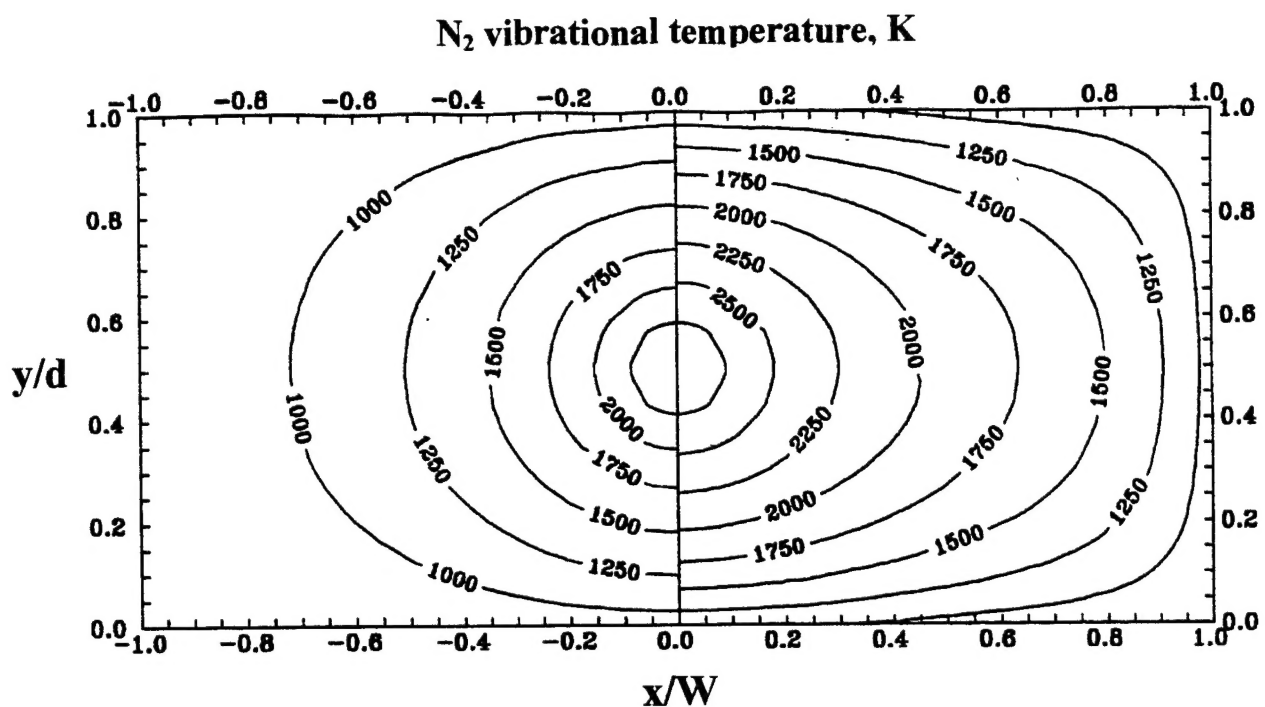
Figure 8. First level vibrational temperature of N_2 in the optically pumped CO/N_2 plasma without (**left**) and with (**right**) RF field applied.

Translational temperature, K

Figure 9. Translational temperature distribution in the optically pumped CO/N_2 plasma without (**left**) and with (**right**) RF field applied.
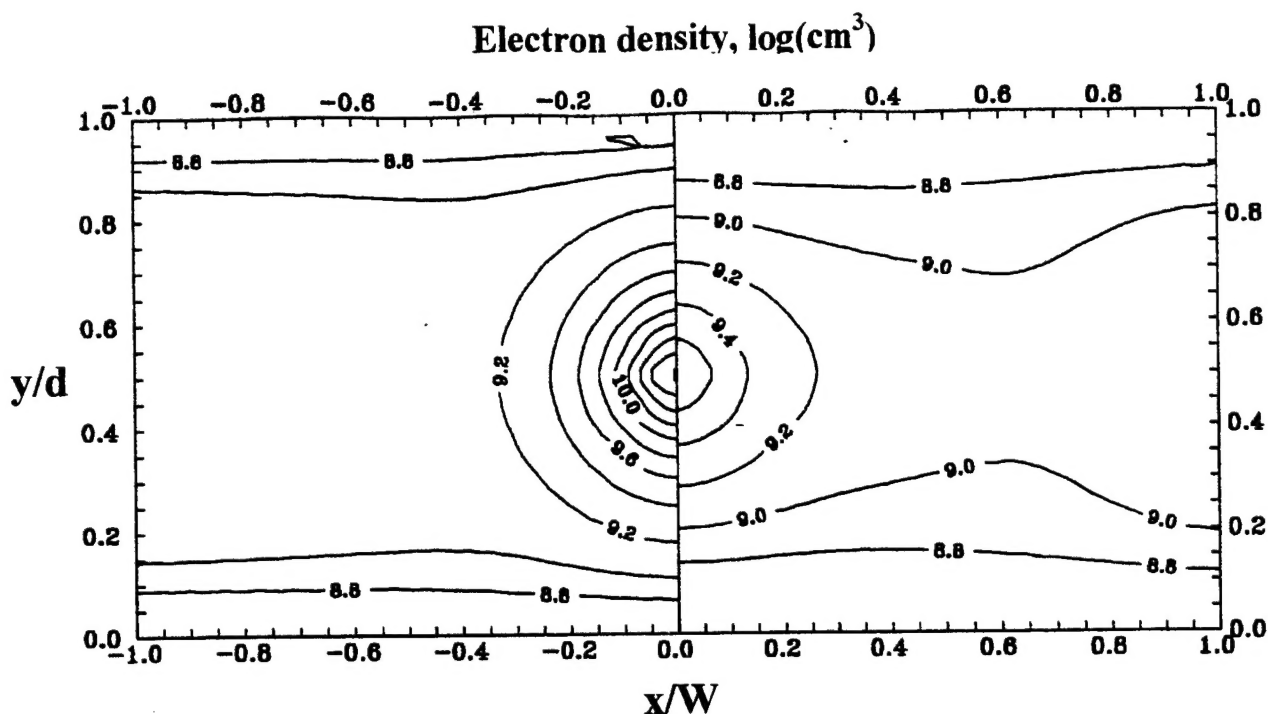
Electron density, log(cm³)

Figure 10. Electron density distribution in the optically pumped CO/N₂ plasma without (**left**) and with (**right**) RF field applied.
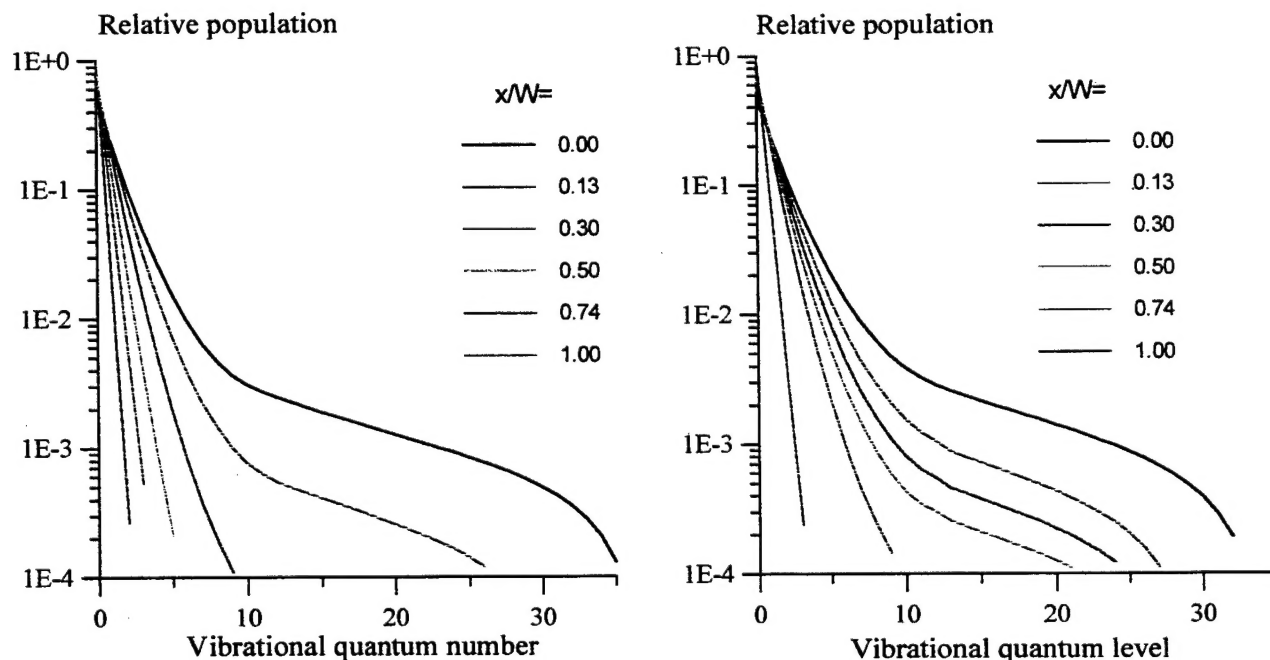

Figure 11. CO vibrational distribution functions along the centerline between the electrodes (at y=0.5) in the optically pumped CO/N₂ plasma without (**left**) and with (**right**) RF field applied.
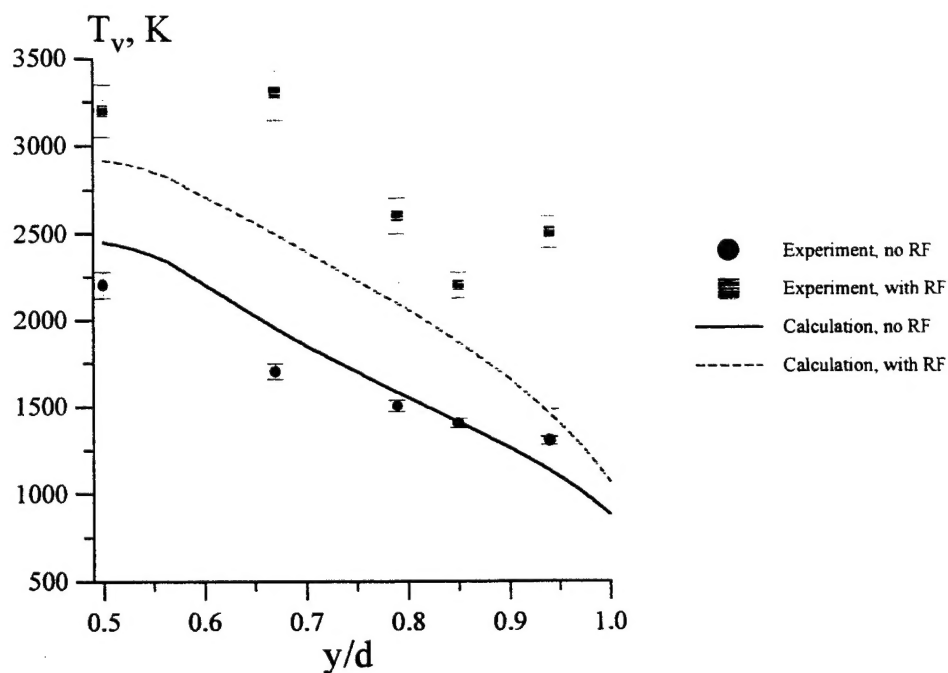
Figure 12. Comparison of the measured and calculated N_2 vibrational temperature in the optically pumped CO/N_2 plasma with and without RF field applied (at x=0).
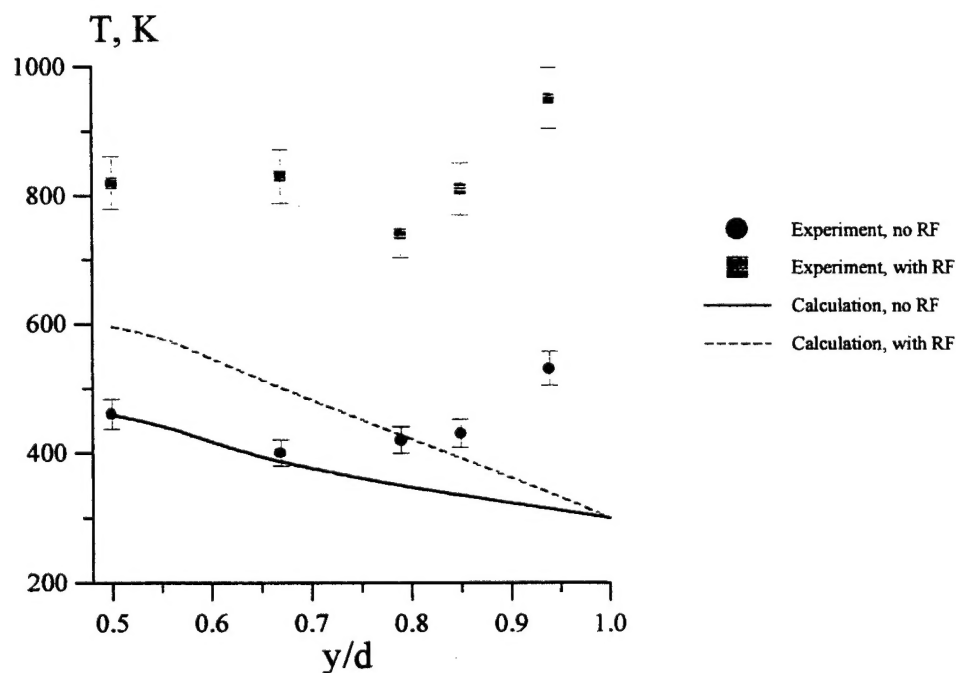

Figure 13. Comparison of the measured and calculated translational temperature in the optically pumped CO/N_2 plasma with and without RF field applied (at x=0).